UNIVERSIDADE FEDERAL DE SANTA CATARINA
CAMPUS JOINVILLE
PROGRAMA DE PÓS-GRADUAÇÃO EM ENGENHARIA E CIÊNCIAS MECÂNICAS

Carlise Ghisleni

THE EFFECT OF INITIAL DISTRIBUTION OF PHASES ON RELATIVE PERMEABILITY CURVES

Joinville, SC
2021

Carlise Ghisleni

THE EFFECT OF INITIAL DISTRIBUTION OF PHASES ON RELATIVE PERMEABILITY CURVES

Dissertation submitted to the Programa de Pós-Graduação em Engenharia e Ciências Mecânicas of Universidade Federal de Santa Catarina to obtain the master's degree in Engineering and Mechanical Sciences.
Supervisor: Prof. Fabiano Gilberto Wolf, Dr.
Co-supervisor: Prof. Diogo Nardelli Siebert, Dr.

Joinville, SC
2021

Ficha de identificação da obra elaborada pelo autor,
através do Programa de Geração Automática da Biblioteca Universitária da UFSC.

Ghisleni, Carlise
The effect of initial distribution of phases on relative permeability curves / Carlise Ghisleni ; orientador, Fabiano Gilberto Wolf, coorientador, Diogo Nardelli Siebert, 2021.
101 p.

Dissertação (mestrado) - Universidade Federal de Santa Catarina, Campus Joinville, Programa de Pós-Graduação em Engenharia e Ciências Mecânicas, Joinville, 2021.

Inclui referências.

1. Engenharia e Ciências Mecânicas. 2. Método de Lattice Boltzmann . 3. Distribuição inicial de fases. 4. Conectividade de fases. I. Wolf, Fabiano Gilberto. II. Nardelli Siebert, Diogo. III. Universidade Federal de Santa Catarina. Programa de Pós-Graduação em Engenharia e Ciências Mecânicas. IV. Título.

Carlise Ghisleni

THE EFFECT OF INITIAL DISTRIBUTION OF PHASES ON RELATIVE PERMEABILITY CURVES

The present master's thesis was evaluated and approved by the examining board composed by the following members:

Prof. Paulo Cesar Philippi, Dr.
Pontifícia Universidade Católica do Paraná

Rodrigo Surmas, Dr.
Centro de Pesquisas Leopoldo Américo Miguez de Mello

Prof. Luis Orlando Emerich dos Santos, Dr.
Universidade Federal de Santa Catarina

We certify that this is a **original and final version** of the conclusion paper that was deemed appropriate to obtain the master's degree in Engineering and Mechanical Sciences.

Documento assinado digitalmente
Rafael de Camargo Catapan
Data: 28/09/2021 15:11:51-0300
CPF: 029.036.159-18
Verifique as assinaturas em https://v.ufsc.br

Prof. Rafael de Camargo Catapan, Dr.
Coordenador do Programa

Documento assinado digitalmente
Fabiano Gilberto Wolf
Data: 28/09/2021 15:16:33-0300
CPF: 025.792.379-92
Verifique as assinaturas em https://v.ufsc.br

Prof. Fabiano Gilberto Wolf, Dr.
Supervisor

Joinville, SC, 30 de julho de 2021.

For all sentient beings that made this possible.

ACKNOWLEDGEMENTS

First, I would like to thank my supervisor, Professor Fabiano G. Wolf, for the e-mail he sent me three years ago asking if I was interested in joining my master on his field of study. Without it, this work could never exist. Also, I would like to thank my co-supervisor, Professor Diogo Nardelli Siebert, who was the one who build this connection.

I would like to say that without the guidance that you two always provided me I could never be able to finish this research. The multiple meetings and the multiple drawings you did about boundary conditions, fluid flow and how lattice-Boltzmann method works made it possible. I am truly grateful for having your support in all the research stages.

I also would like to thank my husband, my family and my friends for the support in this journey and for the understanding during the harsh times. Love you all.

Either, I would like to recognise the importance of Petrobras which was responsible for providing the sponsorship that gave me stability to research. It is important to recognise companies that believe in the power of education and support university researchers.

Also, I would like to thank the Professors Luis Orlando Emerich dos Santos, Eduardo De Carli da Silva, Alexandre Miers Zabot and all my colleges from the lab that always helped me during this project.

RESUMO

Este estudo foi realizado para explorar o efeito da distribuição inicial de fases nas curvas de permeabilidade relativa. A motivação deste estudo foi baseada no uso crescente de simulações computacionais para prever escoamentos multifásicos e suas propriedades. Ao analisar as pesquisas anteriores, observou-se que alguns autores utilizaram a distribuição randômica para iniciar suas simulações, por outro lado, outros autores consideram o método randômico ineficiente por apresentar falta de controle no preenchimento dos poros, o que poderia levar a distribuição de fluido não molhante em poros pequenos ou isolados. Para avaliar o impacto da distribuição inicial das fases, três métodos foram escolhidos para a condução das simulações: método aleatório, a distribuição de fases utilizando a Transformada de Distância Euclidiana Exata, chamado de método EDT e distribuição de fases utilizando a Transformada de Cobertura de Raio, chamado de método CRT. O estudo foi realizado usando o modelo de gradiente de cores baseado em Halliday, Hollis, and Care (2007) and Spencer, Halliday, and Care (2010). As simulações foram realizadas em uma imagem artificial bidimensional e em uma tomografia micro computadorizada tridimensional do arenito Berea. Para definir o método mais confiável para a distribuição inicial das fases, as curvas de permeabilidade relativa foram comparadas com simulações que reproduziam o processo de drenagem. Como resultados, constatou-se que a conectividade das fases está fortemente relacionada à distribuição inicial das fases, o que leva a permeabilidade relativa a apresentar valores diferentes em relação ao método utilizado para a distribuição inicial. A diferença absoluta observada para a permeabilidade relativa da fase molhante e não molhante para a imagem artificial, atingiu quase 40%. Para a rocha Berea, a diferença absoluta foi menor que para a imagem artificial mas ainda atingiu aproximadamente 25%. Com relação a comparação com a simulação de drenagem, o método CRT mostrou uma boa concordância para as curvas de permeabilidade relativa para a fase não molhante, para a imagem 2D artificial e para a rocha Berea 3D. Para as permeabilidades relativas da fase molhante, o método CRT apresentou concordância apenas para a rocha Berea. Para a curva de permeabilidade relativa da fase molhante da imagem artificial, os métodos randômico e EDT apresentaram melhor concordância, uma vez que o método CRT pareceu superestimar os valores para a permeabilidade relativa. Em relação às mudanças na molhabilidade, as diferenças nas curvas de permeabilidade relativa foram observadas para as condições de molhabilidade total e parcial da fase molhante.

Palavras-chave: Métodos para distribuição inicial de fases. Método de Lattice-Boltzmann. Conectividade de fases.

RESUMO EXPANDIDO

Introdução

Na engenharia de petróleo, o escoamento de fluidos aparece em várias etapas da produção. Dentro do reservatório, existem inúmeras propriedades físicas e químicas que podem afetar o deslocamento imiscível. Algumas das mais estudadas são porosidade, permeabilidades absolutas e relativas, número capilar e molhabilidade. Nesse trabalho, a permeabilidade relativa será estudada por se tratar de uma propriedade relacionada a permissividade do fluido em um meio saturado por múltiplos fluidos. Nessa análise, as curvas de permeabilidade relativa, obtidas por simulação computacional, serão analisadas em função do efeito da distribuição inicial de fases. Para isso, as simulações serão conduzidas utilizando o método de Lattice Boltzmann associado ao modelo de gradiente de cor. Essas simulações serão realizadas em duas imagens, uma 2D artificial e outra 3D obtida por micro-tomografia-computadorizada, considerando a obtenção de dados no regime permanente.

Objetivos

O objetivo principal consiste em estudar curvas de permeabilidade relativa em função das diferentes distribuições iniciais de fases, utilizando o método de Lattice Boltzmann para simular escoamentos em regime permanente em rochas artificiais e digitais.

Metodologia

Para a realização do trabalho, inicialmente foram definidas as imagens que seriam utilizadas e os métodos que seriam utilizados para a distribuição inicial das fases. Sendo assim, duas imagens, uma 2D e uma 3D foram utilizadas. A primeira, uma imagem artificial, criada especialmente para este estudo, já a segunda, uma imagem 3D foi obtida por Dong (2007). Já, quanto aos métodos de distribuição de fases, foram escolhidos três métodos: o método randômico, que distribui aleatoriamente as fases; o método EDT, baseado na Transformada de Distância Euclidiana, que distribui a fase molhante próximo a parede do sólido e a fase não molhante no centro do poro e; o método CRT, baseado na Transformada de Cobertura de Raio, que distribui o fluido molhante nos poros menores e o fluido não molhante nos poros maiores. Para validação valores obtidos para permeabilidade relativa, uma simulação de drenagem foi realizada, considerando o mesmo número capilar, para verificar os valores mais aderentes aos observados fisicamente.

Considerações Finais

Dos principais resultados obtidos nesse estudo, destaca-se que diferentes distribuições iniciais de fases incorrem em diferentes padrões de conectividade de fases, os quais afetam diretamente os valores de permeabilidade relativa. Para a imagem artificial, o método CRT mostrou uma boa concordância para curva de permeabilidade relativa da fase não molhante, mas os métodos randômico e EDT foram mais concordantes para a curva de permeabilidade relativa da fase molhante. Ainda para a imagem artificial, o método CRT indicou conexão excessiva para toda a curva de permeabilidade relativa da fase molhante. Para a validação da aderência dos métodos, foi realizada uma simulação de drenagem na rocha artificial. Já, para a validação dos resultados da imagem 3D, um estudo realizado por Raeini, Blunt e Bikeljic (2014) foi utilizado para comparação dos dados. Nesta comparação, o método CRT mostrou melhor concordância para as curvas de permeabilidade relativa das fases molhante e não molhante. Entretanto, é necessário ressaltar que, apesar de ter número capilar e imagens com propriedades similares, a simulação feita por Raeini, Blunt e Bikeljic (2014) considerava uma simu-

lação em regime transiente. Como sugestões para estudos futuros, indica-se a análise do método CRT para uma variedade de ângulos de contato e a realização da simulação de drenagem para a mesma imagem usada neste trabalho.
Palavras-chave: Métodos para distribuição inicial de fases. Método de Lattice-Boltzmann. Conectividade de fases.

ABSTRACT

This study has been performed to explore the effect of the initial distribution of phases in the relative permeability curves. The motivation of this study was based on the increasing use of computational simulations to predict the multiphase fluid flow and its associated properties. By analysing earlier research, it was observed some authors used random distribution to start their simulations, otherwise, other authors consider the random method inefficient since it presented a lack of control in filling pores, which may incur on distributing non-wetting phase in small or isolated pores. To evaluate the impact of the initial distribution of phases, three methods were used to conduct the simulations: random method, a distribution of phases using Exact Euclidean Distance Transformation, called EDT method and, a distribution of phases using Covering Radius Transform, called CRT method. The study was conducted using the color-gradient model based on Halliday, Hollis, and Care (2007) and Spencer, Halliday, and Care (2010). The simulations were performed in a two-dimensional artificial image and in a microcomputed tomography of a three-dimensional Berea sandstone. To define which was the most reliable method for the initial distribution of phases, the relative permeability curves were compared with a drainage flooding simulation. As result, it was found the connectivity of phases is strongly related to the initial distribution of phases, which leads the relative permeabilities to present different values regarding the method used for the initial distribution. The absolute differences observed for the non-wetting phase and wetting phase relative permeability curves achieved almost 40% for the artificial image. For the Berea sandstone, the absolute differences are lower than the observed for the artificial image but, still achieved almost 25%. Regarding the comparison with the drainage flooding, the CRT method showed a good agreement for non-wetting phase relative permeability curves for the artificial 2D image and the 3D Berea sandstone. For the wetting phase, the CRT method only presented an agreement with relative permeabilities for the Berea sandstone. For the wetting phase relative permeabilities in the artificial image, the random and EDT methods presented a better agreement, since the CRT method seemed to overpredict the values for the relative permeability. Regarding the changes in the wettability, for both strongly and partially wetting conditions, the differences in the relative permeability curves regarding the initial distribution of phases were observed.

Keywords: Methods for initial distribution of phases. Lattice-Boltzmann Method Phases connectivity.

LIST OF FIGURES

LIST OF TABLES

LIST OF ABBREVIATIONS AND ACRONYMS

BGK	Collision operator developed by Bhatnagar, Gross and Kook
CFD	Computational fluid dynamics
CRT	Covering radius transform
CT	Computed-tomography
D2Q9	Lattice configuration for 2 dimensions and 9 velocities
D3Q19	Lattice configuration for 3 dimensions and 19 velocities
DT	Distance transformation
EDT	Euclidean distance transformation
EOR	Enhanced oil recovery
FDM	Finite Differences Method
FE	Free-Energy multiphase model of Swift et al. (1996)
FEM	Finite Elements Method
FVM	Finite Volume Method
LBE	Lattice Transport Equation
LBM	Lattice Boltzmann Method
LGA	Lattice gas automata
NWP	Non-Wetting Fluid
REV	Representative elementary volume
RK	Rothmann and Keller (1988) lattice gas model
SC	Shan and Chen (1993) multiphase model
TRT	Two Relaxation Time
WP	Wetting Fluid

LIST OF ABBREVIATIONS

f_i	Distribution Function
ϕ	Porosity
V_P	Porous Volume
V_B	Bulk Volume
N_c	Capillary Number
σ	Interfacial Tension
u	Fluid Velocity
μ	Fluid Viscosity
S_i	Saturation of a Given Phase
V_i	Volume of a Given Phase
k_a	Absolute Permeability
k_i	Effective Permeability
k_{ri}	Relative Permeability
q	Flow Rate
A	Normal Cross-Sectional Area
S_{wc}	Irreducible Water Saturation
S_{orw}	Residual Oil Saturation
$\boldsymbol{r}$	Position of Particles
t	Time
c_i	Discrete Velocity
f_i^{eq}	Equilibrium Distribution Function
τ	Relaxation Time
W_i	Weight in Direction i
$\nabla\omega_r$	Gradient of Red Fluid Saturation for Each Direction
c_s	Speed of Sound in Lattice Units
ω_r	Concentration of Red Fluid
$\widehat{\boldsymbol{n}}$	Unitary Normal Vector to the Interface
$f_{s,i}$	Distribution Function for Symmetric Decomposition Part
$f_{a,i}$	Distribution Function for Anti-Symmetric Decomposition Part
F_i	External Force
f_i^*	Distribution function with external force operator
w_{wr}	Concentration of Red Fluid on the Wall
θ_r	Contact Angle
S_i	Initial Saturation
M	Viscosity Ratio
β	Recoloring Coefficient
D_e	Equivalent Diameter

CONTENTS

1 INTRODUCTION

The characterisation of fluid transport in porous media has been usually a target of attention in engineering and in academy. Particularly, the comprehension of fluid flow inside rocks has attracted interest in areas such as Enhanced oil recovery (EOR), capture and sequestration of carbon dioxide, remediation of non-aqueous liquid phases, remediation and transport of contaminants in aquifers, and others (KANG et al., 2010; DAI et al., 2013; CHEN; KANG, et al., 2013).

In petroleum engineering, the fluid flow appears in many production stages. It can show up either in migration stage, production or, injection inside the columns.

At the reservoir fluid flow stage, there are numerous physical and chemical properties that can affect immiscible displacement. Some of the most studied properties are porosity, absolute and relative permeabilities, capillary number, and wettability. As relative permeability has a considerable effect on flow, this property will be studied in this work.

The relative permeability is a key parameter for describing two-phase fluid flows. By definition, relative permeability is a property related to flow permissiveness in a porous medium saturated by multiple fluids (LYONS, 2010). But more than that, relative permeability is an interdependent property, which means its determination depends on other flow parameters such as saturation of phases, viscosity ratio, driving forces, wettability, pore structure, among others (SHI; TANG, 2018). Whenever any of these parameters change, relative permeability also changes.

Historically, the first experiment to determine relative permeability was carried out by Wyckoff and Botset, in 1936, for a two-phase water-gas system in an unconsolidated sandstone. Years later, in 1941, Leverett and Lewis measured relative permeability for a water-oil-gas system in a similar porous medium (ALIZADEH; PIRI, 2014). Since then, a lot of laboratory work has been done to understand how relative permeability behaves and how properties influence its curves.

Experimentally, there are two main methods to measure relative permeability: steady-state flow and transient flow. In the steady-state flow method, two phases are injected simultaneously at a fixed and constant ratio and when the system reaches equilibrium conditions, relative permeability is measured. Differently, in the transient flow method, a fluid is injected into the sample to displace another fluid that already fills the porous medium, called in-situ fluid (JIANG; TSUJI, 2016) and the relative permeability is measured as the experiment evolves.

Both approaches have advantages and disadvantages. As advantage, the transient method does not depend on saturation to reach equilibrium, each experiment provides a complete relative permeability curve and it, also, returns results quickly. However, this method is characterised as an indirect measure, since the relative per-

meability value is not obtained as an experimental result but as a function of the flow rate, which leads to some uncertainties. On the other hand, the steady-state method presents less controversial results, as it may be considered a direct measurement, but its tests are time-consuming since each experiment returns only two values, one for wetting and one for non-wetting relative permeability (ALIZADEH; PIRI, 2014).

However, to avoid time-consuming data attainment and uncertain conditions in a laboratory environment, several studies have been conducted computationally using Computational Fluid Dynamics (CFD) tools. The core of the simulations focused on reproducing the fluid flow as seen in experiments, analysing specific properties of flow including its interactions with other properties.

The use of CFD started back in 60', using methods known as Finite Volume Method (FVM), Finite Elements Method (FEM), Finite Differences Method (FDM). Late in 90', Lattice Boltzmann Method (LBM) has been proposed as an alternative method for simulation of two-phase flow through complex geometries of the porous medium. Unlike continuum CFD schemes which are based on discretization of macroscopic continuum equations, LBM is based on the mesoscopic kinetic equations. The fundamental advantage of LBM is its computational efficiency (ALPAK; ZACHAROUDIOU, et al., 2019).

This method gained attention as a simulation fluid flow method by its simplicity at formulation and implementation. Lattice Boltzmann Method is capable of simulating a wide variety of problems related to fluid flow in different geometries, both in single and multiphase conditions (CHEN; DOOLEN, 1998). Its basic premise is to apply the Lattice Transport Equation (LBE) for flow simulation in a discrete domain by modeling fluid motion through the evolution of particle distribution function (f_i) (APOURVARI; ARNS, 2016).

To find a research niche that joined relative permeability and LBM, several articles were analysed. As result, it was possible to observe that the researches followed two main ways: i. replicate relative permeability experiments; ii. comprehend how changing fluid properties or rock properties can influence relative permeability curves.

For the first strand, Ramstad, Idowu, and Nardi (2011) explored the relative permeability conduct by using LBM to reproduce experiments in steady-state and transient regimes. For this study, digital images of Berea and Bentheimer sandstones were obtained using micro computed-tomography and the porous medium was initially randomly saturated by two immiscible fluids. The research aimed to compare the results for steady-state and transient fluid flow with experimental data previously obtained by Øren, Bakke, and Arntzen (1998) and Oak, Baker, and Thomas (1990).

In their results, Ramstad, Idowu, and Nardi (2011) noticed there was no satisfactory correlation between simulated drainage curves in the transient flow compared to experimental curves obtained under steady-state conditions. From this observation,

they concluded that it is not possible to compare these flow regimes, especially for the non-wetting phase which is the least connected phase. According to Schlüter et al. (2016), the non-wetting phase is affected by snap-off and fingerings formation, which violate Darcy's law for two fluids, and that is the reason by its definition being more difficult than the wetting phase.

Ramstad, Idowu, and Nardi (2011), Alpak, Berg, and Zacharoudiou (2018) also compared experimental and simulated relative permeability curves. For it, it was used a micro computed-tomography (CT) image of Gildehauser sandstone obtained by Berg et al. (2016). The study focused on the topology of the non-wetting phase. The results were supported by Berg et al. (2016) and Liu et al. (2017), based on the fact that relative permeability has a strong correlation with connectivity.

In the second strand, which is more abundant in literature, the influence of rock and fluid properties on relative permeability got more focus on the analysis. Zhao et al. (2017) evaluated the effects of changing the capillary number, viscosity ratio, and wettability. Shi and Tang (2018) focused on studying the variation of the driving force, wettability, the effects of grain distribution, and phase saturation. Landry, Karpyn, and Ayala (2014) studied the effects of homogeneous and mixed wettability in relative permeability and Li et al. (2018) the effect of different contact angles.

The influence of porous medium heterogeneity, regardless of the degree and the distribution of micro-heterogeneity, was studied by Dou and Zhou (2013). Zhang, Papadikis, and Gu (2016) also studied geometric characteristics of the porous medium and its influence on relative permeability, by creating a set of artificial geometries based on circles and ellipses.

What is valuable to observe about these researches is that there is no standard regarding the choice of the initial distribution of phases or porous geometry. Many authors adopted digital images (ZHAO et al., 2017; RAMSTAD; IDOWU; NARDI, 2011; ALPAK; BERG; ZACHAROUDIOU, 2018) for considering it has better similarity with physical features observed in rocks, while other researchers used artificial geometries composed by spheres (SHI; TANG, 2018), circles (LI et al., 2018; ZHANG; PAPADIKIS; GU, 2016), ellipses (ZHANG; PAPADIKIS; GU, 2016) or squares (DOU; ZHOU, 2013).

Regarding the initial distribution of phases, some authors, such as Ramstad, Idowu, and Nardi (2011), Dou and Zhou (2013), Landry, Karpyn, and Ayala (2014) and Zhang, Papadikis, and Gu (2016) used random distribution to start their simulations. However, Jiang and Tsuji (2016) and Alpak, Berg, and Zacharoudiou (2018) considered it inefficient since the method presented a lack of control in filling pores, which may incur on distributing the non-wetting phase in small or isolated pores. Also, the absence of the notion of the drainage-imbibition hysteresis makes it difficult to compute the imbibition relative permeability function.

Dou and Zhou (2013) also pointed that the use of random distribution at the

beginning of the LBM simulations causes the obtaining of different distributions at the end of the simulation even for an identical initial degree of saturation. The results for relative permeability for each set of random distribution also presented differences.

As observed, there is another group of researchers that avoid using random distribution. For example, Jiang and Tsuji (2016) applied oscillatory body forces to cause spontaneous phases separation; Li et al. (2018) used a random method to place the fluids in the porous medium but, by the imposition of gravitational forces, redistributed them on the sample; Shi and Tang (2018) considered the wetting phase next to the walls and the non-wetting phase at the centre of the porous and redistributed it by applying body forces and; Alpak, Berg, and Zacharoudiou (2018) reproduced imbibition and drainage processes. However, as seen, each study deals with an initial distribution of phases differently, having no consensus on which technique has a better fitting for calculating fluid-related properties.

What was realised evaluating these studies is that there is no research exploring how the behaviour of the initial distribution of phases can interfere in relative permeability. We know from Alpak, Berg, and Zacharoudiou (2018), Jiang and Tsuji (2016) and others, that random saturation may not be the best approach, but there is no study that quantifies how relative permeability values change by using or not using random distribution. Being so, this work seeks to solve the question: How does the initial distribution of phases affect the relative permeability?

What was realised evaluating these studies is that, there is no research exploring how the behaviour of initial distribution of phases can interfere in relative permeability. We know from Alpak, Berg, and Zacharoudiou (2018), Jiang and Tsuji (2016) and others, that random saturation may not be the best approach, but there is no study that quantifies how relative permeability values change by using or not using random distribution. Being so, this work seeks to solve the question: How does the initial distribution of phases affects the relative permeability?

The simulations will be performed until the system reaches steady-state flow conditions, which closely mimics the steady-state flow for the relative permeability experiment. After convergence, the effective permeability for the wetting and non-wetting phase will be computed.

Regarding the content of this work, Chapter 2 brings the literature review about rock and fluid properties and an overview of the history and the basic formulation of the single-phase Lattice Boltzmann method. Chapter 3 explains the methodology applied in this research, such as the porous media used for simulation, the distribution methods and the specific formulation for the used LBM. Chapter 4 presents the results and the analysis for the simulations and Chapter 5 ties all it in, with the conclusions and the key findings.

1.1 OBJECTIVES

1.1.1 General Objective

The main objective consists in study relative permeability curves as a function of the different initial distribution of phases, using Lattice Boltzmann Method (LBM) to simulate steady-state flows in artificial and digital rocks.

1.1.2 Specific Objectives

In order to achieve the overall objective, the study was divided in:

i. verification of the simulation model for a conventional case;

ii. define the porous media that will be used;

iii. define initial phase distributions that will be simulated;

iv. determine the measurement of relative permeability curves for each case considered in item iii;

v. analyse uncertainties associated to random method;

vi. define the most reliable method for the initial distribution of phases basing the results in the drainage flooding;

2 BACKGROUND

Reservoir engineering is the heart of petroleum engineering once it predicts the total amount of trapped oil, the reservoir characteristics and the techniques for extraction. In the 1930's and 1940's, reservoir engineering evolved as a separate and important discipline in petroleum engineering, which deals with the flow of oil, gas, and water through porous media and also with the associate recovery efficiency (SATTER; IQBAL; BUCHWALTER, 2007).

To comprehend how fluid flow process occurs and how the properties influence this process, it is important to lean on rock and fluid characteristics. Section 2.1 brings important aspects of porous media and concepts associated to fundamental parameters of rock and fluid, such as porosity, wettability, capillary number, saturation and permeability. The understanding of these concepts are important to comprehend how fluid flow behaviour.

As reservoir engineering does not exist without multiphase flow, this section will also discuss about a numerical method used for fluid flow simulations: the Lattice Boltzmann Method. Section 2.2 outlines the history of LBM, the concept of particle distribution, a brief formulation for single-phase flow and the usual boundary conditions used in simulations.

2.1 THE POROUS MEDIUM

The porous medium detain information about the reservoir rocks which is crucial for understanding the fluid flow and oil production. The chosen properties only scratches the surface of the topic "rock and fluid properties", but they are fundamental to understand this work.

2.1.1 Porosity

Petroleum reservoirs can be characterised as porous material due to the presence of a microscopic pore network in which oil, gas and water may coexist. Knowing that, it is possible to define a property called porosity.

The porosity is a measure which quantifies the capacity of a reservoir rock contains or stores fluids in its pores. These fluids can be gas, oil and water. High porosity values indicate high capacities of the reservoir rocks to contain these fluids while low porosity values indicate the opposite (EZEKWE, 2011).

The porosity, which is based on the void spaces also depends of its surroundings, in this case, the grains. The huge amount of shapes, sizes and patterns dictate the nature of the pore channels through which subsurface fluids will be able to move (SATTER; IQBAL; BUCHWALTER, 2007).

The porosity (ϕ) is a dimensionless property calculated by:

$$\phi = \frac{V_P}{V_B}, \tag{1}$$

where V_P is the porous volume of the rock and V_B is the bulk volume.

During geological formation, there are two stages for porosity in reservoir rocks. The primary porosity is initially developed during bulk deposition in prehistoric times. In the other hand, secondary porosity is developed due to various geological and geochemical processes, leading to significant alteration in rock characteristics. Examples of secondary porosity are vugs, cavities, circulation of certain solutions, dolomitization of carbonate rocks, and development of fractures in the rock matrix (SATTER; IQBAL; BUCHWALTER, 2007).

2.1.2 Wettability

The wettability is a property that measures the tendency of one fluid do adhere to the surface in the presence of other immiscible fluid (COSENTINO, 2001). The importance of wettability is critical to microscopic flow under capillary-dominated regime, because it is related to the distribution of fluids within a porous network. In other words, a water-wet and an oil-wet reservoirs behave differently with respect to the displacement process (COSENTINO, 2001). Figure 1 shows two cases of wettability, one for water-wet and other for an oil-wet surface.

According to Satter, Iqbal, and Buchwalter (2007), the water-wet reservoirs are considered to be better candidates for enhanced oil recovery by water flooding since water is expected to adhere to the rock surface, creating a lubricating effect and improving the flow of oil through the pore channels. In contrast, if the reservoir is oil-wet, the use of water flooding is not so efficient and the ultimate recovery will be lower.

For Cosentino (2001) and Satter, Iqbal, and Buchwalter (2007) it is believed that reservoir rocks are more likely to be water-wet than oil-wet, since porous medium were originally occupied by formation water through geologic times. However, oil-wet or mixed wettability reservoirs are not uncommon.

2.1.3 Capillary Number

The capillary number (N_c) is the ratio of viscous forces to the capillary forces arising out of interfacial tension (SATTER; IQBAL; BUCHWALTER, 2007) as shown:

$$N_c = \frac{u\mu}{\sigma}, \tag{2}$$

where u is the fluid displacing velocity, μ is the fluid viscosity and σ is the interfacial tension between fluids.

Figure 1 – Contact angle and wettability.

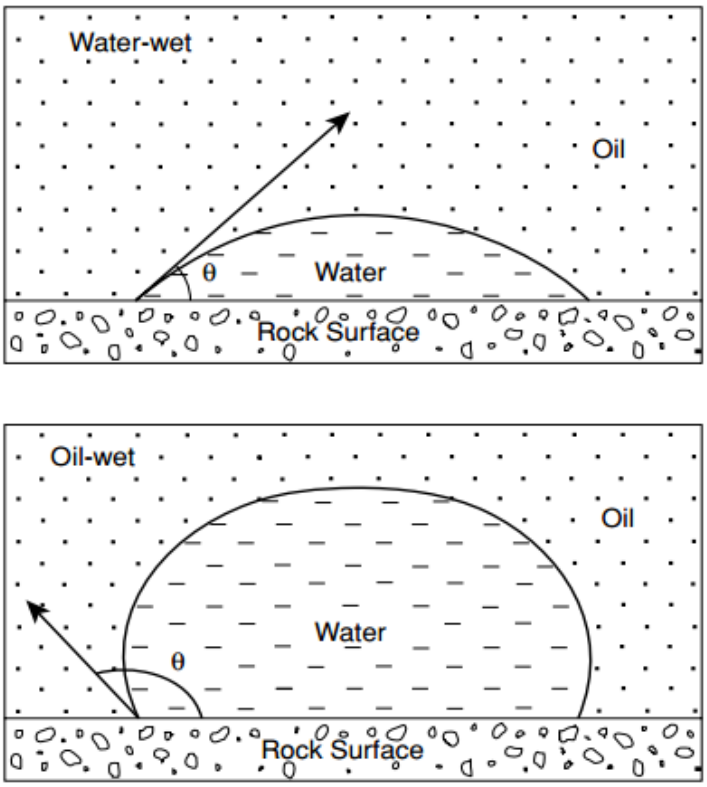

Source – Adapted from Ezekwe (2011)

The viscous forces are present in fluid flow when velocity gradients are encountered. These velocity gradients can be generated by driving forces, gravitational forces, differential of pressure, etc. According to Bird, Stewart, and Lightfoot (2006), viscous forces are strictly related to viscous stresses which are the linear combination of all velocity gradients.

On the other hand, interfacial tension arises from the simple existence of two fluids in porous medium. When two immiscible fluids, such as oil and water coexist in a porous medium, one of the fluids can preferentially wets the porous surface over the other and, as result, a pressure differential is found to exist between the two fluids.

In a common reservoir, the capillary numbers may typically vary from 10^{-8} to 10^{-2} during the displacement of fluids. For a successful production operation, as high as capillary number can be, more efficient will be the oil recovery (SATTER; IQBAL; BUCHWALTER, 2007).

2.1.4 Fluid Saturation

The understanding of the fluid saturation concept is useful in diverse stages of the oil production. At the discovery stage, the fluid saturation is used to estimate the initial volume of the in-situ phases. At the recovery stage, it is used to identify

the reservoir zones where a large quantity of hydrocarbons was left behind (SATTER; IQBAL; BUCHWALTER, 2007).

The fluid saturation (S_i) is usually expressed as the ratio of the volume of a given phase (V_i) to the porous volume (V_P),

$$S_i = \frac{V_i}{V_P}, \tag{3}$$

and it is represented as a fraction of pore space or a percentage.

For instance, if a two-phase reservoir has the non-wetting phase saturation equal to 70% (or 0.7), it means 70% of the pore space is occupied by this phase. The means, the remaining 30% (or 0.3) is occupied by the wetting phase.

2.1.5 Permeability: Absolute, Effective and Relative

When a new reservoir is discovered, the permeability is one of the most valuable characteristics engineer seeks to determine since the general visualisation of the future performance depends on it (SATTER; IQBAL; BUCHWALTER, 2007).

The permeability is a measure of the capability of a porous medium to transmit fluids through a network or microscopic interconnected channels under a certain driving force. In subsurface, the driving force originates from a pressure differential that exists between two points in the flow, i.e., velocity gradients originated due to pressure differential between the producing wells (lower pressure) and drilled areas (higher pressure).

There are three types of permeability: absolute permeability (k_a), effective permeability (k_i) and relative permeability (k_{ri}). If the porous medium is completely saturated by one fluid, the measured permeability is the absolute permeability. For two or more fluids, the permeability measured is the effective permeability to that particular fluid or the relative permeability, which is a normalisation of effective permeability by absolute permeability,

$$k_{ri} = \frac{k_i}{k_a}. \tag{4}$$

The desire of measuring permeability dates back to 1856, when Henry Darcy conducted his first experiment to study fluid flow behaviour on a packed sand column which emulated a subsurface aquifer. He observed that the volumetric flow rate of water through the packed bed was a function of the dimension of porous medium and the difference in hydraulic head, as given,

$$q = \frac{k_a A}{\mu} \left(\frac{\Delta p}{L} \right), \tag{5}$$

where q is the flow rate, μ is fluid viscosity, A is the normal cross-section area to the fluid flow and $\Delta p/L$ is the pressure gradient in flow direction. By modifying equation 5, it is possible to calculate absolute permeability.

Since only water saturated the porous media, the property that Darcy measured was the absolute permeability. Although, for a multiphase system, the effective and relative permeability values for each individual phase need to be calculated. An adaption of Darcy's law for multiphase flow was proposed by Blunt (2017) and can be calculated by,

$$q_i = -\frac{k_{ri}k_a}{\mu_i}(\nabla P_i - \rho_i \boldsymbol{g}). \tag{6}$$

According to Blunt (2017), the macroscopic flow is integrated over a representative volume of space, containing many pores. That way, it is possible to define an average velocity $\overline{u}$ as the average in some representative element of volume, V,

$$\overline{u} = \frac{1}{V}\int \boldsymbol{u} dV, \tag{7}$$

where the velocity is calculated over the entire porous volume. From the equation 7, the capillary number is also obtained (equation 2, but instead of u, $\overline{u}$ is used.

The measure of relative permeability by laboratory methods can be classified under two groups, namely, steady-state or unsteady-state (known as transient flow) methods. The steady-state method is widely used and considered more reliable than unsteady-state methods. However, it is time-consuming and requires elaborate equipment. Some measurements in steady-state may require days of experimental time in comparison to hours for unsteady-state method (EZEKWE, 2011).

But laboratory experiments for relative permeability present a drawback. To run an experiment it is necessary to prepare the samples. The laboratory must cut, clean, dry and re-saturate the cores with water and refined oil. The key issue in this whole process is to restore the initial wettability, which has a large impact on relative permeability curves (DONNEZ, 2007). Figure 2 shows the schematic draw of a laboratory experiment.

Figure 2 – Laboratory assembly for relative permeability experiments.

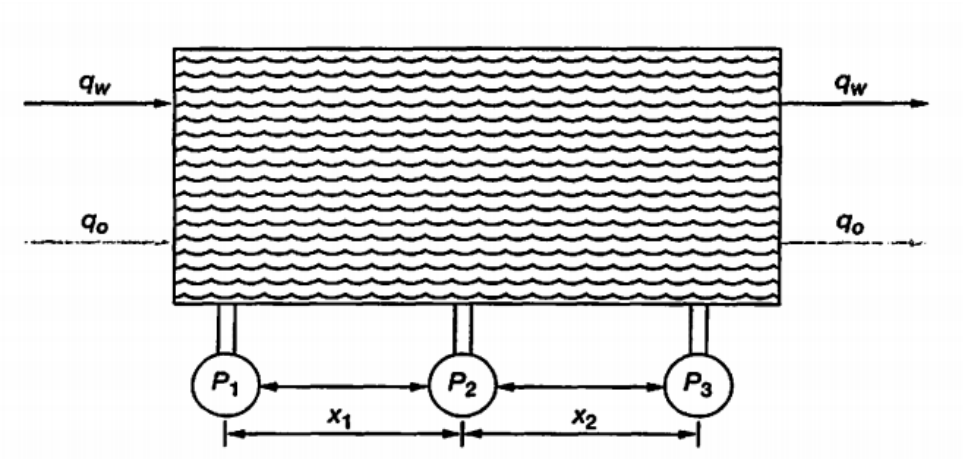

Source – Adapted from Donnez (2007)

where q_w and q_o are the flow rate of the water and oil, respectively; P_1, P_2 and P_3 are the pressures measurements at input, intermediate and output lengths; and x_1 and x_2 are the lengths used obtain the differential pressure.

For the steady-state method, a fixed ratio of fluids is forced through the test sample, until pressure and saturation equilibrium is reached. The effective permeability of each fluid phase is calculated as function of saturation by direct application of Darcy's law, by measuring volumetric flow rate, the pressure drop and the saturation of each individual phase (COSENTINO, 2001). According to Ezekwe (2011), the steady-state method yield the most reliable relative permeability data because capillary equilibrium is achieved in the method.

The entire range of saturation can be measured in a step-wise fashion by changing the ratio of injection rates and repeating the procedure. The problem is that it requires many days, or even months, to complete because equilibrium conditions must be attained at each saturation level.

Unlikely steady-state method, the relative permeability data can be obtained by unsteady-state method very quickly, once it does not require the attainment of equilibrium in the displacement process, so the data can be acquired in a few hours (EZEKWE, 2011).

Unsteady-state experiments are performed by measuring the effluent from a core during an imposed displacement process, in terms of cumulative production, and back calculating the relative permeability ratio consistent with that outcome (COSENTINO, 2001). In other words, the in-situ fluid is displaced by the injection of another at constant rate or pressure, while the produced fluids is continuously measured.

In the other hand, the data from unsteady-state method can be affected by displacement problems, such as viscous fingering and channeling, including instability of the displacement process. This way, the method is recommended to be used to

measure relative permeability at the saturation endpoints, while steady-state methods are used to infill the data between the endpoints (EZEKWE, 2011). A typical relative permeability curve can be seen in Figure 3.

Figure 3 – Relative permeability curves.

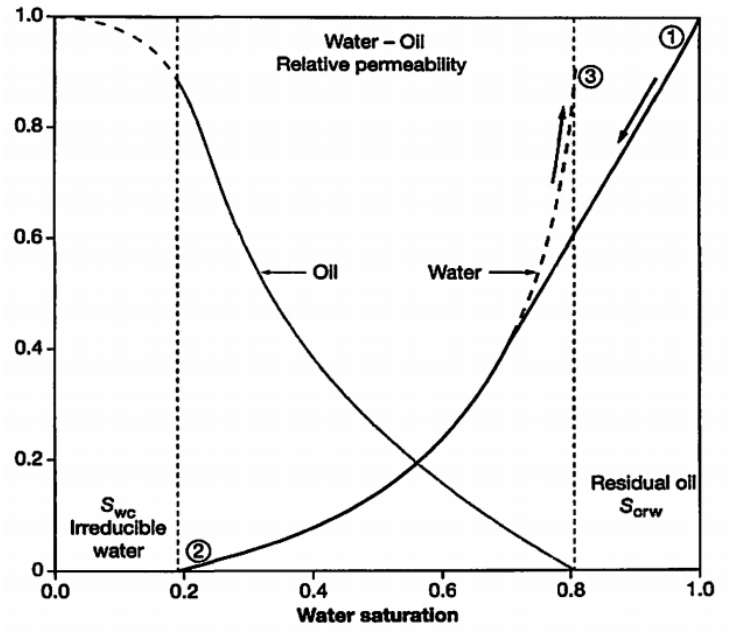

Source – Adapted from Donnez (2007)

where label 1 represents 100% water saturation, label 2 is the irreducible water saturation (S_{wc}) and, label 3 is the residual oil saturation (S_{orw}).

In order to avoid time-consuming laboratory experiments, some computational techniques have been developed to obtain relative permeability curves. These simulations can mimic both steady-state and unsteady-state methods, keeping under control relevant properties and be run in different types of sample.

2.2 LATTICE BOLTZMANN METHOD

There are two main approaches in simulating the transport equations (heat, mass, and momentum): continuum and discrete. In continuum approach, ordinary or partial differential equations are obtained by applying conservation of energy, mass, and momentum for an infinitesimal control volume, which represents a macroscopic scale. Since, it is difficult to solve the governing equations, schemes like Finite Volume Method (FVM), Finite Differences Method (FDM) and Finite Elements Method (FEM) can be used to solve differential equations, considering a given boundary and initial conditions.

On the other extreme, the medium can be considered to be made of small particles, known as discrete approach, and these micro-scale particles collide to each

other. The main issue here is the necessity to identify location and velocity of each particle at each time step in order to identify inter-particle forces and solve ordinary differential equation of Newton's Second Law.

For considering both approaches with advantages and disadvantages, Lattice Boltzmann Method remains in the middle of both aforementioned techniques. The main idea of LBM is to bridge the gap between micro-scale and macro-scale, by not considering each particle behaviour alone, but the behaviour of a collection of particles as a unit, using a property called distribution function (MOHAMED, 2011).

This section provides an overview about the Lattice Boltzmann Method (LBM), explaining the history, the single-phase formulations and the most used boundary conditions. This review helps to create a context from where the method came and how it works.

2.2.1 The History of Lattice Boltzmann Method

The Lattice Boltzmann Method has experienced a fast pace development in the last two decades and has become a powerful computational fluid dynamics tool. This method is particularly successful in applications involving interfacial dynamics and fluid flow through complex geometries (CHEN; DOOLEN, 1998).

The LBM trace their roots to Lattice Gas Automata LGA, which was originally conceived by Stanislaw Ulam and John von Neumann in the 1940s. The philosophy behind the LGA considers fluid behaviours at macroscale nothing but statistical results of the micro-dynamics. The method itself consists of a discretization of space, on which individual cells exist in a particular state, and update their state at each time step according to a rule that takes as input the states of some set of neighbours cells (HUANG; SUKOP; LU, 2015).

The popularity of LGA starts to increase when Frish, Hasslacher and Pomeau (1986) presented a study that could properly simulate the two-dimensional Navier-Stokes equations. As advantage, LGA exhibited itself as a straightforward method based on the collision-streaming paradigm, boolean operations with no round-off errors and, unconditional stable computation. On the other hand, the method also presented downsides like statistical noise arising from boolean variables, violation of Galilean invariance and, dependence of the velocity of the pressure (GUO; SHU, 2013).

A second major step towards the modern LBM was the elimination of statistical noise proposed by McNamara and Zanetti (1988), who replace the individual particles of the LGA with an averaged discrete distribution function. Another major simplification was introduced by Qian et al. (1992), who exchange the collision matrix of Higuera et al. (1989) by a single relaxation time, leading to the collision operator developed by Bhatnagar, Gross, and Krook BGK, which enhances greatly the computational efficiency and makes the implementation of the collision process much easier than other models

(HUANG; SUKOP; LU, 2015; SANTOS; FACIN; PHILIPPI, 2003).

After that, the LBM developed quickly in different fields of study, from material science and engineering to biophysics. In section 2.2.2, the method itself will be explained for a single-phase flow, in order to explain the collision and streaming stages, the function distribution and the lattice scheme.

2.2.2 Single Phase Lattice Boltzmann Method

A major breakthrough in LB theory happened when the direct derivation of the LB equation (LBE) was obtained from the continuous Boltzmann equation. It successfully established the theoretical foundation of the LB method (PHILIPPI et al., 2006).

The Lattice Boltzmann Method is a mesoscopic method that describes a mechanical system of particles. It may be expressed as a discrete for of the Boltzmann transport equation, where the system is described by a particle distribution function $f_i(\boldsymbol{r}, t)$, which represents a probable number of particles at position $\boldsymbol{r}$ and time t, with discrete velocity c_i.

Density and momentum, respectively, can also be obtained from the distribution function, as expressed:

$$\rho = \sum_i f_i, \tag{8}$$

$$\rho u = \sum_i f_i c_i. \tag{9}$$

In LBM, a discrete cartesian lattice scheme is utilised to confine the particles in the space. These particles are allowed to move in a finite number of directions, depending on the structure used. The Lattice configuration for 2 dimensions and 9 velocities (D2Q9) is used for two-dimensional structures and the Lattice configuration for 3 dimensions and 19 velocities (D3Q19) is used for three-dimensional structures. These structure representations can be seen in Figure 4.

The evolution of the particles inside lattice structures, in terms of movement, is given by two distinct stages: collision and streaming. During the collision, particles interact with each other within lattice nodes. At this stage no information is exchanged between nodes and quantities of mass and momentum are conserved (GUNSTENSEN, A K et al., 1991a).

Otherwise, during streaming, particles propagate in defined directions according to the lattice structure considered. For each time step, the collision and streaming stages repeatedly occur until a defined number of time steps or until the system reaches equilibrium. The equation that describes the evolution of particle distribution is Lattice

Figure 4 – D2Q9 and D3Q19 lattice structures.

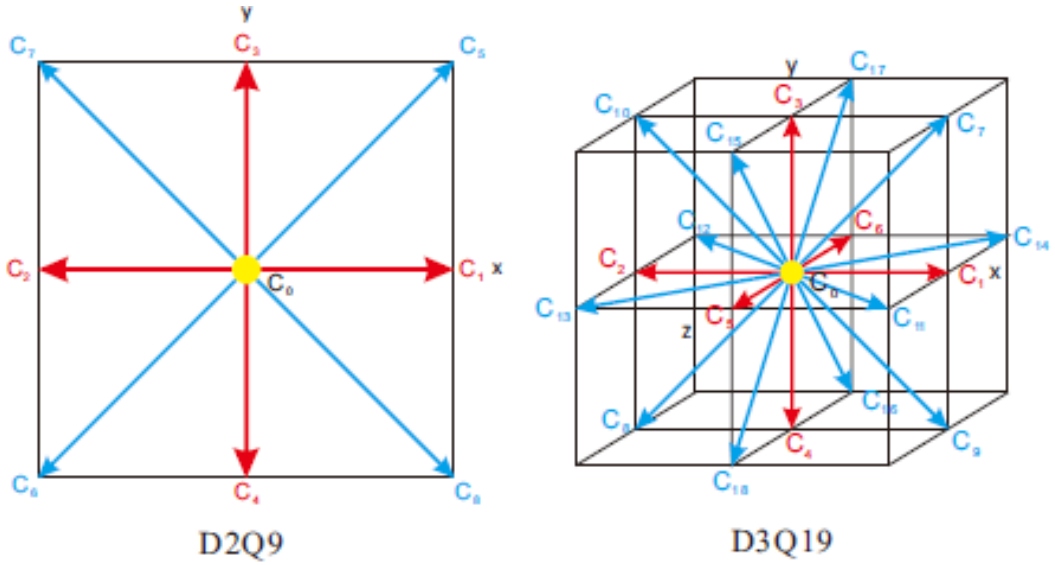

Source – Adapted from Guo, Liu, and Xuo (2017)

Transport Equation (LBE):

$$f_i(\boldsymbol{r} + c_i, t+1) - f_i(\boldsymbol{r}, t) = \Omega_i[\rho(\boldsymbol{r}, t), u(\boldsymbol{r}, t)], \tag{10}$$

where Ω_i is the collision operator and $u(\boldsymbol{r}, t)$ is the velocity, defined as:

$$u(\boldsymbol{r}, t) = \frac{\sum f_i c_i}{\sum f_i}. \tag{11}$$

In Equation 10, the left side describes the streaming stage, and the right side describes the collision stage. Even both stages coexist in mathematical formulation, during computational implementation each stage is build up individually.

The collision operator Ω_i captures the relaxation of the distribution function towards the equilibrium distribution. When properly chosen, it guarantees that mass and momentum can be properly conserved, mathematically,

$$\sum_i \Omega_i = 0, \tag{12a}$$

$$\sum_i \Omega_i c_i = 0. \tag{12b}$$

The simplest and most widely used collision operator for LBE is called Collision operator developed by Bhatnagar, Gross and Kook (BGK),

$$\Omega_i = -\frac{1}{\tau}(f_i - f_i^{eq}). \tag{13}$$

Its formulation was driven by the need for larger density fluid simulation (remember LBM evolve from LGA, therefore the first collision operator was suitable only for gas

simulations) and its formulation takes into account the populations f_i and the equilibrium populations f_i^{eq}. Physically, it can be interpreted as the tendency of the population f_i to approach its equilibrium state f_i^{eq} after a time τ. The relaxation time τ, determines the speed of this equilibrium (KRÜGER et al., 2017).

To achieve the correct macroscopic behaviour of fluids governed by the Navier-Stokes equation, the equilibrium distribution must be properly chosen. Qian, d'Humières, and Lallemand (1992) proposed the following expression:

$$f_i^{eq}(\rho, u) = \rho W_i \left[1 + \frac{3(\boldsymbol{c} \cdot \boldsymbol{u})}{c_s^2} + \frac{9(\boldsymbol{c} \cdot \boldsymbol{u})^2}{2c_s^4} - \frac{3\boldsymbol{u}^2}{2c_s^2}\right], \tag{14}$$

where W_i and c_s lattice dependent. For D2Q9 structure, $c = |\boldsymbol{c_i}|$, $W_0 = 4/9$, $W_1 = W_2 = W_3 = W_4 = 1/9$ and $W_5 = W_6 = W_7 = W_8 = 1/36$. The values for W_i are selected in order to achieve macroscopic isotropy and Galilean invariance (SUKOP; THORNE, 2006). The same distribution can be obtained by the Maxwell-Boltzmann distribution proposed by Philippi et al. (2006). For D3Q19 structure, to calculate f_i^{eq}, the values for W_i and c_i are different. This approach can be seen in Wolf-Gladrow (2005).

In the section 2.2.3, the multi-component models for Lattice Boltzmann will be discussed and the Color-Gradient model will be explained in terms of its implementation.

2.2.3 Multi-component Models for Lattice Boltzmann Method

The multiphase fluid flow is found in a myriad of applications, ranging from advanced oil recovery to micromodel development and studies in biology. Usually, the evolution of this system is modelled by applying the Navier-Stokes equations inside each phase, with the interface acting as a moving boundary, where the Young-Laplace equation gives rise to a stress jump normal to the interface.

Soon after its initial conception, the Lattice Boltzmann Method showed to be a suitable tool for the simulation of this kind of flow and in the following decades, various multi-component models using the LB framework were developed. Among them, three of the most known are: the RK model, the SC model, and the FE model.

The earliest one, called the color-gradient multiphase model or RK model, was proposed by A. K. Gunstensen et al. (1991b), based on (ROTHMANN; KELLER, 1988) lattice gas model. In this model, each component is represented by one distribution function and associated with colors: red-colored fluid (R_i) and the blue-colored fluid (B_i). The collision step is performed over a colorblind distribution function, which is the sum over the single-phase distributions. An additional term is added to the collision operator to account for the force due to the interface curvature. Before the streaming step a recoloring step reconstructs the colored distributions functions.

The Shan-Chen model (SC) proposed by Shan and Chen (1993) appeared soon after and it is based on the incorporation of an attractive or repulsive force between

particles of different fluids, which leads to phase separation (HUANG; SUKOP; LU, 2015). In this model, each component is represented by its own distribution function, with its own collision operator, which adds an inter-particle force term. Although capable of simulating immiscible fluid flow with moderate density ratios, the SC model does not allow the independent adjustment of the density ratio and the interface length, both depending on the surface tension. Other drawbacks of this model are the high values for the spurious currents and the non-negligible diffusivity component.

The third type of multiphase LBM model is the Free-Energy (FE) of Swift et al. (1996). This model intends to be more thermodynamic consistent by using the Cahn-Hillard equation for the free energy which results in a density gradient dependent equation of state. To retrieve such relation for pressure in the LBM the authors propose a new equilibrium distribution for the BGK collision step. This FE model permits the simulation of two-phase pore-scale flow of fluids that exhibit significant viscosity contrast, such as vapour-liquid flow in porous media, colloidal suspension, surfactant adsorption into interfaces, among others (HUANG; SUKOP; LU, 2015).

2.2.3.1 Color-Gradient Model

In this work, the color-gradient model was chosen to perform the simulations since the research did not treat significant viscosity contrast or high-density ratios. Also, this model had already been implemented and tested by the Poro Research Team, providing the benefit of simulating using multiple CPUs or GPUs.

In a two-phase system, the amount of particles with velocity $\boldsymbol{c_i}$ at nodal position $\boldsymbol{r}$ and time t, are described by the red (R_i) and blue (B_i) distribution functions. For the collision step, a colorblind distribution is defined,

$$f_i(\boldsymbol{r}, t) = R_i(\boldsymbol{r}, t) + B_i(\boldsymbol{r}, t). \tag{15}$$

Density and velocity were obtained, respectively, by equations 8 and 9, using the distribution function in its formulation.

According to Halliday, Hollis, and Care (2007), the proper definition of the phase-field is important to recover correct dynamics for continuum regime and kinematics. With that purpose in mind, a discrete approximation for the phase-field gradient is computed by following second-order finite difference scheme,

$$\nabla\omega_r \approx \frac{1}{c_s^2}\sum_i W_i\omega_r(\boldsymbol{r} + \boldsymbol{c_i})\boldsymbol{c_i}, \tag{16}$$

where c_s is the speed of sound in lattice units and ω_r is the local red fluid concentration (SPENCER; HALLIDAY; CARE, 2010; SANTOS; FACIN; PHILIPPI, 2003). Since the

gradient points from the blue to the red phase, a normal vector to the interface can be computed from the equation,

$$\widehat{\boldsymbol{n}} = -\frac{\nabla\omega_r}{|\nabla\omega_r|}. \tag{17}$$

To compute collision, it was used the Two Relaxation Time (TRT) model proposed by Ginzburg (2005). This model improves significantly the problem of non-zero slip velocity near the walls for small channels existing in the BGK collision operator (PAN; LUO; MILLER, 2006). Briefly, the TRT uses a decomposition of the distribution function into a symmetric $f_{s,i}$ and an anti-symmetric $f_{a,i}$ part, for which, to perform collision the BGK operator was applied,

$$f_{s,i} = \frac{f_i + f_{-i}}{2}, \tag{18}$$

$$f_{a,i} = \frac{f_i - f_{-i}}{2}, \tag{19}$$

$$\Omega_i = -\frac{f_{s,i} - f_{s,i}^{eq}}{\tau_s} - \frac{f_{a,i} - f_{a,i}^{eq}}{\tau_a}, \tag{20}$$

here, τ_s is the relaxation time of the symmetric part for each fluid and τ_a is a function of τ_s in order to vanish high order spurious terms.

Additionally, a perturbation term F_i, used to model the stress jump on the interface,

$$f_i^* = \Omega_i + F_i. \tag{21}$$

Its formulation was based on a viscous stress perturbation that promotes a Laplace pressure step between the fluids in the interfacial region (SPENCER; HALLIDAY; CARE, 2010). The force term due to interfacial tension in Einstein notation was,

$$F_i(\boldsymbol{r}, t) = \rho W_i \left(\frac{\alpha|\nabla\omega_r|}{c_s^2\tau}\right)[(\hat{n}\cdot c_i)^2 + (D-1)c_s^2 + c_i^2], \tag{22}$$

where W_i is a directional-dependent weight. Using this force term (SPENCER; HALLIDAY; CARE, 2010), the interfacial tension is given by,

$$\sigma = 2\rho c_s^2\alpha. \tag{23}$$

The RK model also includes a re-coloring step (HALLIDAY; HOLLIS; CARE, 2007), where, after a colorblind collision, the two coloured distribution functions are reconstructed individually by the following equations,

$$B_i(\boldsymbol{r}, t) = \omega_b f_i - W_i\beta\rho\omega_r\omega_b(\widehat{n}\cdot\boldsymbol{c_i}), \tag{24}$$

$$R_i(\boldsymbol{r}, t) = \omega_r f_i - W_i \beta \rho \omega_r \omega_b (\widehat{n} \cdot \boldsymbol{c_i}). \tag{25}$$

The last procedure on the computation of a new time step is the streaming of each colored distribution function to its neighbours following,

$$B_i(\boldsymbol{r} + \boldsymbol{c_i}, t + 1) = B_i(\boldsymbol{r}, t), \tag{26}$$

$$R_i(\boldsymbol{r} + \boldsymbol{c_i}, t + 1) = R_i(\boldsymbol{r}, t). \tag{27}$$

To implement the effect of wettability on a solid wall, it is assumed that the solid wall is a mixture of two fluids with constant proportions, which is controlled by a parameter called the concentration of red fluid on the wall (w_{wr}). If the contact angle to the red component is θ_r, then

$$w_{wr} = \frac{cos\theta_r - 1}{2}, \qquad 0 \leq w_{wr} \leq 1. \tag{28}$$

If $\theta_r = 0°$, then w_{wr} is 0, and the red fluid will be strongly non-wetting, which means, the droplets cannot adhere to the solid surface. Otherwise, if w_{wr} is 1 the red fluid will be strongly wetting and the droplets spread out at the periphery due to greater affinity with the solid surface.

2.2.4 Boundary Conditions

Boundary conditions are essential in LBM in order to ensure consistency and guarantee physical aspects for the model. During this section, the most common boundary conditions will be briefly described. In the following figures, the grey sites indicate the solid sites and, the white sites indicate the pore sites.

i. Bounce-back: this scheme is the most widely used rule for stationary no-slip walls. It assumes the momentum of a particle is just reversed when it hits the wall, going back into the flow domain, as seen in Figure 5. If the particle is reversed, it means that the macroscopic velocity at the wall is zero. The grey sites indicate the solid sites.

ii. Periodic: this condition considers that when the system becomes closed by the edges, it can be treated as if it is attached to the opposite edge. In that way, periodic boundaries are applied to open ends, so when the fluid reaches one end of the system, it 'reappears' in the other end. Figure 6 represents periodic boundary.

iii. Mirror: this condition is applied to simulate smooth boundaries with negligible friction exerted upon the fluid, called commonly free-slip. It may be imposed as a reflection process as seen in Figure 7.

Figure 5 – Bounce back boundary condition.

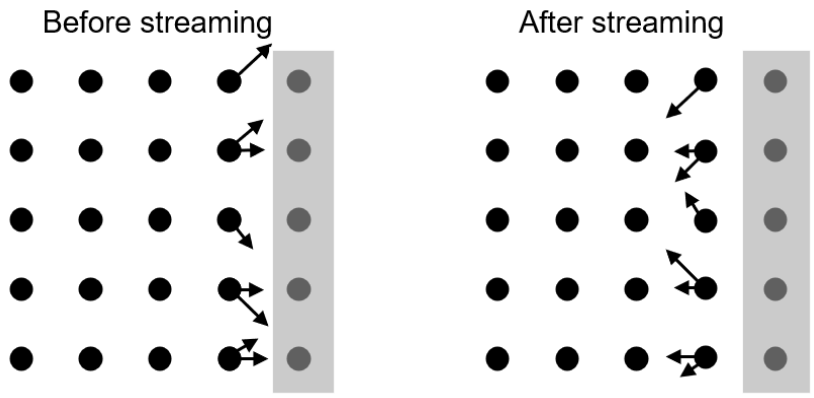

Source – Elaborated by the author

Figure 6 – Periodic boundary condition.

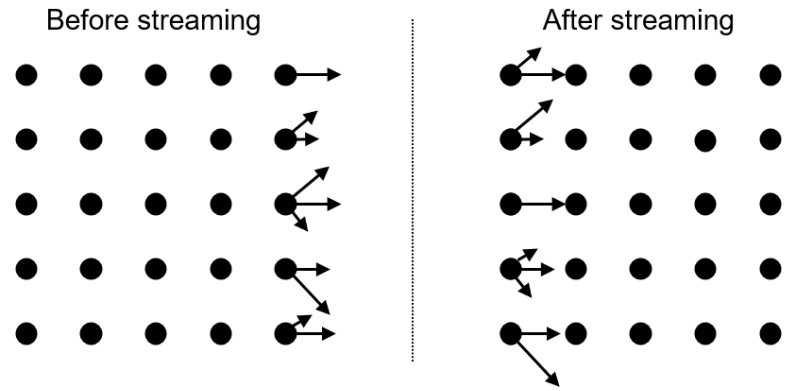

Source – Elaborated by the author

iv. Von Neumann: this condition constraints the flux at the boundaries, fixing the velocity of the flux. It implies that distribution function, density and pressure are computed at the nodes to maintain constant velocity (KRÜGER et al., 2017).

v. Dirichlet: this condition constraint the pressure/density at the boundaries. The solution for these boundaries is closely related to that given above for the velocity boundaries, but instead of velocity, density is fixed (specifying density is equivalent to specifying pressure because its relation in the equation of state) (SUKOP; THORNE, 2006).

Other boundary conditions can be implemented for specific problems. Furthermore, body forces, such as gravitational forces, can be incorporated into the model by rearranging velocity during equilibrium distribution function calculation (SUKOP; THORNE, 2006).

Figure 7 – Mirror boundary condition.

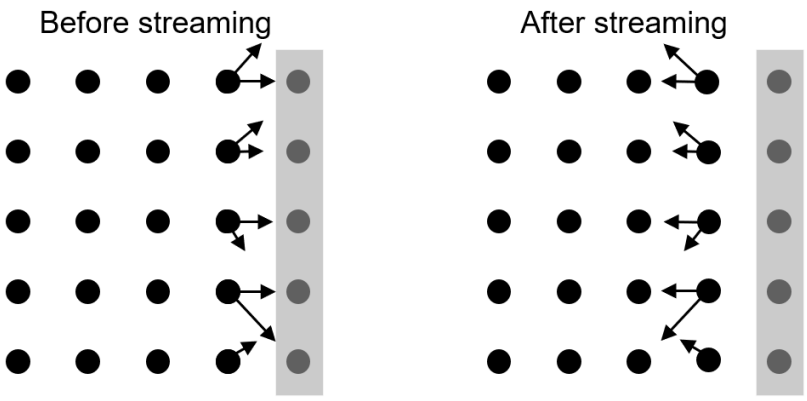

Source – Elaborated by the author

3 METHODOLOGY

To avoid time-consuming experiments and errors associated with indirect laboratory measurements, computational simulation has emerged as a trustworthy and efficient method. Although, in order to obtain reliable results, it is necessary to outline well the problem.

In this chapter, four different subjects will be discussed. In the section 3.1, the properties of the artificial image and the representative-tomography Berea sandstone will be explained. In the section 3.2, the three methods for the initial distribution of phases - random, EDT and CRT methods - will be discussed by using a hypothetical sample to place the phases. In section 2.2.3, the LBM approach for immiscible fluids, implemented for the simulations will be presented. The last, section 3.3 brings an overview of the simulation setup.

3.1 IMAGES CHARACTERISATION

The importance of knowing the reservoir rock is fundamental for petrophysics once, the behaviour of fluid flow is intrinsically related to it. According to Cosentino (2001), the close relationship existing between porous network, rock properties and fluid flow forms a cornerstone of a whole reservoir study.

Although sometimes, it is not that simple to simulate real reservoir rocks. First, because it is not easy to obtain a micro-computed-tomography of sandstone or carbonate. Second, because computational processing demand for simulations can be high. Third, because of the challenges to visualise the path of fluid flow in three-dimensional geometries. That way sometimes it is needed a step back to simpler geometries, in order to improve the understanding of fluid flow by simplifying visualisation.

The next sections will deepen in the two porous media used in this work. A two-dimensional artificial image and a three-dimensional micro-CT of the Berea sandstone.

3.1.1 Artificial Image

To start a simulation, it is necessary to define a porous medium, in which the fluid will flow. For the two-dimensional simulations, it was chosen an artificial image as seen in Figure 8.

The image was build with a set of squares with measures of 12^2, 32^2, 52^2, 72^2, 92^2, and 112^2 sites, distributed in an aleatory way. The initial size of the image is equal to 2000x1000x1 and it is possible to see it is formed by two regions. One with macropores and other with micropores. This construction intended to understand the flow in both regions.

To respect the periodic boundary condition and avoid inconsistencies at the

Figure 8 – Artificial porous medium.

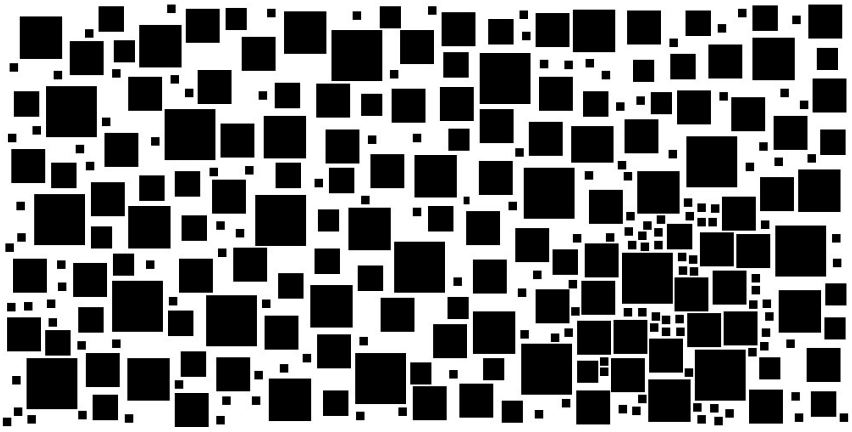

Source – Elaborated by the author

edges due to the inequality of right and left sides, the image from Figure 8 was mirrored, in the flow direction, turning into Figure 9.

Figure 9 – Mirrored artificial porous medium.

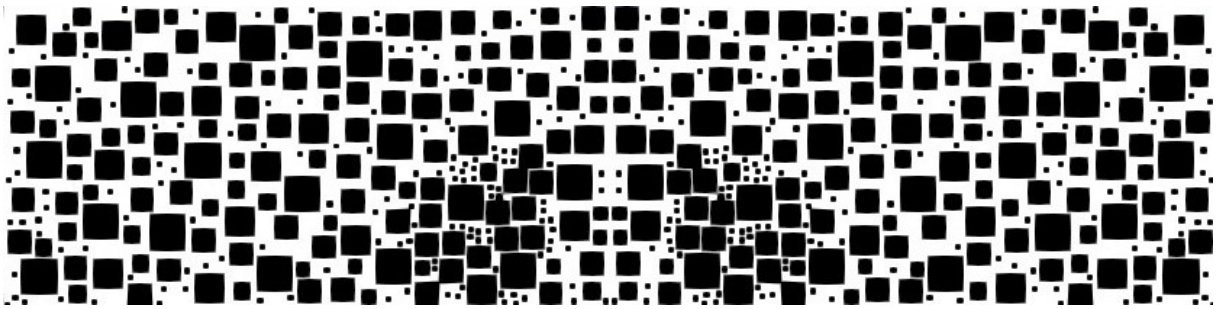

Source – Elaborated by the author

The properties of the artificial image are seen in Table 1. The scale considered is $1\mu m/voxel$.

Table 1 – Rock properties for artificial image.

Image size	**Porosity (ϕ)**	**Absolute Permeability (k_a)**
4000 x 1000 x 1	47.0%	111 D

Source – Elaborated by the author

3.1.2 Three-dimensional Image

To the three-dimensional analysis, it was chosen a micro-CT image obtained by Dong (2007), called Berea sandstone. This sandstone forms the middle layer of the Waverly group rock formations in Ohio and its deposition occurs during Mississipian

geological period between 360 and 325 million years ago. This rock is also found in oil and gas-producing formation in Michigan Basin.

The Berea sandstone is frequently used in flooding experiments due to its fine-grained and well-sorted characteristics with closely spaced planar bedding. However, according to Dong (2007) the sample still is heterogeneous. To provide a better look at its characteristics, Figure 10 shows a cross-section of the micro-CT image.

Figure 10 – Cross-section of a micro-CT image of Berea Sandstone.

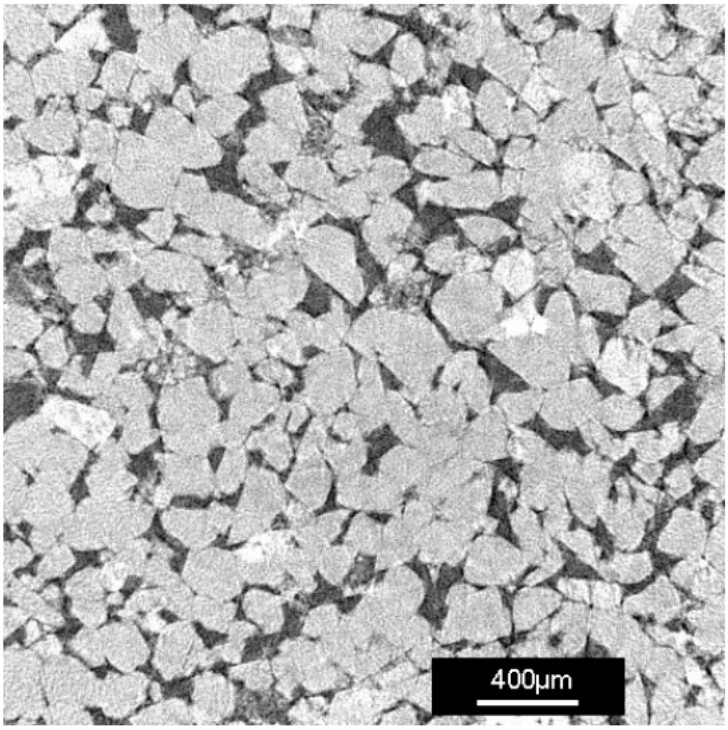

Source – Adapted from Dong (2007, p. 109)

The three-dimensional visualisation of Berea sandstone, already duplicated, can be seen in Figure 11 and the rock properties are displayed in Table 2.

Considering the physical size of the Berea sandstone is equal to $2138^3\mu^3$ and the digital image size is 400^3 voxels, resulting in a scale of $5.345\ \mu m/voxel$.

Table 2 – Rock properties for Berea sandstone.

Image size	**Porosity (ϕ)**	**Absolute Permeability (k_a)**
800 x 400 x 400	19.6%	0.657 D

Source – Elaborated by the author

The Berea sandstone was chosen considering the number of articles who cited it (RAEINI; BLUNT; BIKELJIC, 2014; FULCHER; ERTEKIN; STAHL, 1985; OAK; BAKER; THOMAS, 1990; AMAEFULE; HANDY, 1982; KREVOR; PINI; BENSON, 2012; AK-BARABADI; PIRI, 2013). Also, Mostaghimi, Blunt, and Bijeljic (2012) indicated that for

Figure 11 – Duplicated Berea Sandstone.

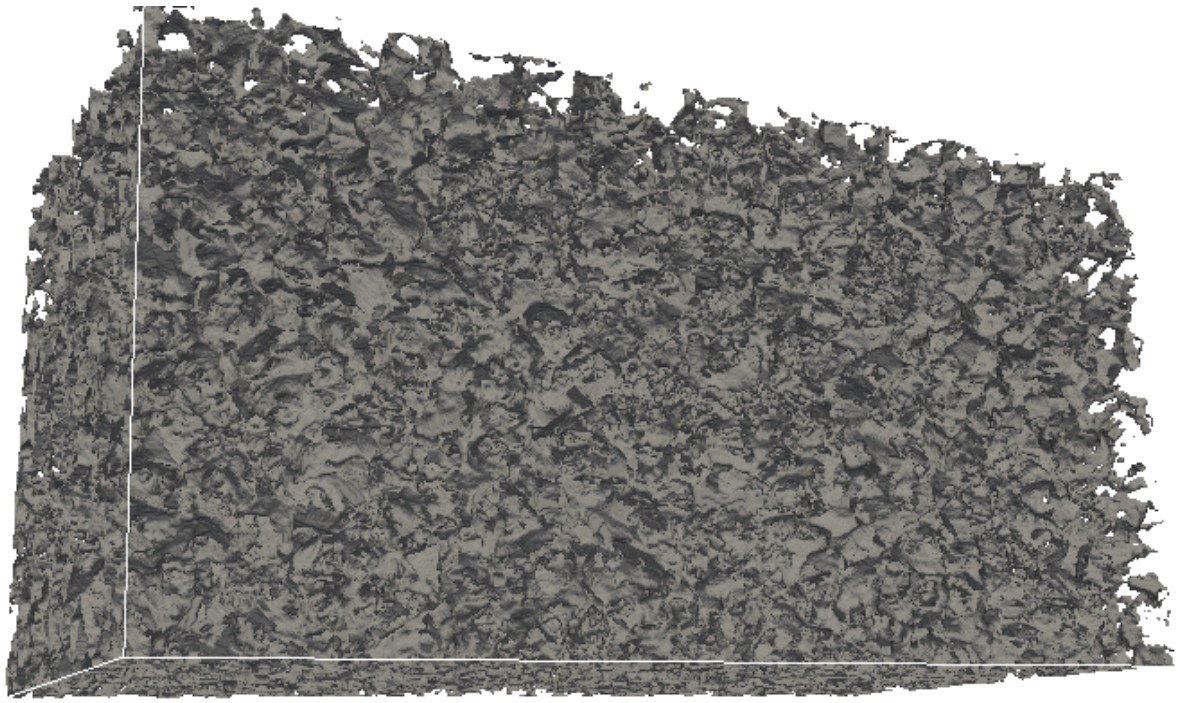

Source – Elaborated by the author

porosity and specific surface area, an image of Berea sandstone larger than 80^3 sites have constant properties. For the permeability variation, the sizes larger than 150^3 sites can be considered for representative elementary volume REV, which is in accordance with the 400^3 sites Berea sandstone image used in the research. However, the REV was not simulated to the specific geometry used in this work.

3.2 CHARACTERISATION OF INITIAL DISTRIBUTION OF PHASES

Different from an experiment, where one fluid is placed inside the sample and another fluid is injected to displace it, mimicking a drainage flooding, when working with numerical simulation, the phases can be distributed in a variety of ways, including, reproduce a drainage flooding.

Authors like Ramstad, Idowu, and Nardi (2011), Dou and Zhou (2013), Landry, Karpyn, and Ayala (2014) and Zhang, Papadikis, and Gu (2016) preferred to randomly distribute the phases, Jiang and Tsuji (2016) and Shi and Tang (2018) preferred to apply body forces to cause spontaneous phases separation, Li et al. (2018) imposed gravitational forces to redistribute the phases and Alpak, Berg, and Zacharoudiou (2018) reproduced imbibition and drainage processes.

Seeing there is no consensus about the initial distribution of phases, the proposal of this work is to analyse if relative permeability curves are affected by different initial saturation. The three methods chosen to place phases inside the porous medium were

i. random distribution; ii. EDT method, that places wetting fluid next to walls and non-wetting fluid in the centre of the porous and; iii. CRT method that places wetting fluid into smaller pores and non-wetting fluid into larger porous.

The random distribution of phases (section 3.2.1) was chosen because it was commonly quoted in articles and be the object of disagreement between authors. Otherwise, the EDT method (section 3.2.2) and the CRT method (section 3.2.3) were based on Dou and Zhou (2013) and Ghassemi and Pak (2011) that said for a strongly wetting system, non-wetting fluid tends to occupy a larger pore space, while the wetting phase tends to occupy a smaller pore space. For Rosa, Souza Carvalho, and Xavier (2006), during drainage flooding, this configuration is also expected.

During the explanation of the methods for the initial distribution of phases, an hypothetical sample will be used to better explain the arrangement of the fluids, where blue is assigned to the wetting fluid (WP) and red to the non-wetting fluid (NWP).

3.2.1 Random Distribution

The random distribution of phases, or the random method, is one of the most mentioned methods used to place phases before performing or as an initialisation condition for fluid flow simulations, probably because of its simplicity in implementation. Basically, the process of randomly arrange fluids consists in counting the number of void sites and, considering a given initial saturation (S_i), fill these voids with given fluids.

For instance, let's consider a hypothetical porous medium, as seen in Figure 12. Black pixels represent the solid sites and white pixels represent the fluid sites. The amount of fluid sites is equal to 150.

If the initial saturation of the non-wetting phase is 30%, the wetting phase is equal to 70%. It means, 45 sites will be filled with the non-wetting phase and 105 sites will be filled with the wetting phase. Figures 18 and 13b shows two sets of fluid distribution. In these images, red is assigned for NWP and blue for assigned for WP.

What is relevant to mention is that each time the fluid is placed in the sample, the sites for wetting and non-wetting phase change, leading to different results. This may be an issue, according to Jiang and Tsuji (2016) and Alpak, Berg, and Zacharoudiou (2018), due to the lack of control in filling pores might interfere with the simulation results.

3.2.2 Distribution of phases using Exact Euclidean Distance Transformation

Distance transformation (DT) was first defined by Rosenfeld and Pfaltz (1966) and ever since it has become an important tool for shape analysis in digital picture processing.

Its operation converts a binary matrix, represented by an image made of 1-sites and 0-sites, into another, the distance map, in which, each element has a value

Figure 12 – Hypothetical porous medium for random saturation representation.

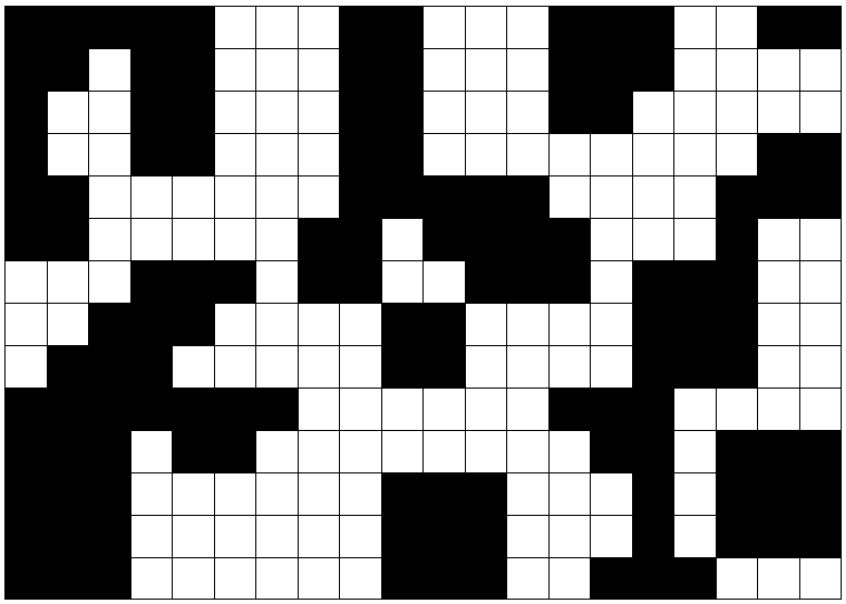

Source – Elaborated by the author

Figure 13 – Random distribution of phases.

(a) Example 1. (b) Example 2.

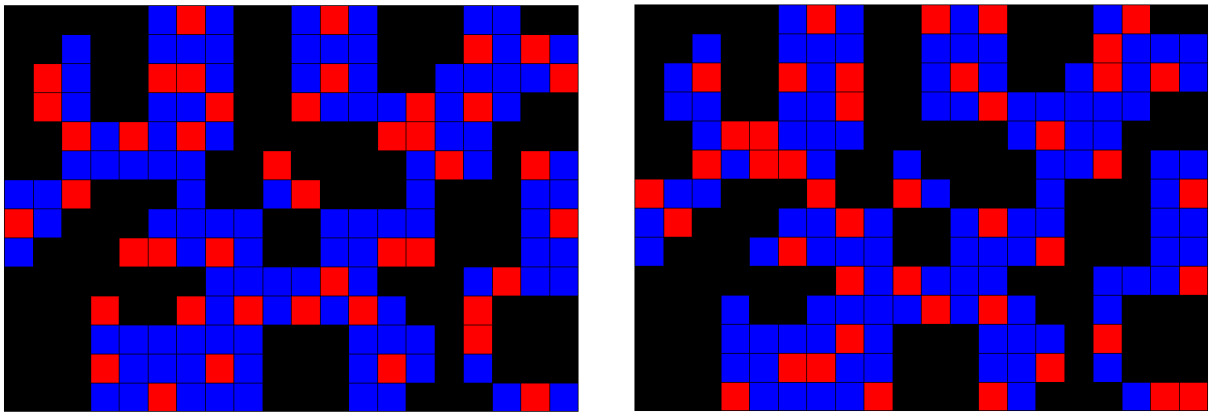

Source – Elaborated by the author

corresponding to the distance from the corresponding 1-site to the nearest 0-site by given a distance function (TORELLI et al., 2010).

The distance between two points of an image can be calculated according to different approaches. The most common of them is Euclidean distance transformation (EDT) due to its property of invariant rotation (ASSIS ZAMPIROLLI, 2003). By using the EDT method, it is possible to dilate and erode features, find the minimum path between two pixels, measure fractal dimension, calculate Voronoi diagram, comprehend aspects of mathematical morphology, among others (TORELLI et al., 2010).

The first one to study Euclidean Distance Transformation was Danielsson (1980), who proposed to generate the Euclidean distance map with no significant errors, but not

totally error-free. While non-exact EDT is good enough for some applications, there are applications where an Exact (error-free) Euclidean Distance Transformation is required. According to Maurer and Raghavan (2003), various approximations of EDT have been used to generate skeletons of binary objects, but only the exact EDT can produce an accurate skeleton that is reversible, rotation invariant, and minimal.

To obtain the Euclidean distance map of a binary matrix/image, it is necessary to assume that for any site there is another one, in its neighbourhood, with the same nearest distance. Figure 14 shows a binary image and its respective Euclidean distance map. For each pixel in the left image, there is a corresponding pixel in the right image which stores the exact euclidean distance between this pixel and the nearest border pixel. Note that, only in sites equal to 1 the distance function is applied to generate the distance map.

So, for position $(3, 4)$ starting from the left top side, the distance between the pixel and the nearest zero, which is the border pixel, is equal to 1. Although, for position $(4, 4)$ the distance between the pixel and the nearest zero is $\sqrt{2}$, once the minimum distance is given by the diagonal. It is valuable to point out, that diagonal values are required because its approach considers the exact value for the distance map.

Figure 14 – Exact EDT scheme for distance map.

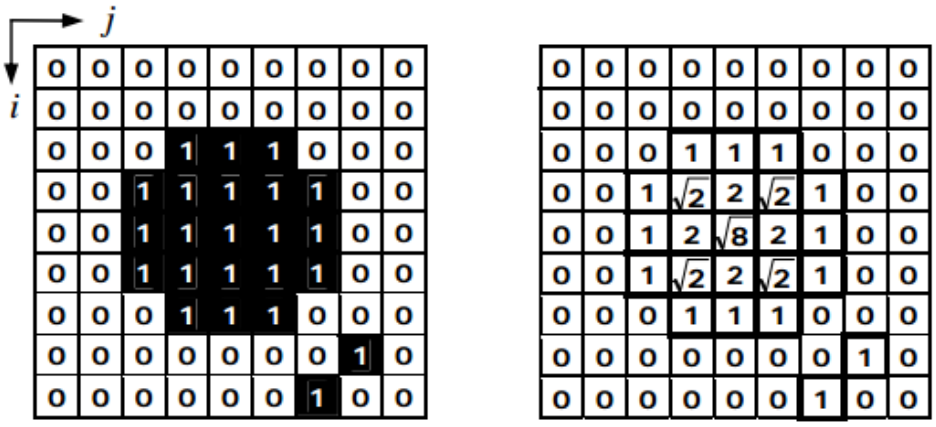

Source – Adapted from Torelli et al. (2010)

As this research deals with fluid concentration inside porous media, it is interesting to exemplify how the distribution algorithm was applied, based on Figure 14. For placing wetting fluid next to the solid interface, the EDT method analyse the desired concentration of wetting fluid and place it into the pixels with a lower value in distance map (since these values are next to the walls). As wetting fluid saturation gets higher, the values of the distance map increase.

To calculate the EDT in this work, the exact approach was preferred to avoid any input errors in subsequent simulations. To set the wetting phase next to the wall and the non-wetting phase in the centre of pores, Exact-EDT available on Scipy Python Library

was utilised. Figure 15 shows an example of how this algorithm place fluids into the sample.

Figure 15 – EDT distribution of phases.

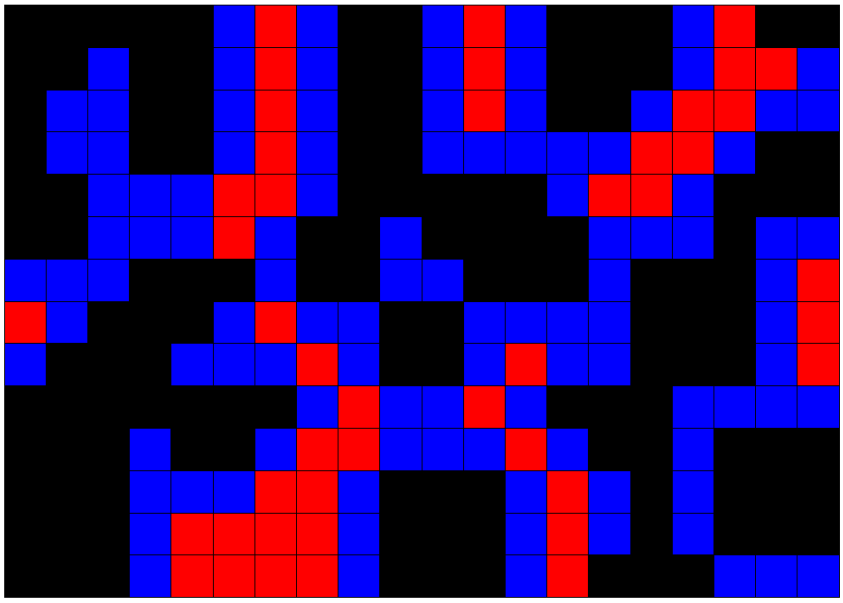

Source – Elaborated by the author

3.2.3 Distribution of phases using Covering Radius Transform

The euclidean distance transformation map also originates another method called Covering radius transform (CRT). This method assigns to each pixel of a given phase, the maximal radius of a sphere (3D porous medium) or circle (2D porous medium) which can cover the pixel under consideration (APOURVARI; ARNS, 2016).

According to Lang et al. (2013), the CRT approach assigns to every pixel which is a porous site, the value of the radius of the largest possible sphere or circle, placed anywhere, that covers that pixel. This results in complete coverage of the fluid space by overlapping spheres with a distribution of radius.

To apply this method in this study, the "largest possible circle" will be assigned to the non-wetting phase. It means, the NWP will be placed in the larger pores and smaller pores will be occupied by WP, which agrees with Rosa, Souza Carvalho, and Xavier (2006) citation of how fluids are placed inside reservoir rocks.

In terms of implementation, the CRT method also uses the EDT algorithm to analyse the pore radius, once smaller pores have lower values in the distance map. Taking Figure 14 as example, the two isolated pores with distance equal to 1 will be filled with WP, otherwise the central pore with values equal to $\{1, \sqrt{2}, 2, \sqrt{8}\}$ will be filled with NWP. Using the hypothetical sample, CRT distribution is shown in Figure 16.

Figure 16 – CRT distribution of phases.

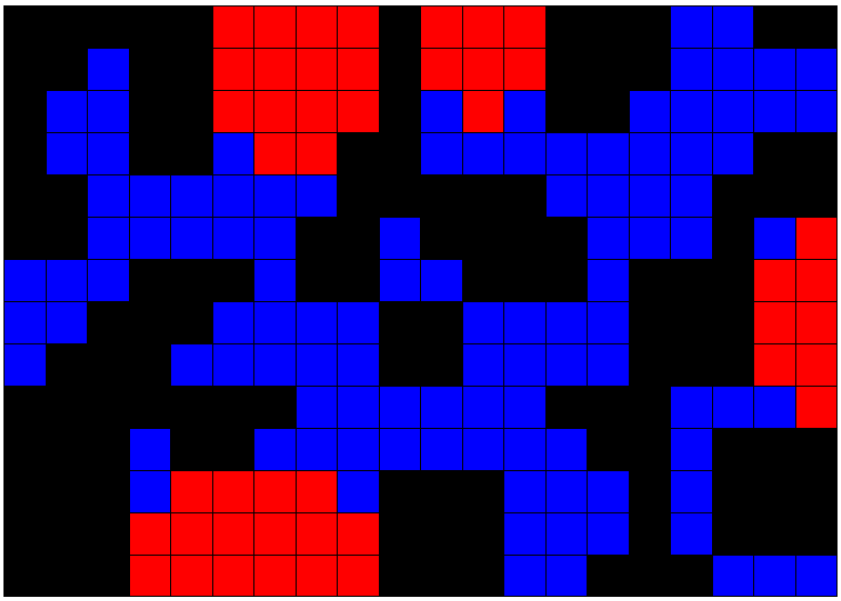

Source – Elaborated by the author

3.2.4 Considerations about different distribution methods

The seek for different approaches intends to achieve a level of detail that mimics reservoir scale conditions. Since numerical simulation deals with a huge variety of properties, it is necessary a good definition in order to obtain reliable results.

To Rosa, Souza Carvalho, and Xavier (2006) during the imbibition process, wetting fluid tends to be placed close to the walls and in pores with smaller sizes. On the other hand, for the drainage process, non-wetting fluid tends to occupy larger pores.

This approach expected by Rosa, Souza Carvalho, and Xavier (2006), either can or cannot happen in random saturation. When focusing in two regions from Figures 18 and 13b, it is possible to see non-wetting phase placed in isolated pores, as seen in Figures 17a and 17a.

It happened because the random algorithm fills the porous media in a way that does not distinguish which pores are open or close. Otherwise, in Figures 15 and 16, these lack of control in filling pores does not appear. For Ghassemi and Pak (2011), random distribution of the phases at the beginning of the LBM simulations causes the obtain of different relative permeabilities even for identical initial saturation levels.

3.2.5 Drainage

As discussed in earlier sections, it is expected to find the wetting phase next to the solid surface or in small pores and, it happens due to the hydrocarbons movement from source rock into reservoir rock in the primary migration.

Before the primary migration, the reservoir rock is filled with connate water that

Figure 17 – Lack of control in random distribution of phases.

(a) Example 1 (b) Example 2

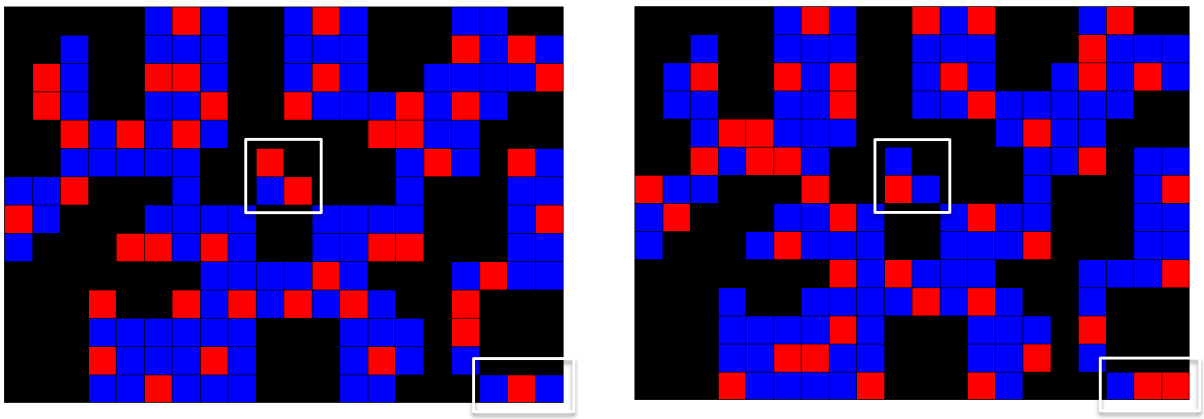

Source – Elaborated by the author

occupies the entire porous space. During the primary migration, the connate water is expelled by the oil, mimicking a drainage process.

As the capillary pressure is higher in the small pores, the connate water remains static in these spots. In the meantime, the superficial tension also tends to keep up the connate water attached to the solid surface. That way, it is expected the oil, in most the cases, occupies the centre of the larger porous spaces while the connate water occupies small pores and creates a thin film over the solid surface.

By reproducing a physical reservoir event, the drainage flooding simulation intends to act as a guider for the random, EDT, and CRT method simulation results.

To set this simulation, the geometry is initially filled with the wetting phase while the non-wetting phase is injected into the sample. During the displacement process, the wetting saturation decreases while the non-wetting saturation increases until the wetting phase achieves the irreducible saturation value.

3.3 SIMULATION SETUP

For the simulations, a set of properties was defined as seen in Table 3.

The contact angle was set as $\theta_r = 0°(w_{wr} = 0)$ between solid-fluid interface, characterising strong wetting condition for the blue fluid to the solid. For the drainage, non-wetting phase also assumed $\theta_r = 0°$. The choice for this contact angle was made to keep all analysis consistent, once the changes on contact angle affect the displacement process and residual saturation.

To analyse the expressiveness of lubrication effect in the results, another set of simulations were conducted to the artificial image, considering $\theta_r \approx 80°$. To implement wettability on a solid wall, the property w_{wr} was controlled by the eq. 28.

For the parameters viscosity, density and interfacial tension the values were

Table 3 – Initialisation properties in lattice units.

(a) Artificial image.

Parameter	**Value**
M	1
τ_s	0.9
α	0.1
β	0.9
θ_r	$0°$
w_{wr}	0
N_c	$\approx 3 \times 10^{-3}$

(b) Berea sandstone.

Parameter	**Value**
M	1
τ_s	0.9
α	0.1
β	0.9
θ_r	$0°$
w_{wr}	0
N_c	$\approx 3 \times 10^{-5}$

Source – Elaborated by the author

defined in lattice units as 0.133, 1 and 0.0667, respectively. This is obtained by setting $\tau_s = 0.9$, $\alpha = 0.1$ $\beta = 0.9$.

As mentioned in the previous section, for all initial distribution methods simulations, a driving force was imposed into the domain to allow the fluid to flow since there was no fluid being injected. The periodic boundary condition is used to keep the fluid circulating into the sample. To maintain the capillary number similar to the entire set of initial saturation, some simulations were repeated, with higher or lower driving force values, in order to achieve an appropriate N_c.

For the drainage flooding simulation, instead of using a mirrored image as Figure 9, it was used a non-mirrored artificial 2D image in order to reduce the computational time cost. To avoid instabilities at the boundaries, 10 columns of buffer layers were added at the inlet and outlet faces and 10 lines of closed layers were added in top and bottom sides as seen in Figure 18. It prevents numerical instabilities due to the null gradient of the material derivative that is imposed at the outlet.

Figure 18 – Added buffer layers for the artificial image in drainage flooding.

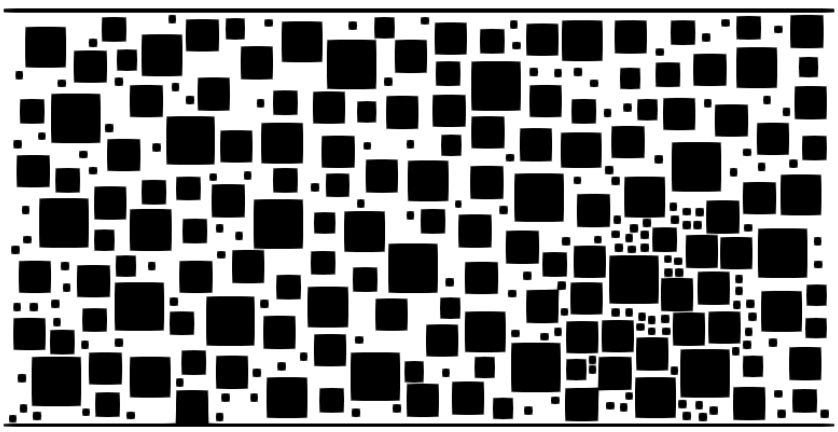

Regarding boundary conditions, the periodic condition was applied by mirroring

the samples and a no-slip boundary condition was imposed in all solid sites via the bounce-back scheme.

For the drainage flooding, the Dirichlet condition was applied at the inlet by fixing the velocity value and, a convective boundary condition (null gradient) was imposed at the outlet.

4 RESULTS AND DISCUSSION

This chapter presents the results of simulations in which the methodology proposed in the last chapter was applied.

The division consists of three different subject sections: the first shows the results that verify the LB multiphase model and its capacity to physically reproduce accurately interfacial phenomena with similarity; the second presents the results for relative permeability curves based on the different initial distribution of phases and; the third presents the relative permeability curves for a three-dimensional image of sandstone rock.

4.1 MODEL VERIFICATION

In order to verify the implementation of the proposed Lattice-Boltzmann Method two tests were conducted: the Young-Laplace law verification, and the viscous coupling during co-current flow in a 2D channel. Both verification simulations are described below.

4.1.1 Young-Laplace law verification

The first simulation tested the the model's ability to relate pressure difference, the radius of curvature, and interfacial tension in the situation that a droplet of one fluid is immersed into another fluid. In other words, this test intends to reproduce the Young-Laplace law.

The Young-Laplace law says that the internal pressure of a drop can be modified both by varying the surface tension σ and by varying the radius of the drop R,

$$\Delta p = \frac{\sigma}{R}. \tag{29}$$

To reproduce computationally this test, a non-wetting phase, shaped like a droplet was placed at the centre of a system filled with a wetting phase. The system was left to relax until a steady-state circle of non-wetting fluid was achieved. Then, the pressure difference between fluids and the droplet diameter was measured.

The results of the tests, considering different initial droplet sizes, are presented in Figure 19. The dots in the image represent the simulated results while the line represents the analytical solution.

Figure 19 – Comparison between simulated results and analytical solution.

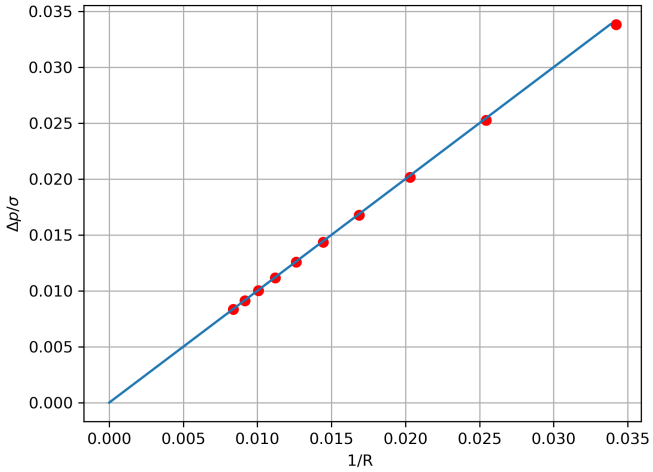

Source – Elaborated by the author

The results of the tests considering different initial droplet sizes and different α can be seen in Figure 20. The pressure difference inside and outside the droplet is proportional to the inverse droplet radius for all α values as expected by Young-Laplace law. The slope of fitted lines increased for increasing α, in accordance to equation 23.

Figure 20 – Young-Laplace law verification for different surface tension values.

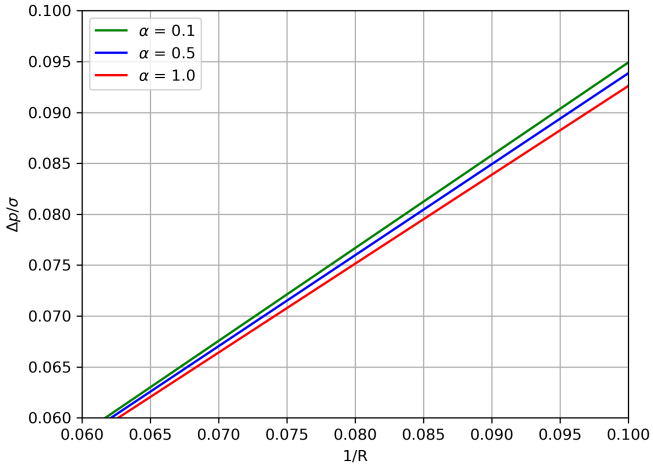

Source – Elaborated by the author

4.1.2 Viscous coupling during co-current flow in a 2D channel

The second test intended to calculate the relative permeabilities of both phases as a function of the wetting saturation and the viscosity ratio.

As in immiscible two-phase flow in porous media the wetting phase typically covers the surface of the solid (ROSA; SOUZA CARVALHO; XAVIER, 2006) where it

flows in the form of films, the wetting phase was placed next to the slit walls while the non-wetting phase was placed in the centre, as seen in Figure 21.

Figure 21 – Schematic of immiscible two phase flow between parallel plates.

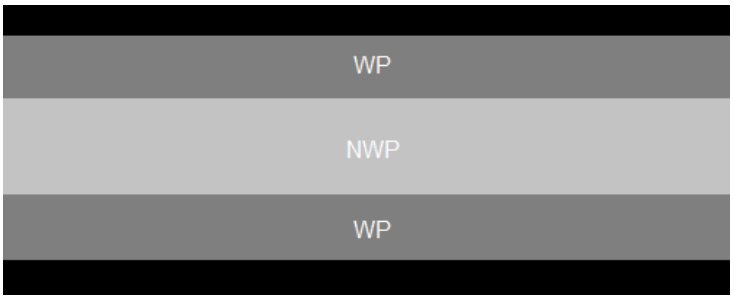

Source – Elaborated by the author

The length of the plates is infinite in the direction of the flow and periodic boundary conditions apply at the sides vertical to the direction of the flow. No-slip boundary conditions apply at the plates. Both fluids have the same kinematic viscosity but different densities which produces different dynamic viscosities. The saturation of fluids varies from 0 to 1 and, for each saturation, the simulation is conducted until steady-state.

The relative permeability of each phase is defined as a function of the wetting saturation (YIOTIS et al., 2007),

$$k_{r,w} = \frac{1}{2} S_w^2 (3 - S_w), \tag{30}$$

$$k_{r,nw} = (1 - S_w) \left[\frac{3}{2} M + (1 - S_w)^2 \left(1 - \frac{3}{2} M \right) \right]. \tag{31}$$

Equation 30 shows that the relative permeability of the wetting phase between two parallel plates is a function of the wetting saturation wetting saturation only. However, Equation 31 shows the relative permeability of the non-wetting phase is a function of both the wetting saturation and the viscosity ratio.

Figure 22 shows the comparison between the analytical solution and the LB simulation. It is possible to see, although both phases are subject to the same pressure gradient, the non-wetting phase accelerates faster than the wetting phase because it is less viscous. The relative permeability calculated with the LB model is in very good agreement with the analytical solution.

Figure 22 – Calculated relative permeabilities for the wetting and non-wetting phases in a slit when M = 0.91

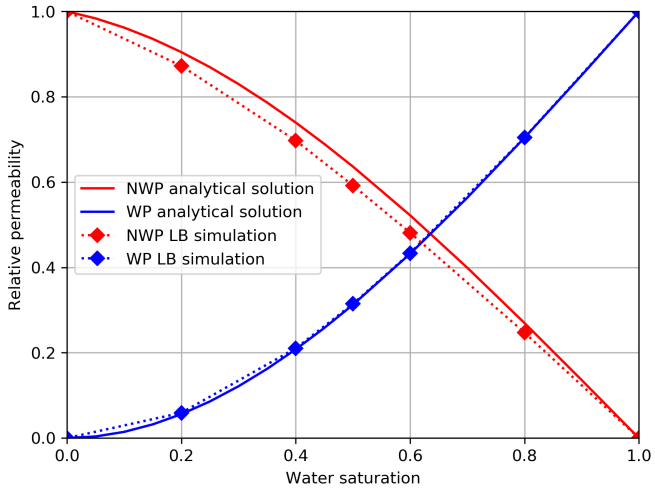

Source – Elaborated by the author

4.2 ARTIFICIAL IMAGE

4.2.1 Initialisation of Distribution Methods

As exposed in the previous chapter, three different methods were used to distribute fluids into the sample. For the random, EDT, and CRT distributions, the abbreviations RAN, EDT and CRT will be used in the tables in order to expose the results.

For the artificial image, the initial distribution of phases for each method can be seen in Figure 23. These images were generated for an initial saturation of WP equal to 40%. The blue is assigned for WP and red is assigned for NWP. This saturation was chosen because it is related to other results, which will be presented later in the text.

Figure 23 – Initial distribution of fluids for artificial image for $S_w = 0.4$.

(a) Random distribution

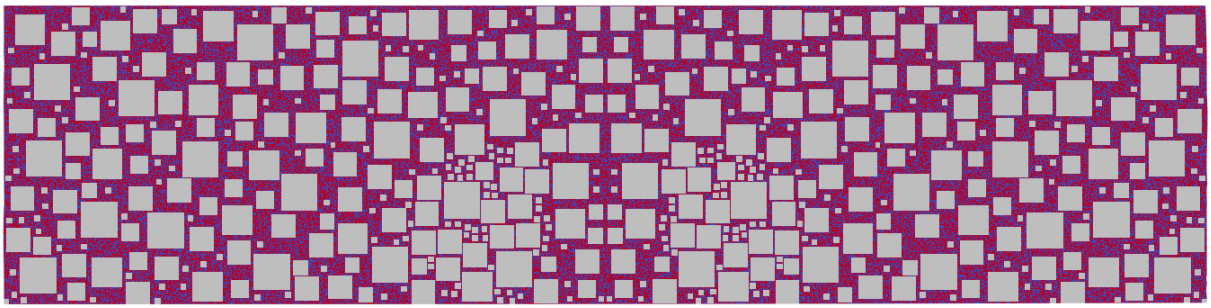

(b) EDT distribution

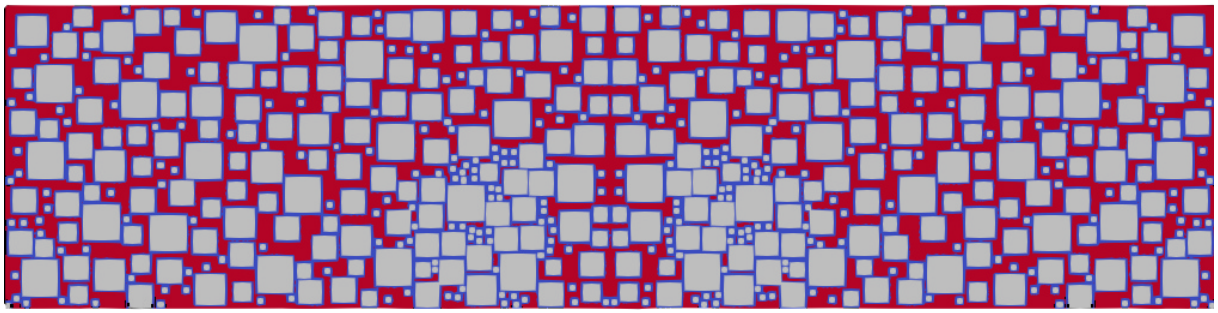

(c) CRT distribution

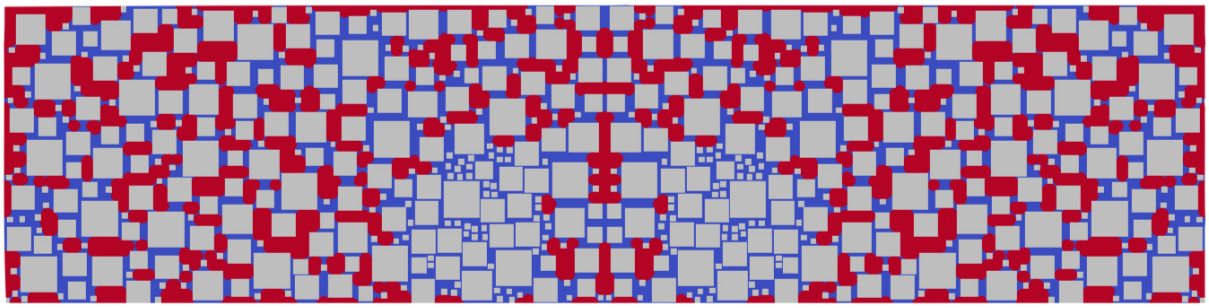

From Figure 23a, it is possible to see that for the random method, the colors are aleatorily distributed, and it is not easy to distinguish which is the red or the blue phase. Differently, for EDT and CRT methods, Figures 23b and 23c, the red and the blue phases have a clear delimitation.

After setting the initial distribution of phases, respecting a determined saturation level, to obtain the relative permeability curves for steady-state flow, it is necessary to carry the simulation until the flow in porous space does not exhibit an appreciable change. For each saturation, two points are obtained: one for WP relative permeability and another for NWP relative permeability. It means the initial saturation of the wetting phase must range from 100% (1) to 0% (0) to obtain an entire relative permeability curve.

In our simulations, the wetting phase initial saturation ranged from 1 to 0 with intervals of 0.1. For each saturation, the simulation was carried out until steady-steady flow was achieved and then, the relative permeability for each phase was calculated

based on equation 6. The absolute permeability was obtained when the rock was saturated only by one phase since this property is only related to the porous medium.

The criteria for steady-steady flow achievement is the equilibrium of phases displacement, in which, the relative permeability does not change appreciably in time. Figure 24a shows the convergence of absolute permeability in time and Figure 24b the convergence of relative permeability of phases for $S_w = 0.4$ in the CRT method. It is possible to see some oscillation in relative permeability values due to the reorganisation of fluids, however, the relative permeability remained in a stability plateau.

Figure 24 – Measurement of the permeabilities in steady-state flow.

(a) Absolute permeability

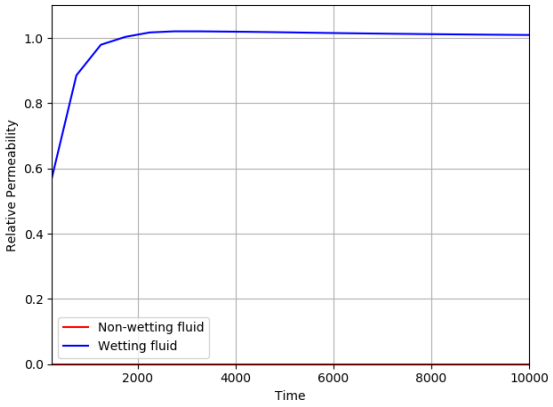

(b) Relative permeability

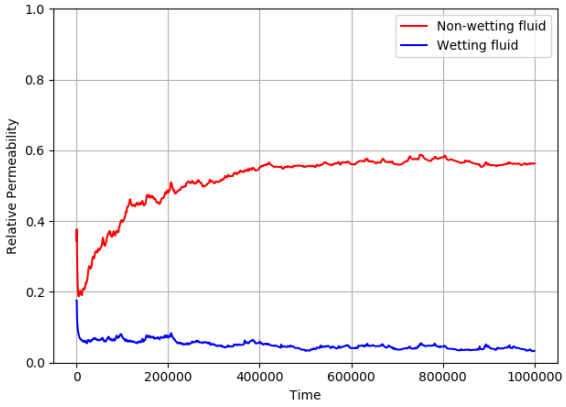

Source – Elaborated by the author

The relative permeability curves for all WP and NWP can be seen in Figure 25. Red curves represent the non-wetting phase and blue curves represent the wetting phase.

Figure 25 – Relative permeability curves for artificial image.

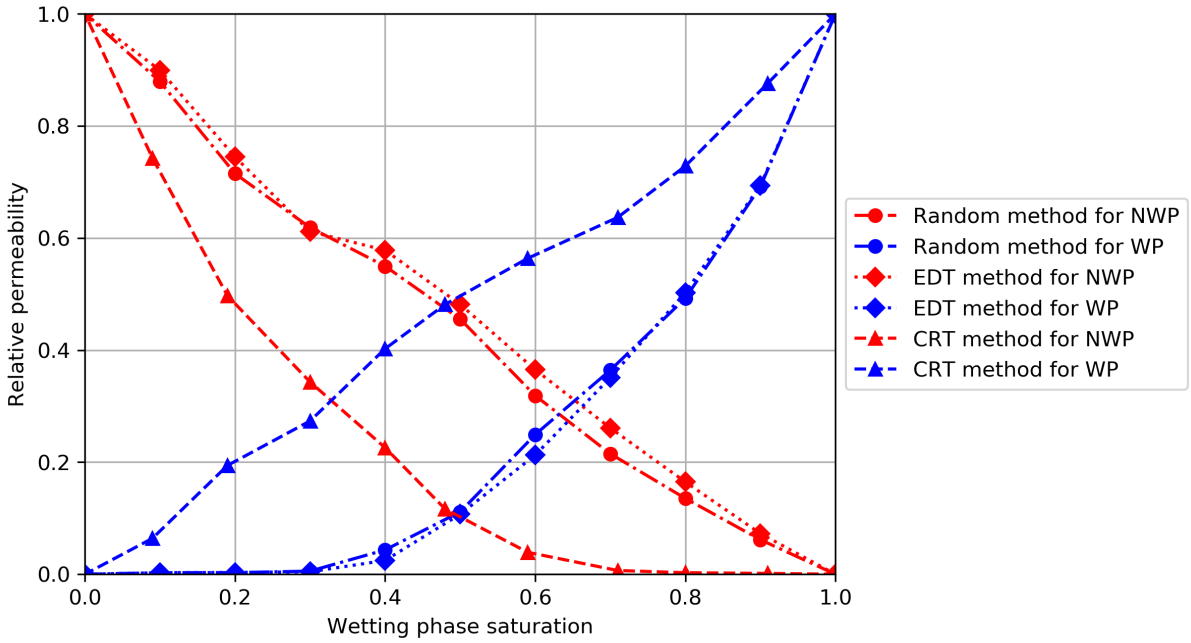

Source – Elaborated by the author

By visual inspection, in Figure 25 it is possible to see that the relative permeability curves for EDT and random method resemble each other for both NWP and WP. Otherwise, the relative permeability for CRT method has a significant difference compared to the others, since the WP curve has higher and the NWP has lower relative permeability values.

According to Dou and Zhou (2013) and Huang, Sukop, and Lu (2015), the relative permeability depends on the final distribution of phases, which depends on the initial distribution of phases. Until now, the initial distribution was discussed. The following analysis will be focused on the final distribution of phases. Figure 26 brings the comparison for the final fluid placement for the methods, equally for $S_w = 0.4$.

Figure 26 – Distribution of fluids under steady-state flow conditions for artificial image.

(a) Random distribution

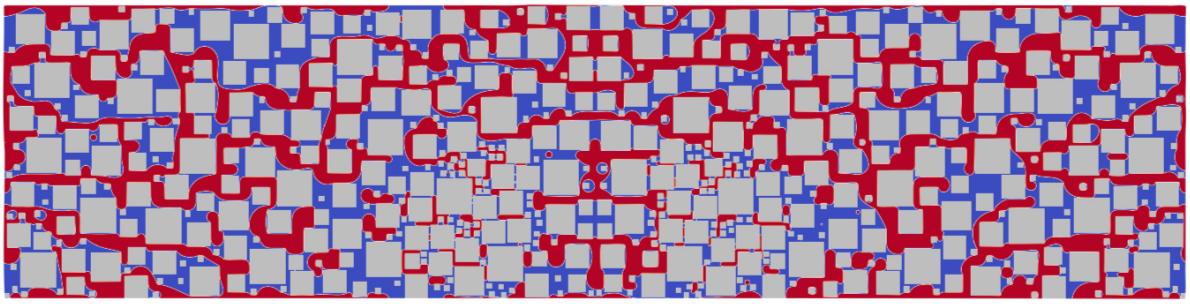

(b) EDT distribution

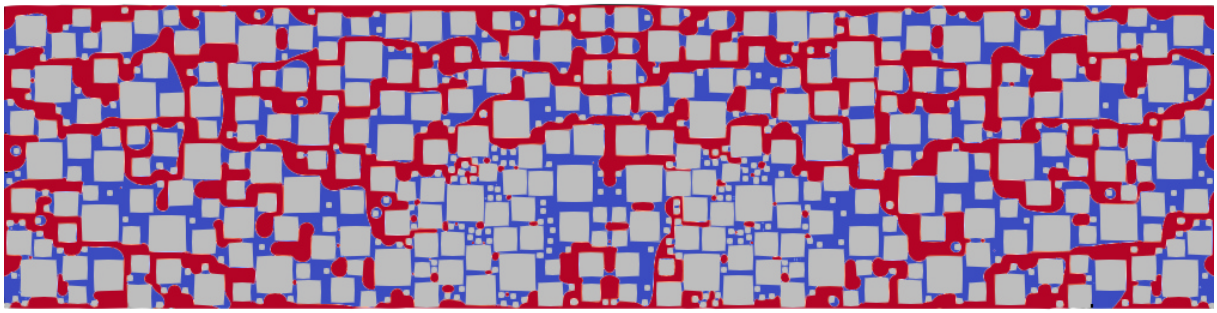

(c) CRT distribution

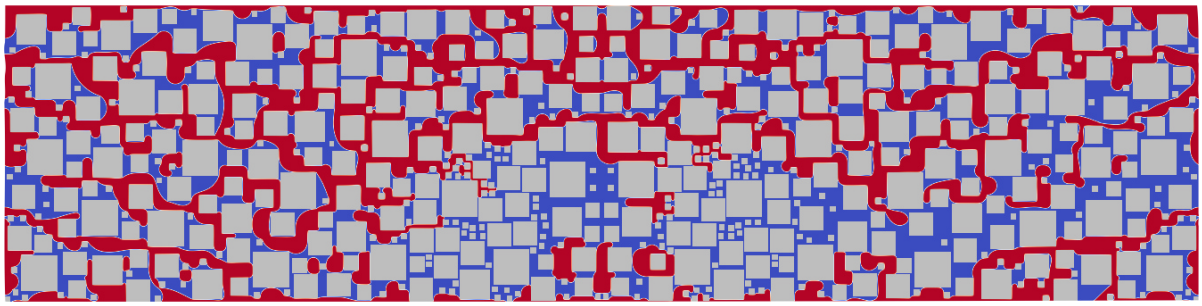

From Figure 26, it is possible to see that the four images have different final distributions due to the initial distribution differences, which is in agreement with Dou and Zhou (2013) and Huang, Sukop, and Lu (2015). Some of the differences can be easily spotted:

i. Random method: Considerable quantity of NWP entrapped into the microporous region and some NWP disconnection in the macroporous region (Figure 26a);

ii. EDT method: NWP regions disconnected from the main flow to the left side of the image, right before the microporous region. In the microporosity, some NWP appears entrapped (Figure 26b);

iii. CRT method: Well-connected region of WP after the microporous region. Less NWP entrapped in microporosity. (Figure 26c).

To quantify the size of the gap for the methods, Table 4 brings an analysis of the absolute difference of NWP relative permeability for each combination of methods, in terms of percentage. Column S_w shows the initial saturation in terms of WP; columns RAN, EDT and CRT present the relative permeability values for NWP and; columns |RAN - EDT|, |RAN - CRT| and |EDT - CRT| show the absolute difference for these combinations.

This analysis is being presented for the non-wetting phase because the non-wetting phase is usually the least connected phase (RAMSTAD; IDOWU; NARDI, 2011), is affected by snap-off and fingerings formation (SCHLÜTER et al., 2016) and its topology is difficult to analyse (ALPAK; BERG; ZACHAROUDIOU, 2018). The absolute differences for WP relative permeability curves can be found in Appendix A.

Table 4 – Relative permeability absolute differences of NWP regarding initial distribution methods.

S_w	**RAN**	**EDT**	**CRT**	**|RAN-EDT|[%]**	**|RAN-CRT|[%]**	**|EDT-CRT|[%]**
1.0	0.0000	0.0000	0.0000	0.00	0.00	0.00
0.9	0.0616	0.0727	0.0016	1.11	6.00	7.11
0.8	0.1354	0.1648	0.0028	2.94	13.26	16.20
0.7	0.2151	0.2610	0.0084	4.59	20.67	25.26
0.6	0.3188	0.3651	0.0370	4.63	28.18	32.81
0.5	0.4554	0.4816	0.0934	2.62	36.20	38.82
0.4	0.5498	0.5783	0.2259	2.85	32.39	35.24
0.3	0.6186	0.6117	0.3431	0.69	27.55	26.86
0.2	0.715	0.7448	0.4893	2.98	22.57	25.55
0.1	0.8792	0.8995	0.7229	2.03	15.63	17.66
0.0	1.0000	1.0000	1.0000	0.00	0.00	0.00

Source – Elaborated by the author

In Table 4, it is possible to see the larger gaps occur between random and CRT or EDT and CRT methods, with higher differences for intermediate saturations of the wetting phase. For the S_w of 50% and 40%, the differences ranged from 32.39% to 38.82%. Otherwise, for the S_w of 90%, 80%, and 10%, lower gaps were observed, ranging from 6% to 17.66%. Therefore, if comparing the values for random and EDT method, the gaps were under 5% for all the saturation range.

The possible reason for lower gaps that appeared at the end of the curves may be related to the connection of the phases. It means, for high-end values such as 90% or 10%, either the wetting or the non-wetting phase will be dominant in the flow and, the other phase will be entrapped and will remain static (DOU; ZHOU, 2013). Otherwise, for an intermediate saturation level, the connectivity of the phases may not be that clear, in terms of the dominance of one phase over another and, that can be one of the reasons

for the higher gaps. Therefore, by comparing random and EDT methods, the absolute difference is relatively the same for intermediate or high-end saturation values.

Considering the debate of the absence of control in filling pores for the random method, the next section brings an analysis regarding the expressiveness of the uncertainties in relative permeability.

4.2.2 Random Method Uncertainty

As some authors such as Jiang and Tsuji (2016) and Alpak, Berg, and Zacharoudiou (2018) debate the lack of control of random method in filling the porous medium can interfere in phase connectivity and relative permeability. To figure out the expressiveness of changes in relative permeability regarding the random method, it was conducted a set of simulations considering different initial phase distributions by the application of the random method.

The chosen saturation for these simulations was 30% and 70% of the wetting phase, since these numbers were in between of higher and lower gaps. To proceed with the simulations, the random method was applied five times for 30% saturation and the other five times for 70% saturation. Simulations were carried out until steady-state flow was achieved and then relative permeability was measured. Initial parameters were kept identical. Table 5a brings results for 30% of WP and, Table 6a for 70% of WP.

The formulation used to calculate the expanded uncertainty associated with these measurements was based on Albertazzi and Souza (2008). The t-Student coefficient was considered equal to 2.7764 for the confidence interval level of 95%. Table 5b shows the results for 30% of WP and Table 6b for 70% of WP. Considering there is only one uncertainty source, the combined uncertainty is, in fact, the standard deviation of the measurements.

Table 5 – Uncertainty analysis for random method considering 30% of wetting phase.

(a) Relative permeability for each application of the random method

Number	**NWP**	**WP**
1	0.6262	0.0047
2	0.6452	0.0085
3	0.5955	0.0078
4	0.6341	0.0081
5	0.6187	0.0046

(b) Uncertainty analysis

	NWP	**WP**
$\overline{k_{ri}}$	0.6240	0.0067
u	0.0187	0.0019
U	0.0518	0.0053

Source – Elaborated by the author

It is possible to see that the expanded uncertainty in Table 5b is 5.18% for NWP and lower than 1% to the WP. It means, the relative permeability varies less than 5.18%

Table 6 – Uncertainty analysis for random method considering 70% of wetting phase.

(a) Relative permeability for each application of the random method.

Number	NWP	WP
1	0.2568	0.3439
2	0.2308	0.3337
3	0.2058	0.3893
4	0.2045	0.3836
5	0.2044	0.3323

(b) Uncertainty analysis.

	NWP	WP
$\overline{k_{ri}}$	0.2205	0.3557
u	0.0230	0.0277
U	0.0645	0.0770

Source – Elaborated by the author

regarding the initial distribution of phases for random method, for an initial saturation of 30%. For Table 6b the expanded uncertainty is 6.45% for NWP and 7.70% to the WP.

This variation in random distribution was also observed by Ghassemi and Pak (2011). In their work, the authors pointed out that the use of random distribution at the beginning of the LBM simulations caused the obtaining of different relative permeabilities values even for the identical initial degrees of saturation.

This analysis brings to light that, by considering the lack of control in filling pores, the absolute difference between random and EDT methods remains below 5%. Therefore, for random and CRT methods, the absolute difference varies from 25.24% to 30.21%.

4.2.3 Drainage Flooding (DRE)

Since the relative permeability curves for the initial distribution methods were not equal, a drainage flooding simulation was conducted in order to understand which of the curves could be the most consistent, with what is likely physically to be observed in reservoir conditions. According to Alpak, Berg, and Zacharoudiou (2018), the drainage closely mimics the steady-state flow for relative permeability experiments.

In the drainage flooding, instead of having an initial distribution of phases, the porous medium was saturated by only the wetting phase. The non-wetting phase was injected with constant velocity, displacing the WP, until the system reaches equilibrium. After having the final distribution of phases, the domain was mirrored in the flow direction and the relative permeability was calculated by the equation 6.

The relative permeabilities obtained for the drainage can be seen in Figure 27, plotted above Figure 25. The final distribution of phases for the drainage flooding can be seen in Figure 28.

From the Figure 27, it is possible to see, the equilibrium saturation for drainage

Figure 27 – Relative permeability of drainage flooding for artificial image.

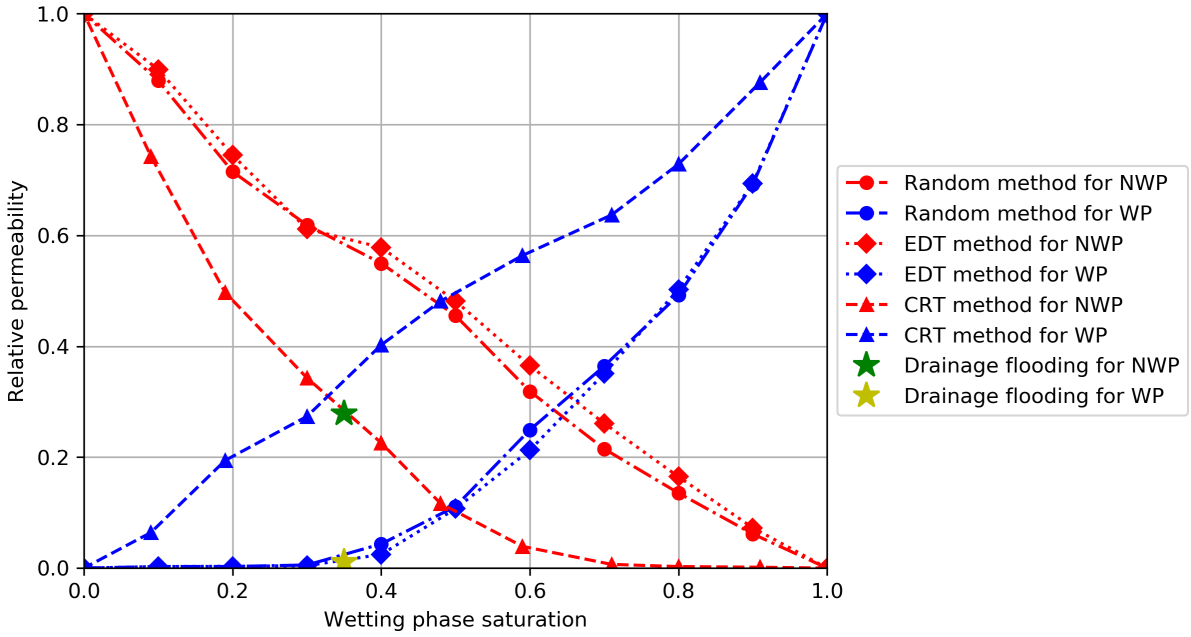

Source – Elaborated by the author

Figure 28 – Drainage flooding under steady-state flow conditions for artificial image.

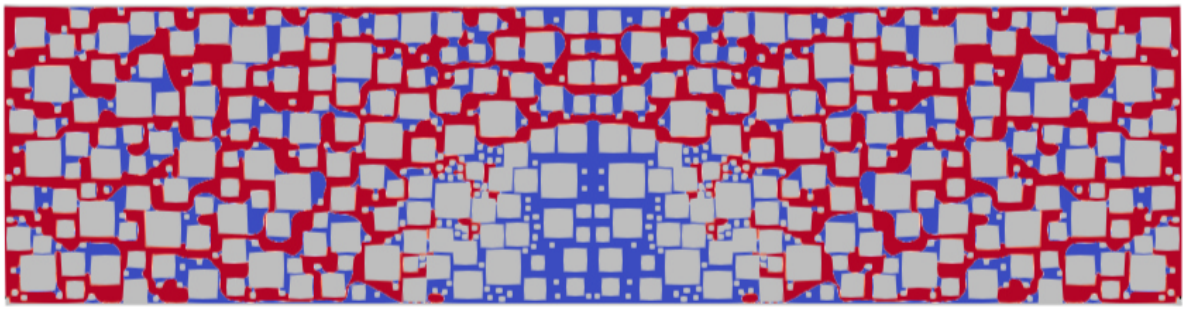

Source – Elaborated by the author

occurred for $S_w = 0.35$. At this saturation, the relative permeability for NWP is closer to the value for CRT method. On the other hand, the relative permeability for WP is closer to the value for EDT and random methods.

According to Raeini, Blunt, and Bikeljic (2014) and Chang et al. (2008), for drainage, the wetting phase at the end of simulation usually presents a very low and close to zero relative permeability. It means, the WP is almost motionless since the equilibrium was reached under steady-state fluid flow. In our results, this result was observed for the random and EDT methods, but not for the CRT method.

To measure the gap between the relative permeability for the initial distribution methods regarding the drainage, the absolute difference was applied, for the drainage saturation value, as seen in Table 7. The first row is assigned for NWP relative permeability. The second row is assigned for WP relative permeability.

Table 7 – Absolute difference of relative permeability for drainage and initialisation methods.

RAN	**EDT**	**CRT**	**DRE**	**|DRE-RAN|[%]**	**|DRE-EDT|[%]**	**|DRE-CRT|[%]**
0.5842	0.5583	0.2850	0.2789	30.53	27.94	0.56
0.0218	0.0269	0.2010	0.0138	0.80	1.31	18.75

Source – Elaborated by the author

The WP relative permeability for the CRT method is considerably higher, having an absolute difference of 18.75% regarding the drainage. The possible reason is the WP is distributed in a way for the CRT method that allows the flow, even for lower saturation levels.

Similarly, these characteristics for the CRT method were observed for all the saturation levels in the WP relative permeability curve, indicating an overprediction regarding the method. The absolute differences for WP relative permeability curve for random, EDT, and CRT methods can be found in Appendix A.

To link the initial distribution simulations with the drainage flooding, the capillary number was kept resembling, as seen in Table 8. It was considered in order to bring cohesion to the analysis since the capillary number affects the relative permeability. According to Zhao et al. (2017), with the increase of capillary number, the relative permeability for the NWP increases significantly while for the WP changes little, for strongly wetting porous medium.

In Table 8, it is possible to see that the capillary number is not exactly the same for random, EDT, and CRT methods. It happens because these simulations do not control velocity, but pressure difference and the capillary number are defined by the velocity.

Table 8 – Capillary number for simulations.

RAN	**EDT**	**CRT**	**DRAINAGE**
0.0035	0.0033	0.0036	0.0034

Source – Elaborated by the author

Considering the final distribution of phases for random, EDT, CRT, and drainage (Figures 26 and 28) presented the existence of the fluid placement differences, the next section will analyse the connectivity of phases.

4.2.4 Phases Connectivity Analysis

According to Chang et al. (2008), the degree of connectivity of the phases could influence the relative permeability values. By considering it, this analysis intends to quantify the amount and the dimension of the NWP and WP elements in the steady-state flow distribution.

In order to do this, the final distribution states were loaded on Fiji Software (SCHINDELIN et al., 2012) and the plugin Find Connected Regions, released by Longair (2006) was applied to quantify the fluid connectivity. The results are displayed in Figure 29. The connected regions for NWP are highlighted in different colors.

From Figure 29d, it is possible to see that the non-wetting phase in drainage flooding is well-connected and it fills almost the entire region of the macroporosity. It goes along with Bultreys et al. (2016) work, that pointed out, when performing a drainage simulation, the macroporosity is completely drained first, followed by the microporosity.

The random, EDT, and CRT methods also presented great connectivity for NWP in the macroporous region, but not exhibiting the same phase connectivity as drainage, through the porous space.

Regarding the connectivity in the microporous region, for the random method, in Figure 29a, the microporosity is marked by a high quantity of NWP entrapped, in droplets with diverse sizes. It occurred due to the initial distribution that placed NWP into a region where, in experimental or reservoir conditions, NWP would not be encountered. Also, in the microporous region, the mobility of the NWP is small, not contributing significantly to the fluid flow. Furthermore, the macroporous region on the left and on the right side of microporosity also presented disconnected areas of NWP. In addition, in these regions, the sizes of connections were larger than the observed in the micropores.

For the EDT method, in Figure 29b, the microporous region had less fluid entrapped than the random method. The small droplets that appeared in this region were also products of the initial distribution and did not present mobility during the simulation. Since the WP was placed next to the walls, the larger porous (in the microporous region) were saturated by NWP, which remained entrapped during the simulation. Similar to the random method, the region on the right and left sides of the microporosity of the EDT method also presented connected regions with larger sizes. It may happen because there is a microporous area in the middle of the domain, which acts as a barrier, impairing the fluid connection.

For the CRT method, in Figure 29c, the microporous region presented the lowest quantity of NWP entrapped, regarding the random and EDT methods. Regarding the mobility, during the simulation, even switching a bit from the original position, the NWP remained enclosed. The region to the left side of microporosity for the CRT method resembles random and EDT methods. Otherwise, to the right side, it is possible to see a free path for wetting fluid.

Figure 29 – Flow connectivity for NWP according final distributions.

(a) Random distribution

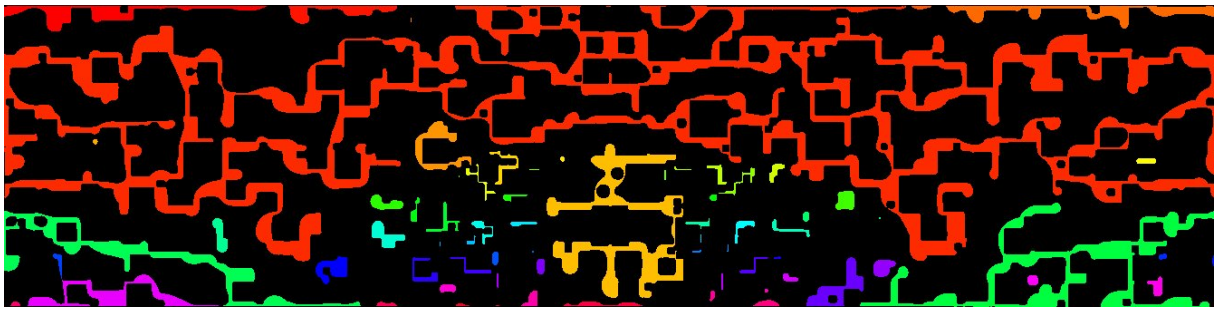

(b) EDT distribution

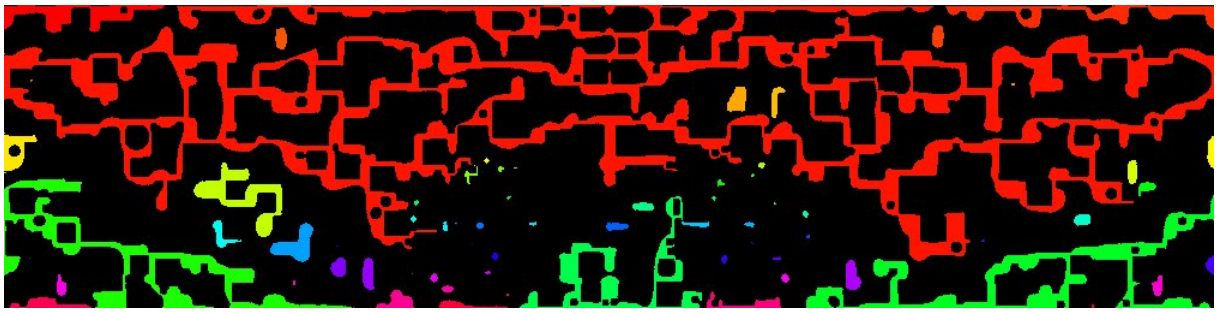

(c) CRT distribution

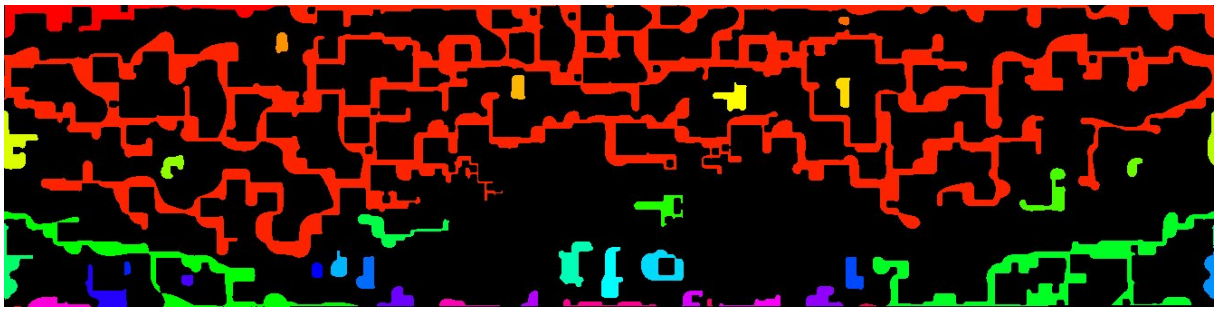

(d) Drainage flooding

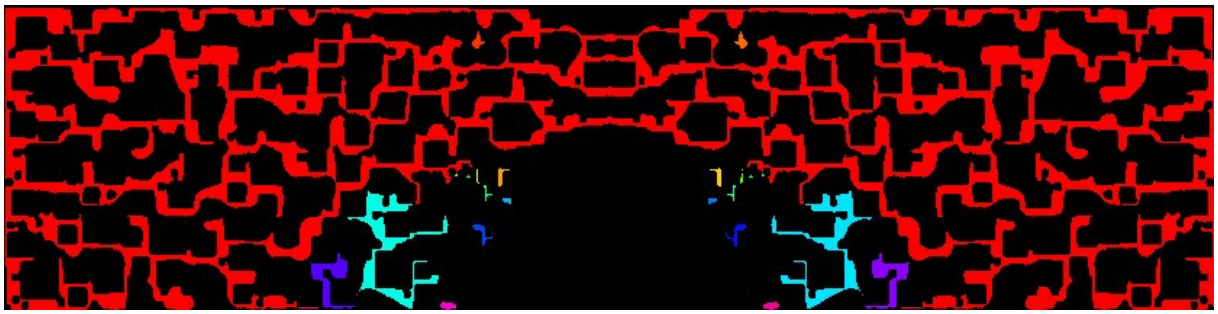

Source – Elaborated by the author

As verified by Figure 29, the NWP is well-connected in macroporous region for all the methods for $S_w = 0.4$. Being so, it was expected to find out some evidence related to the microporous region. Therefore, each method has its own distribution into the microporosity. For instance, for random to EDT methods, the quantity of entrapped NWP gets lower in the microporous region and, nevertheless, the relative permeability curve between the methods still resembles.

This verification may be evidence that the microporosity does not represent a strong contribution to the flow rates and to the relative permeability. It goes along to the study of Oliveira et al. (2019), which found out the relationship between relative permeability and microporosity is only stronger in porous systems dominated by the microporosity. For macropores dominated systems or combined micropores and macropores systems, the relative permeability is dominated by the macroporous region.

According to Bultreys et al. (2016), when performing a drainage flooding in rocks with a dual-porosity, the relative permeability depends greatly on the connectivity structure into the macropores. When a significant part of the macropores is connected to each other the flow through microporosity is likely small compared to the total flow and does not represent a strong contribution to the flow rates, resulting in very small differences in the relative permeability curves.

In order to avoid only visual-based findings, the data obtained for non-wetting phase connection on Fiji Software was plotted as a histogram, as seen in Figure 30. The histogram was based on the equivalent diameter, given by,

$$D_e = \sqrt{\frac{4A}{\pi}}, \tag{32}$$

where A is the total number of fluid phase sites.

From Figure 30, it is possible to see the random and EDT methods presented the higher quantities of elements with higher and lower equivalent diameters. Differently, the CRT method presented an intermediate number of elements and the drainage, the number of elements was the lowerest, compared to the other methods.

It may be strong evidence that the higher values for NWP relative permeabilities, observed in random and EDT methods, may be related to the quantity of high size elements in the fluid flow which incurs in higher phase connectivity.

For the wetting phase elements, the data obtained can be seen in the histogram from Figure 31.

Figure 30 – Histogram of equivalent diameter for non-wetting phase.

(a) Random distribution

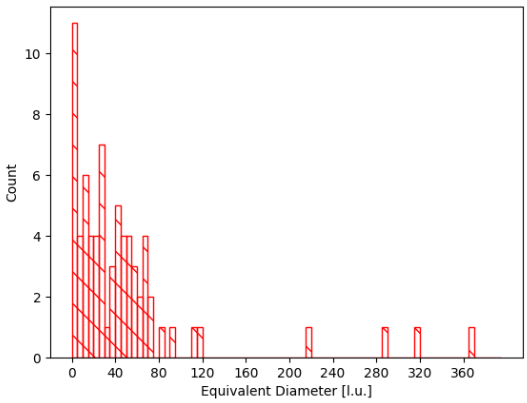

(b) EDT distribution

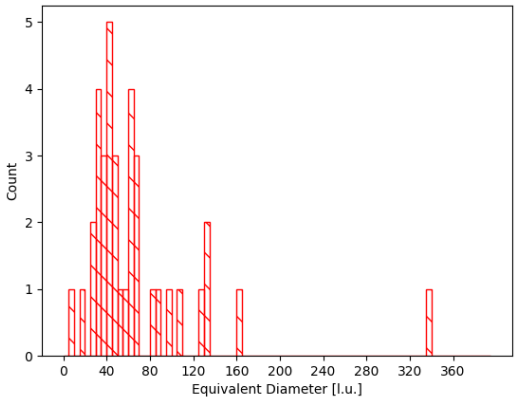

(c) CRT distribution

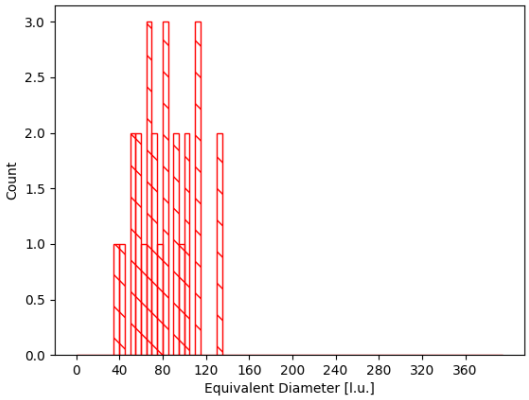

(d) Drainage flooding

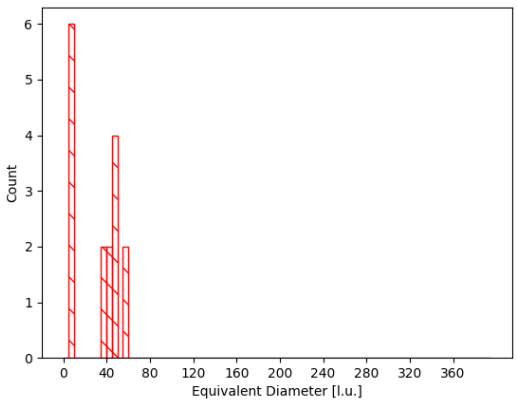

Source – Elaborated by the author

Figure 31 – Histogram of equivalent diameter for wetting phase.

(a) Random distribution

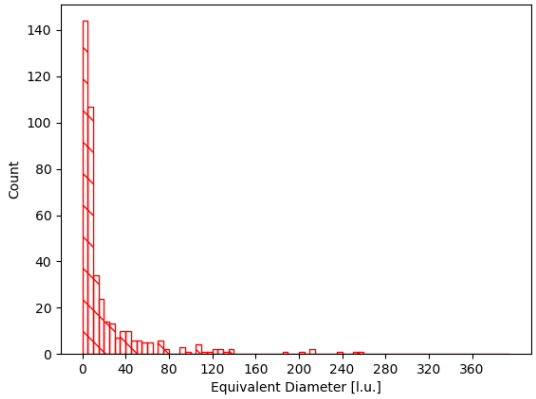

(b) EDT distribution

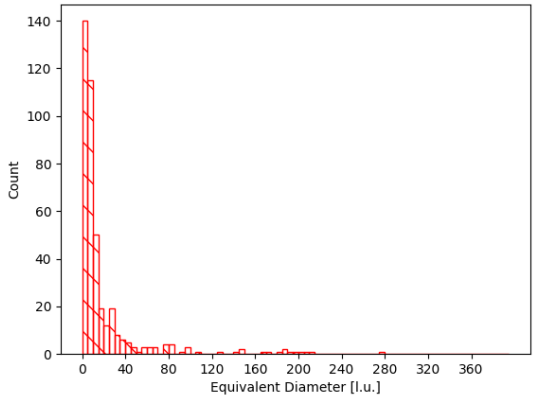

(c) CRT distribution

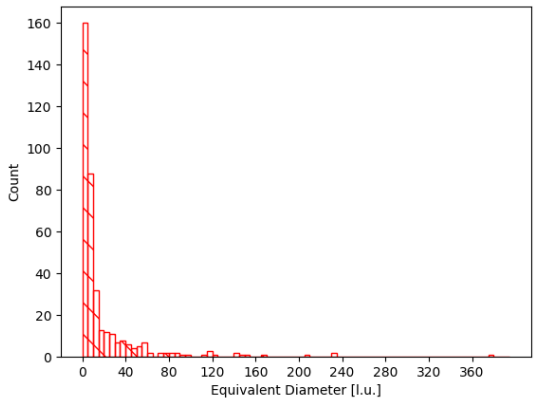

(d) Drainage flooding

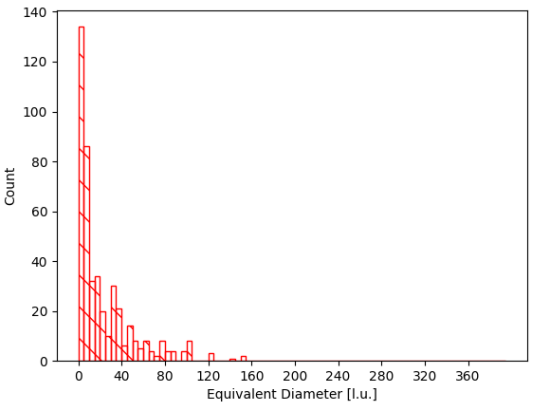

Source – Elaborated by the author

From Figure 31, it is possible to see the random, EDT, and CRT methods resemble one another in terms of the distribution of elements. The three methods presented higher values for small size elements. Equally, the drainage flooding presented a high number for small size elements.

However, for the CRT method, it is possible to verify there is one element with a high value for equivalent diameter ($D_e > 360\ lu$). By analysing Figure 32b, it is possible to see a higher size WP element in the right side of the image, gathering the macro and microporosity, that may be causing the over connection. Otherwise, by analysing the Figure 32a, for the random method, the WP seemed to have more adherence to the walls, not presenting higher size elements of connectivity.

This is evidence that for the CRT method, there is WP flow even for conditions for which no fluid flow was expected. This over connection of the wetting phase may be a possible explanation for the differences seen in WP relative permeability curve for the CRT method when compared with random and EDT methods.

Figure 32 – Flow connectivity for WP according final distributions.

(a) Random distribution

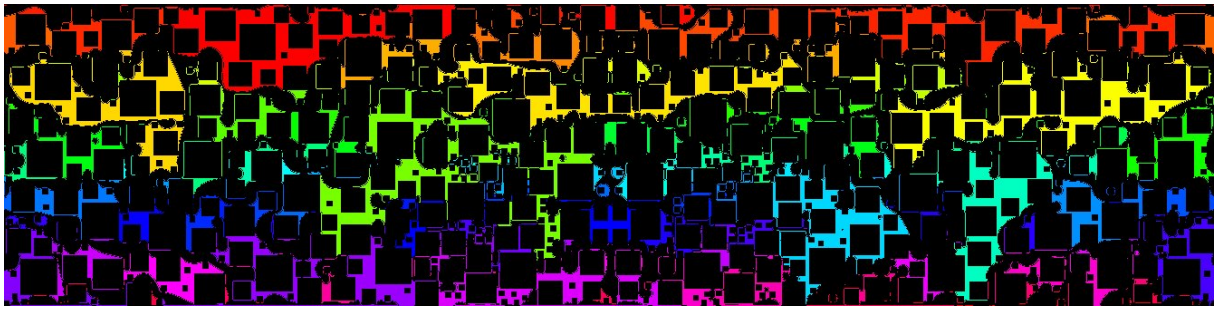

(b) CRT distribution

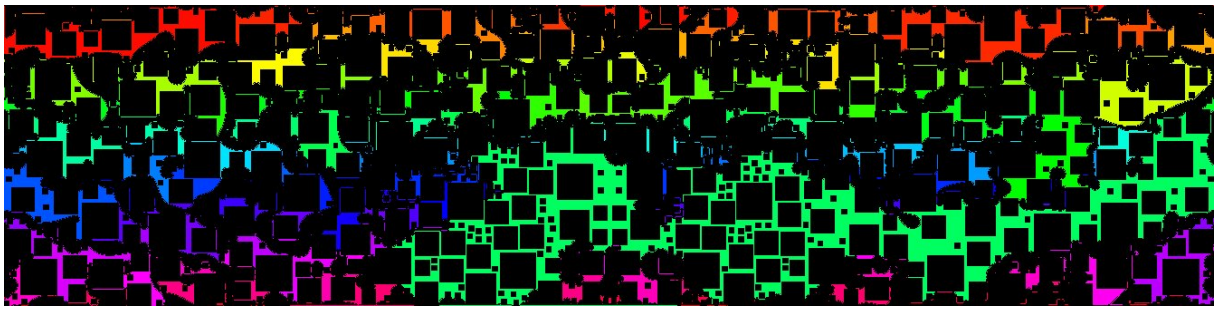

Source – Elaborated by the author

As seen in the final distribution of phases, Figures 26 and 28, in the drainage flooding and in the CRT method, the microporous region is mostly filled with WP, leaving less available quantity to the macropores. Otherwise, in the random method and EDT methods, as the NWP is trapped into the micropores, more WP is available to the macropores.

For a strongly-wetting sample, like the one we simulated, if more WP is available in the macropores, it means more WP fluid will adhere to the walls creating a coat that accelerates the flow increasing NWP relative permeability. This is called the lubrication effect.

According to Dou and Zhou (2013) and Ramstad, Idowu, and Nardi (2011), for a strongly wet medium, most part of the channels are covered by wetting phase. The non-wetting phase flows in the centre of the channel. Thus, if the solid is coated by wetting a film, the non-wetting phase may be able to move faster through a channel than if the film was missing.

As the random and EDT methods had a higher number of NWP elements and more WP phase in the macropores, it is expected the NWP relative permeability presented higher values due to the lubrication effect.

For the CRT method and the drainage, the final distribution indicated that less NWP is entrapped into the micropores, which means more WP remained constricted into this area. With less WP in the macropores, the lubrication effect is less intense. Also, the number of NWP elements in the connectivity analysis, was lower for CRT and drainage resulting in lower relative permeability values.

4.2.5 Effect of Wettability

To verify the expressiveness of the lubrication effect in the connectivity, another set of simulations were performed considering the same initial distribution methods. The only change was regarding the contact angle that became $\theta_r \approx 80^\circ$ ($w_{wr} = 0.4$), a partially wetting condition, instead of $\theta_r = 0^\circ$ ($w_{wr} = 0.0$), a strongly wetting condition. Figure 33 shows the results for relative permeability curves.

Figure 33 – Relative permeability curves for artificial image with lower contact angle.

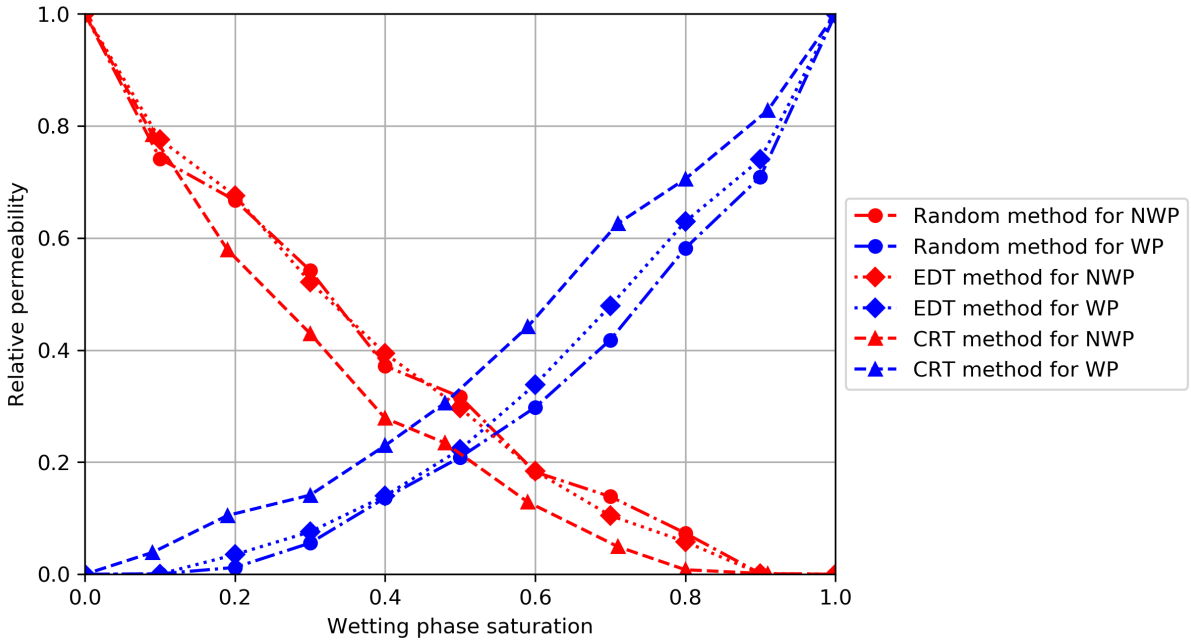

Source – Elaborated by the author

From Figure 33, it is possible to see the random and EDT methods had similar values for WP and NWP relative permeabilities. On the other hand, the CRT method presented a lower NWP relative permeability and a higher WP relative permeability, regarding the other two methods. Nevertheless, the gap between the curves was smaller than observed for the strongly wetting porous medium.

The values for the absolute differences between the relative permeability curves can be seen in Appendix B. The higher differences were found for intermediate saturation levels. The biggest difference occurred between random and CRT methods and EDT and CRT methods, having about 11% difference for NWP relative permeabilities. For random and EDT methods, the absolute difference was no higher than 4% for the entire set of saturation values.

Regarding the comparison between the partially wetting condition and the strongly wetting condition, the absolute differences for relative permeabilities were higher for the strongly wetting porous medium, which may be related to the lubrication effect.

The final distribution of phases for the methods can be seen in Figure 34.

By comparing the results for the final distribution of partially wetting porous medium (Figure 34) to the strongly wetting porous medium (Figure 26), some differences can be observed:

i. NWP for random and EDT methods: by the increase of the contact angle, the amount of NWP occupying the microporous region increased while the

Figure 34 – Final distributions of phases for partially wetting condition for $S_w = 0.4$.

(a) Random distribution

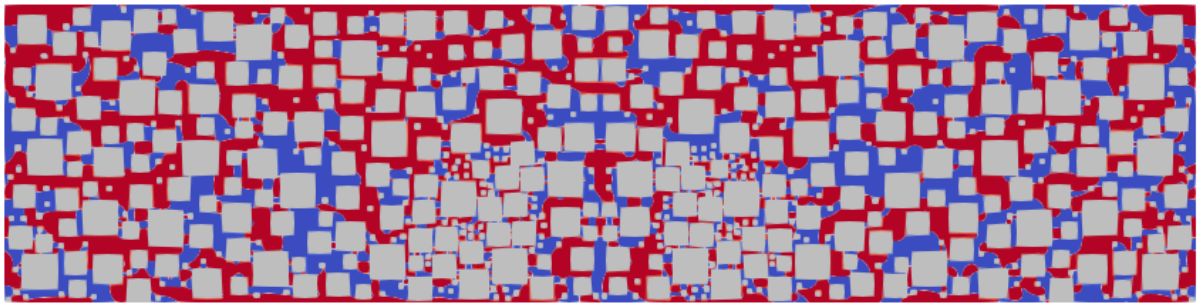

(b) EDT distribution

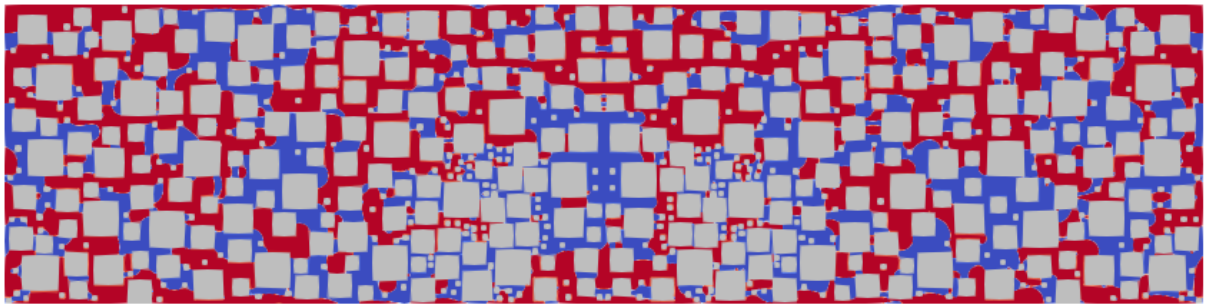

(c) CRT distribution

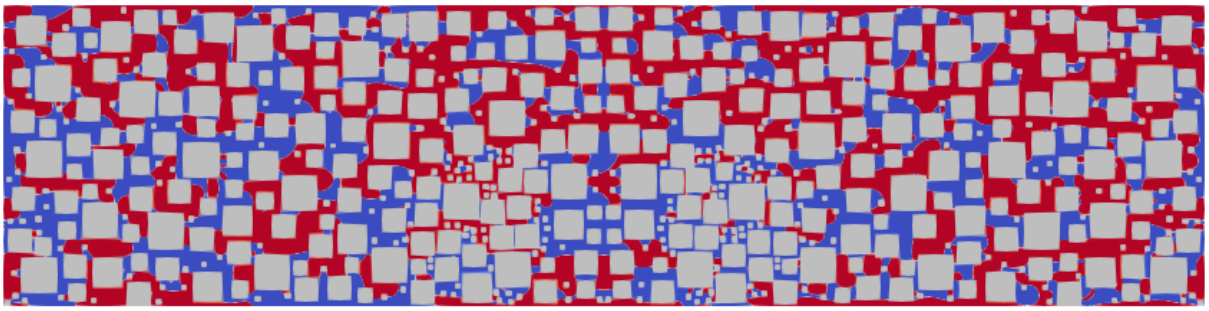

connectivity of NWP in the macroporous region seemed to decrease;

ii. WP for random and EDT methods: the differences in the final distribution of the WP are not easily spotted but, we can infer if more NWP is trapped in the microporous region, more WP is available on macroporosity;

iii. NWP for CRT method: even the quantity of NWP increased into the microporous region, the connectivity in the macroporous region seemed to increase, since the right side of the image is more connected than the observed for the strongly wetting condition;

iv. WP for CRT method: the higher size element of connectivity observed for the strongly wetting condition is not present for the partially wetting condition.

To compare the results for both wettability conditions, Figure 35 presents a direct comparison for relative permeability curves for each method. From the figure, it is possible to visualise the NWP relative permeability for the random and EDT methods had higher values for the strongly wetting porous medium. On the other hand, the contrary is observed for the CRT method. For the WP relative permeability curves, the random and EDT methods had lower values for the strongly wetting porous medium, which was expected due to the adhesion of WP on the solid walls. However, on the opposite way, the CRT method showed higher relative permeability values.

According to Li et al. (2018) and Shi and Tang (2018), when the contact angle increases, the WP phase starts to become connected and, as result, the WP relative permeability increases while the NWP relative permeability decreases. Said that it is possible to observe the results for the CRT method went to the opposite side of the theory, while random and EDT methods followed it.

Figure 35 – Changes in relative permeability regarding the contact angle.

(a) Random analysis

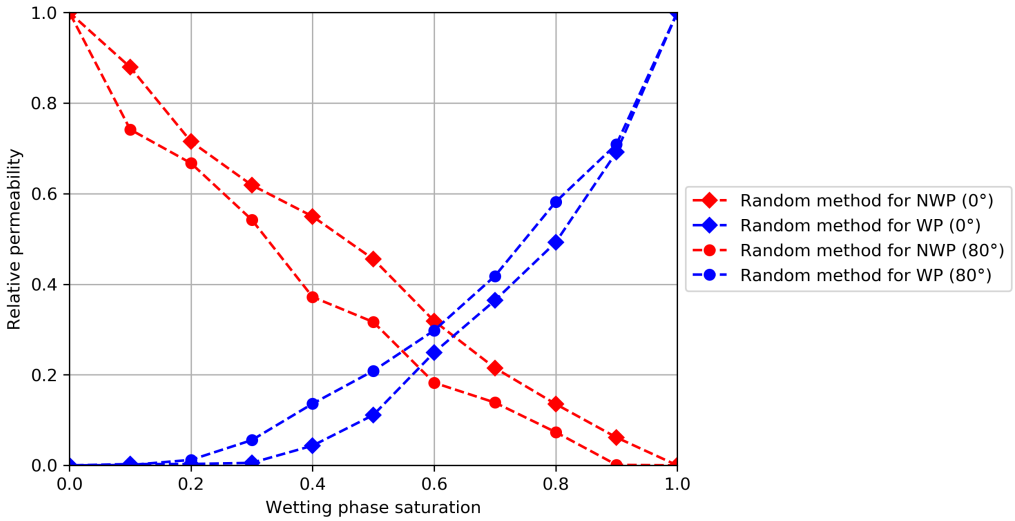

(b) EDT analysis

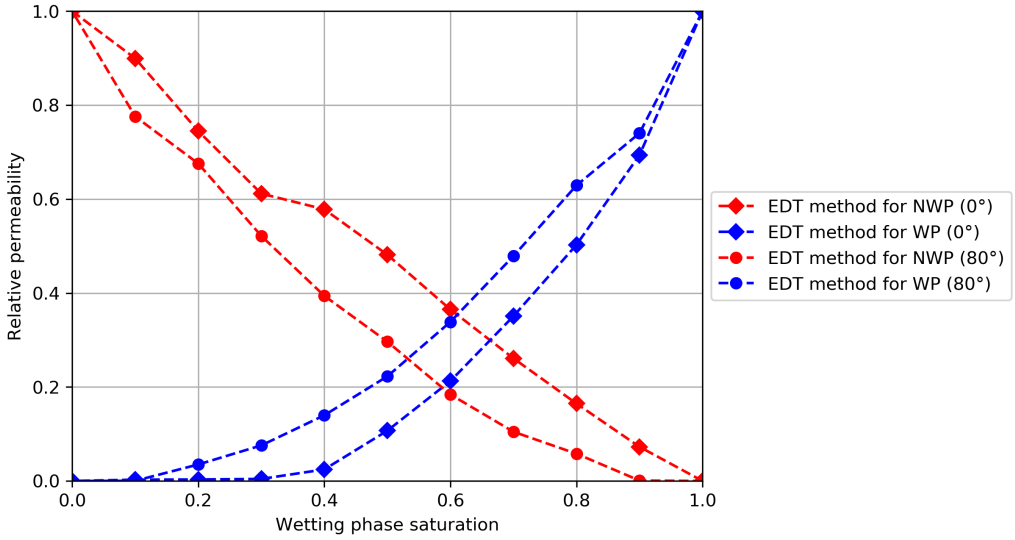

(c) CRT analysis

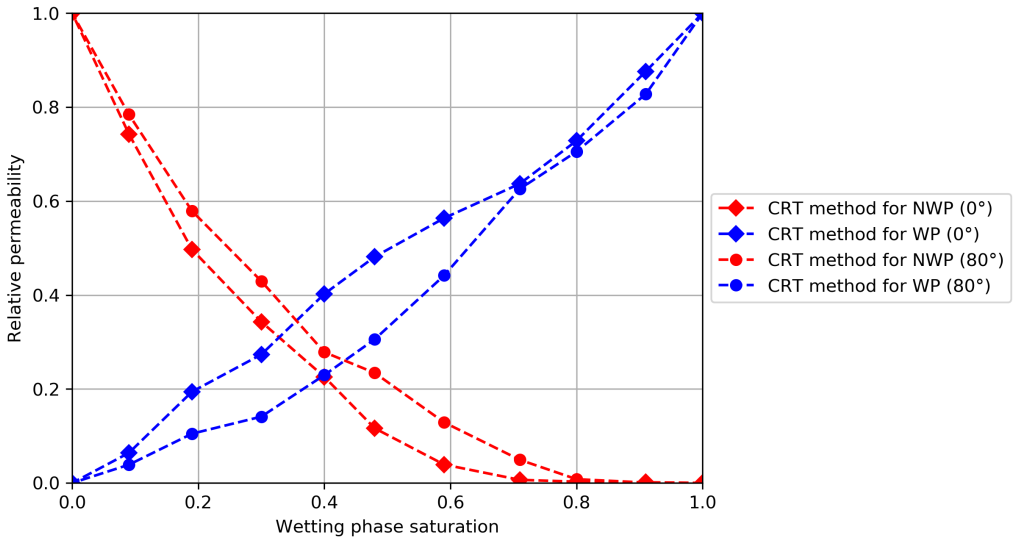

Source – Elaborated by the author

To deepen the analysis of connectivity, the number and size of the elements in the flow were calculated using the Fiji Software. To maintain the connectivity analysis similar to the one before accomplished for the strongly wetting case, the saturation level of 40% was chosen. The results for the NWP histogram can be seen in Figure 36 and for the WP histogram in Figure 37.

Figure 36 – Histogram of equivalent diameter for non-wetting phase.

(a) Random distribution

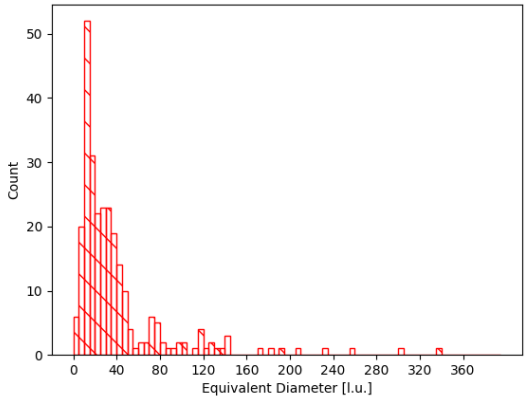

(b) EDT distribution

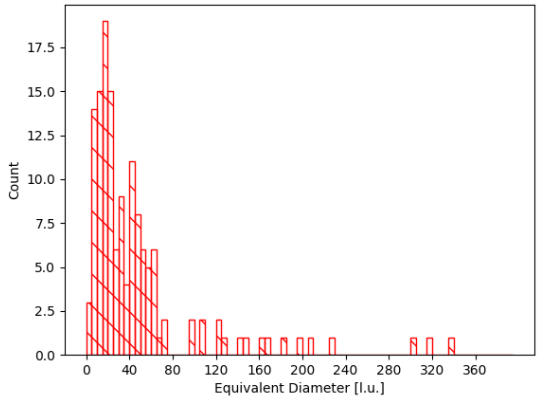

(c) CRT distribution

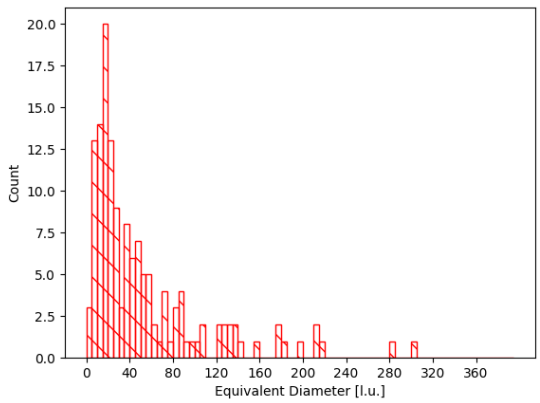

Source – Elaborated by the author

Figure 37 – Histogram of equivalent diameter for wetting phase.

(a) Random distribution

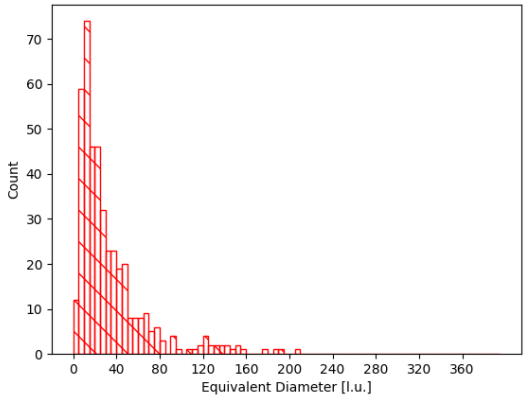

(b) EDT distribution

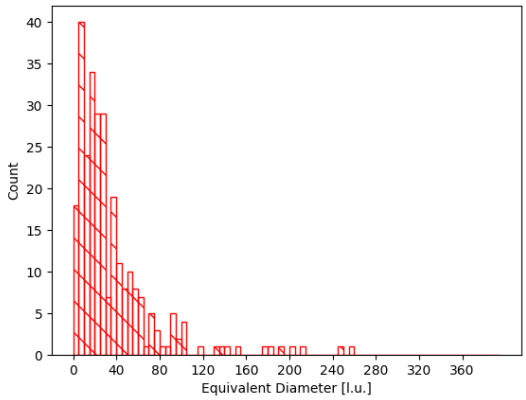

(c) CRT distribution

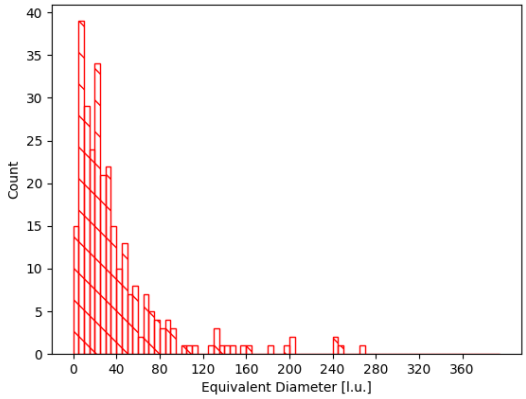

Source – Elaborated by the author

From Figure 36, it is possible to see the random had the highest quantity of elements. Regarding the size, the random and EDT methods presented the higher values, which may indicate a better connection of NWP in random and EDT methods and, may explain the higher results for the NWP relative permeabilities. Otherwise, it is possible to see the CRT method also presented elements with higher size in the fluid flow, nevertheless these elements were smaller than the observed in random and EDT methods. It may be explaining of why the NWP relative permeability curve for the CRT

method is closer to the random and EDT, but still, it had lower values.

For the WP, the random also presented the highest quantity of elements, mainly composed of small particles. Regarding the high size elements, it is possible to see a progression in size from random to EDT to CRT method. The random method had smaller quantities for high size elements and consequently the lower WP relative permeability. The EDT method had an intermediate number of high size elements and consequently it WP relative permeability was higher than the random method. The CRT method had the higher number than the other methods and, consequently, its WP relative permeability was the highest.

By comparing the NWP histogram for partially wetting condition to the NWP histogram for strongly wetting condition, for the random and EDT method, the total number of elements increased in the partially wetting condition but the size of them decreased. However, for the CRT method, the total number of elements increased and the size of them also increase. It may be a possible explanation for the increase of relative permeability for the CRT method when a decrease was expected a decrease.

For the comparison of WP histogram for partially wetting condition to the WP histogram for strongly wetting, the total number of elements for the random and EDT methods increased in the partially wetting condition, justifying the increase of WP relative permeability. Otherwise, the number of elements decreased for the CRT method, regarding quantity and size, explaining the decrease in the relative permeability.

This observation may be an interesting insight to point out. The connectivity of the phases seems to be influenced by the initial distribution of phases. From Dou and Zhou (2013), it is known that different initial distributions lead to different final distributions, and now we may addend, the initial distribution of phases also leads to different connectivity patterns that directly affect the relative permeability.

The next section analyses the adherence of these results by considering an image with features that reproduce a real reservoir.

4.3 BEREA SANDSTONE

4.3.1 Initialisation of Distribution Methods

For the determination of relative permeability curves for Berea sandstone, the EDT, random, and CRT methods were used to place the fluids into the sample. The initial distribution of phases can be seen in Figure 38.

Figure 38 – Initial distributions of phases for $S_w = 0.6$.

(a) Random distribution

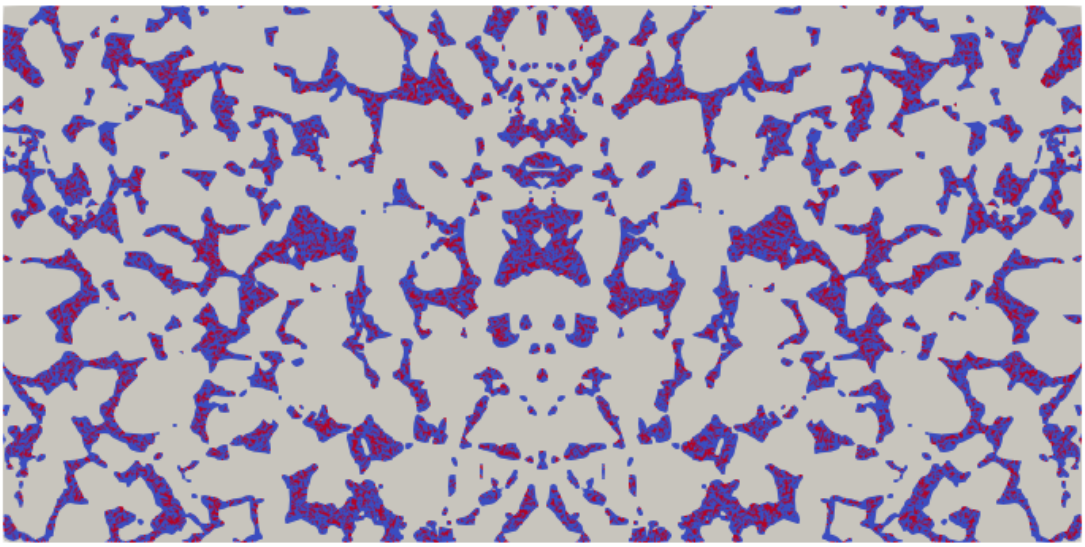

(b) EDT distribution

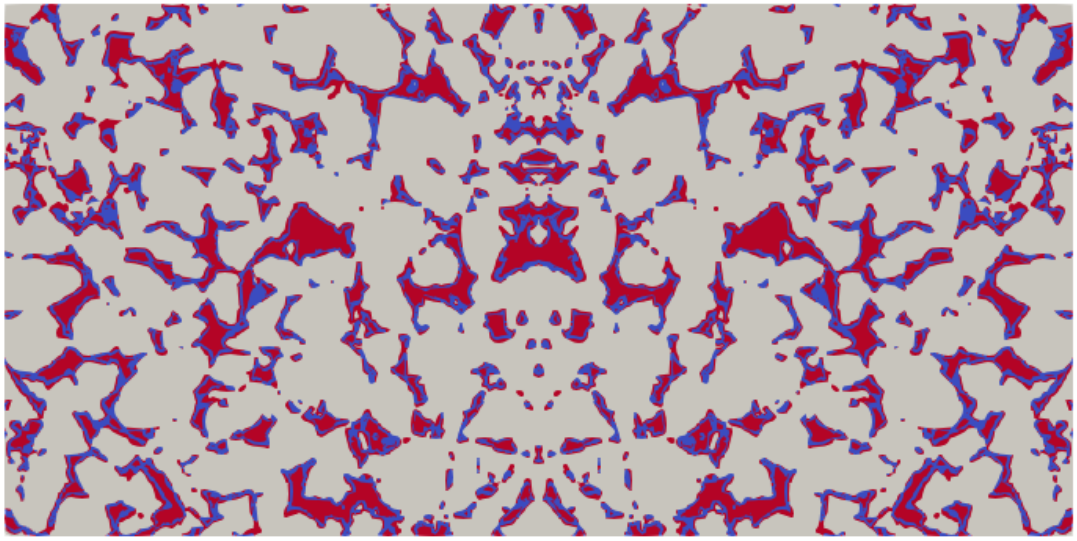

(c) CRT distribution

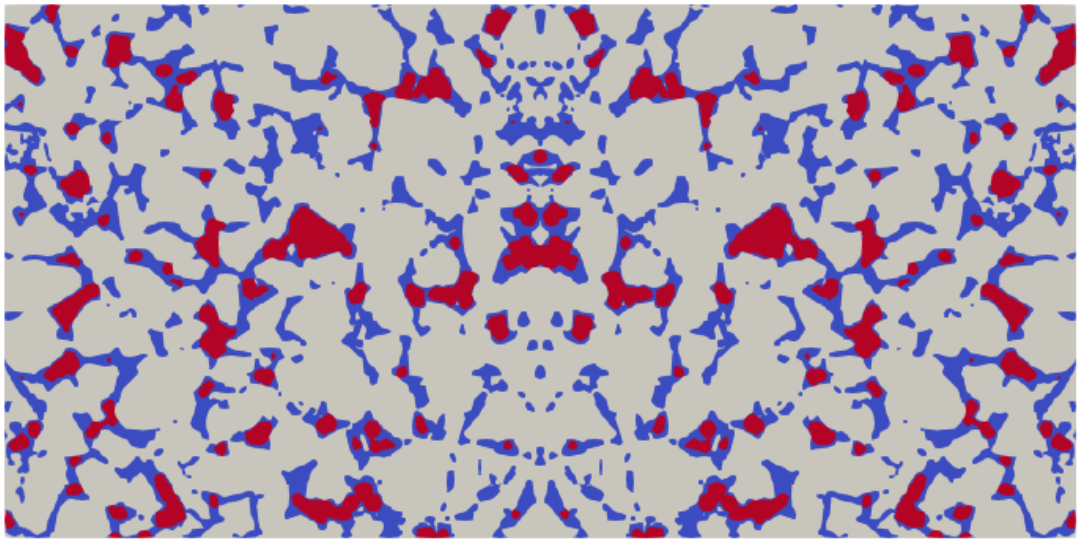

The saturation level for the wetting phase ranged from 0 to 1 in increments of 0.1. The porous medium was considered strongly wetting, with $\theta_r = 0°$. The capillary numbers for these simulations floated around 3×10^{-5}. The simulations were carried out until steady-state fluid flow was achieved then the relative permeabilities were measured. The results can be seen in Figure 39.

Figure 39 – Relative permeability curves for Berea sandstone.

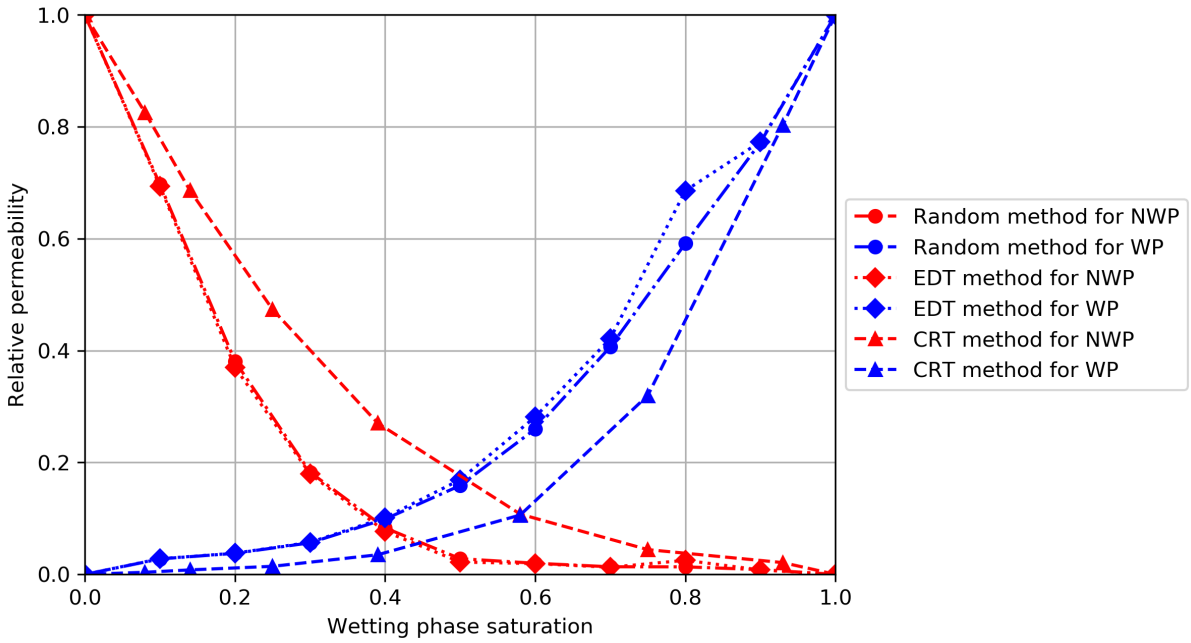

Source – Elaborated by the author

From Figure 39, it was possible to see the gaps between the curves, for the same saturation values, were lower than the observed in the artificial image, however, the differences still exist. The analysis for the absolute differences for NWP and WP relative permeabilities were presented in Appendix C.

The final distribution of phases can be seen in Figures 40, 41 and 42, for random, EDT and CRT method, respectively. The first image shows the contour of the NWP in the porous media and, a representation of the phases position is shown in the slice in the second image.

Figure 40 – Final distribution of phases for the random method.

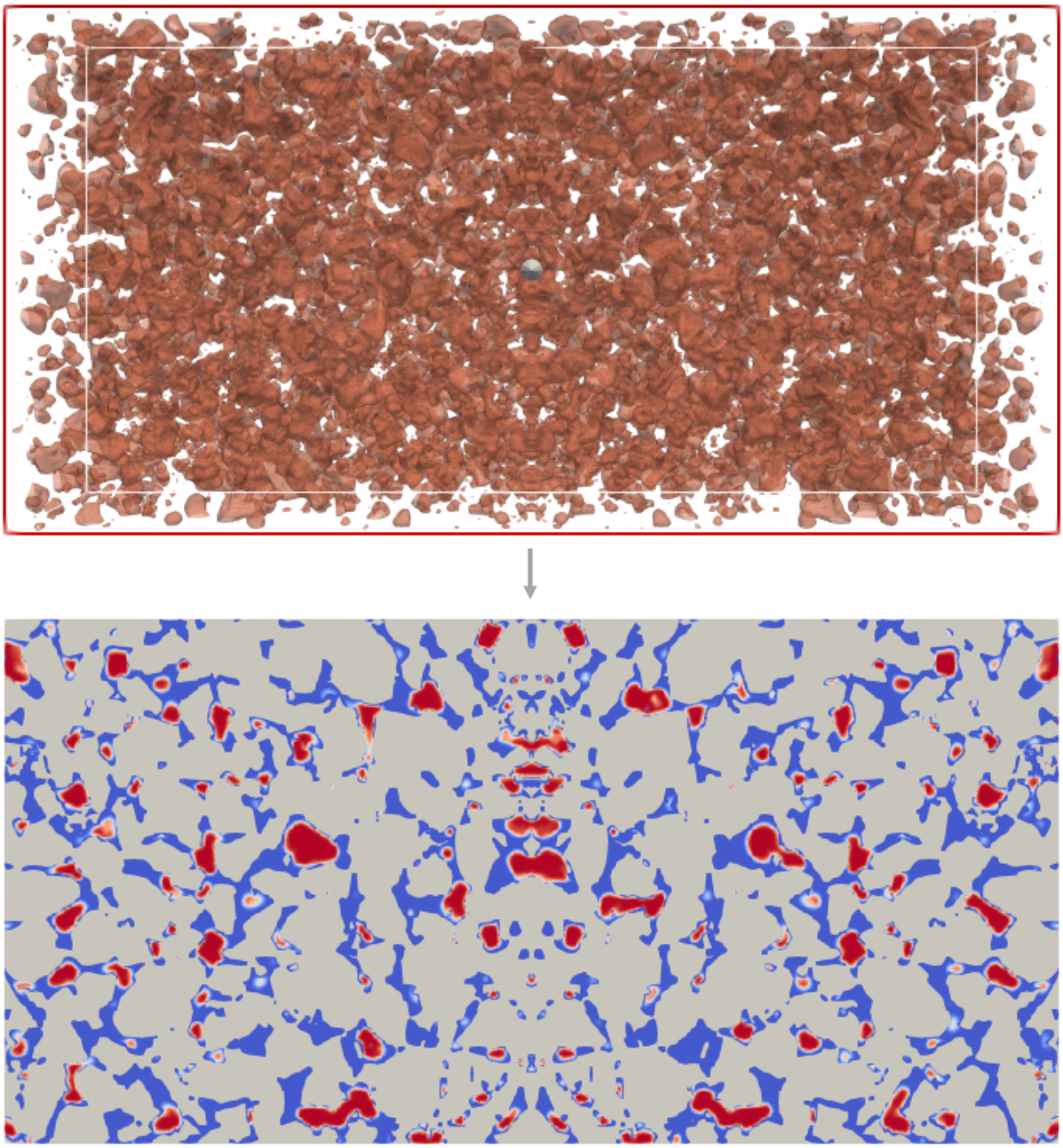

Source – Elaborated by the author

Figure 41 – Final distribution of phases for the EDT method.

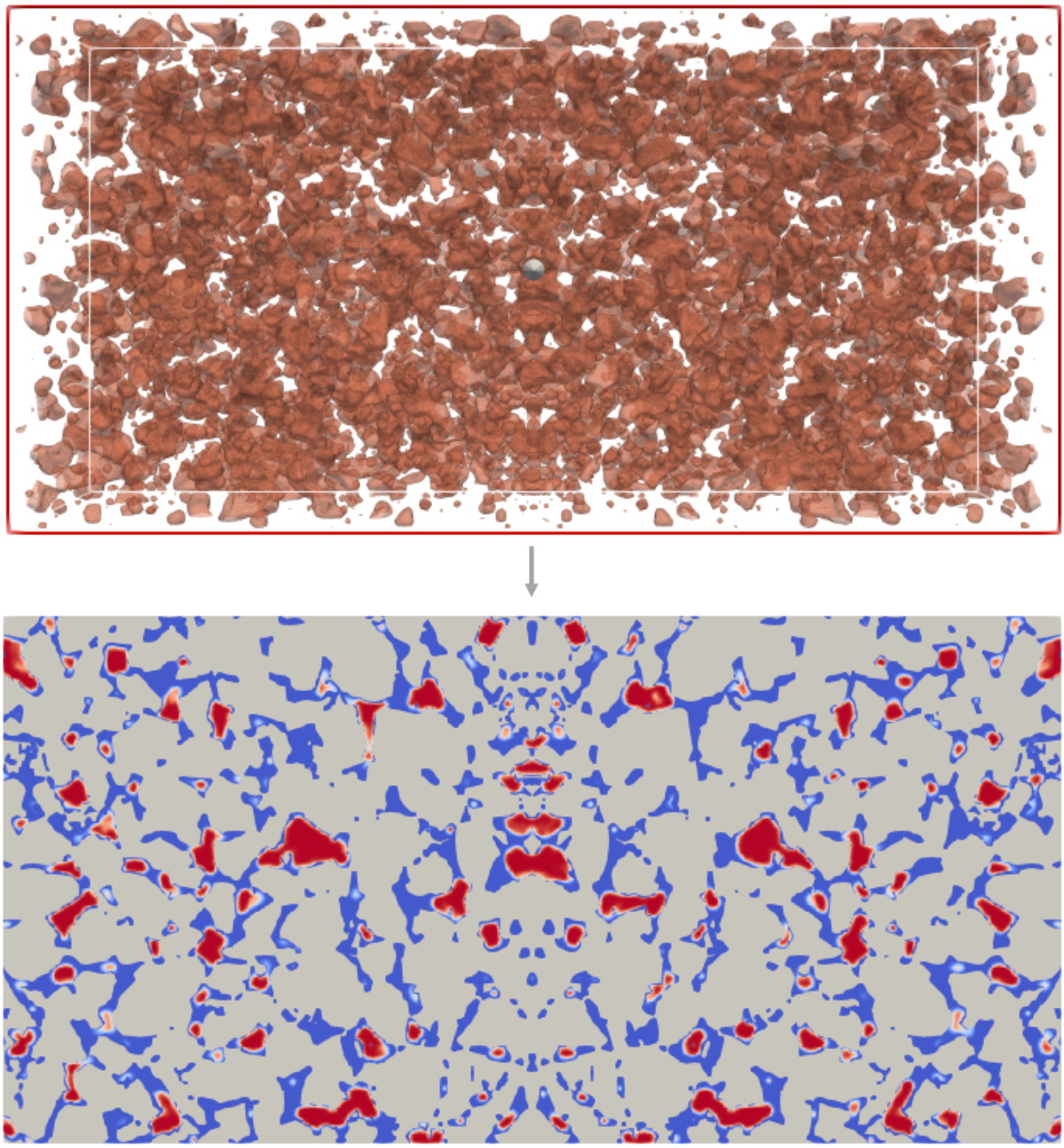

Source – Elaborated by the author

Figure 42 – Final distribution of phases for the CRT method.

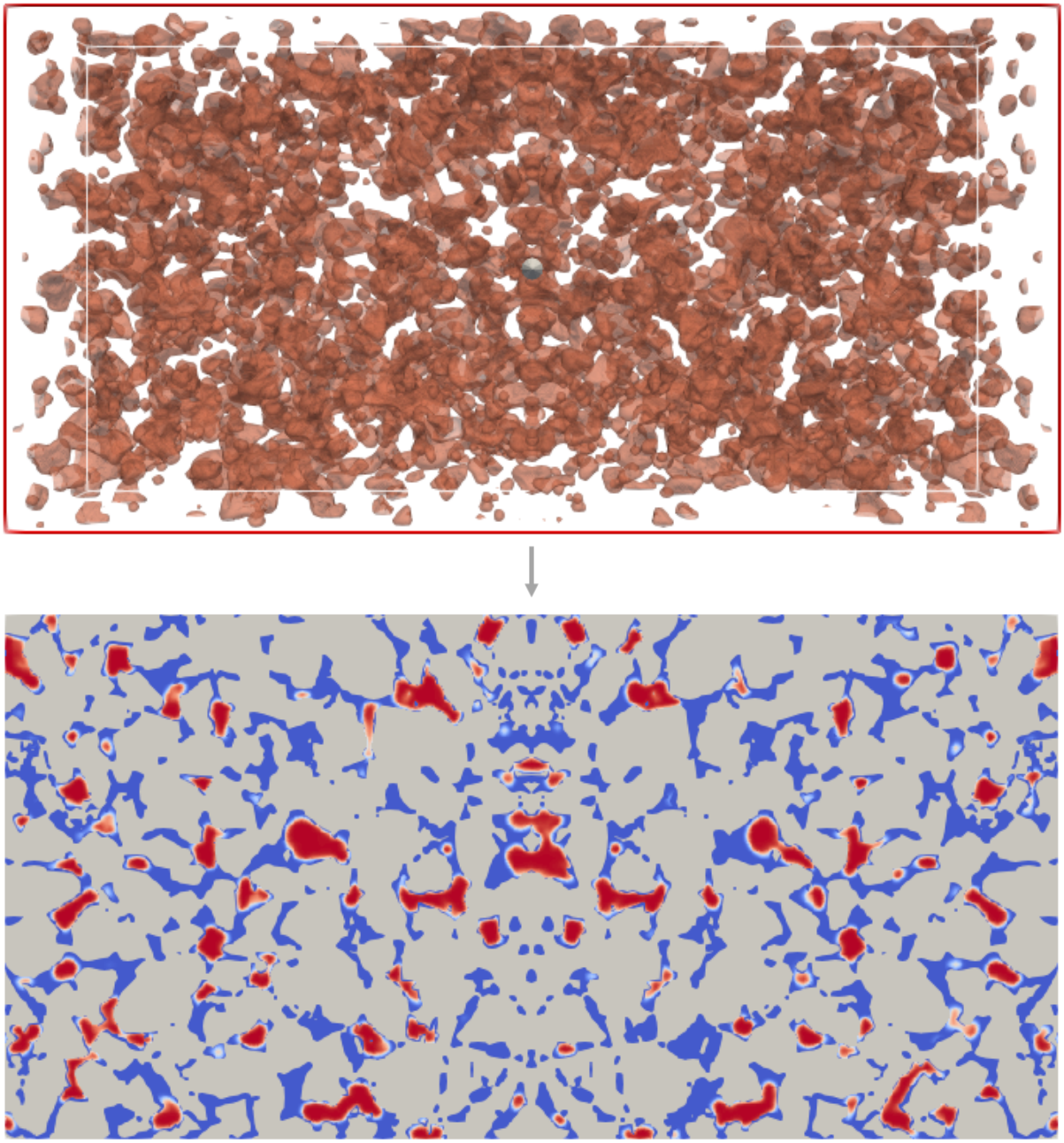

Source – Elaborated by the author

From the final distribution of phases, it is possible to see each method presented its particular final distribution and no visible features could justify the relative permeabilities differences. To deepen this analysis, in the next section, the connectivity will be analysed.

4.3.2 Phases Connectivity Analysis

As the final distribution of phases did not emphasise the similarities or the differences, the software Fiji was used to calculate the number and size of the elements,

in order to provide data about the fluid distribution. The histogram was based on the equivalent diameter, given by,

$$D_e = \left(\frac{6A}{\pi}\right)^{1/3}, \tag{33}$$

where A is the total number of fluid phase sites.

The histogram for the NWP elements can be seen in Figure 43 and for the WP can be seen in Figure 44.

Figure 43 – Histogram of equivalent diameter for non-wetting phase.

(a) Random distribution

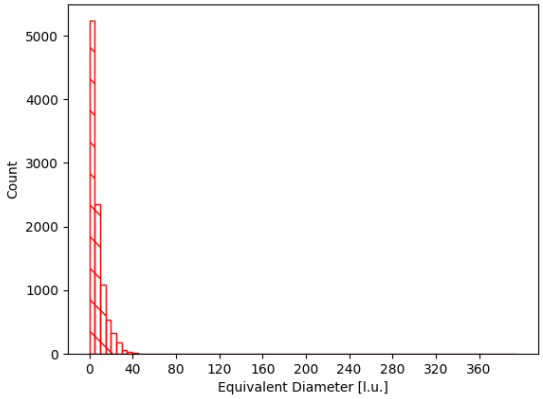

(b) EDT distribution

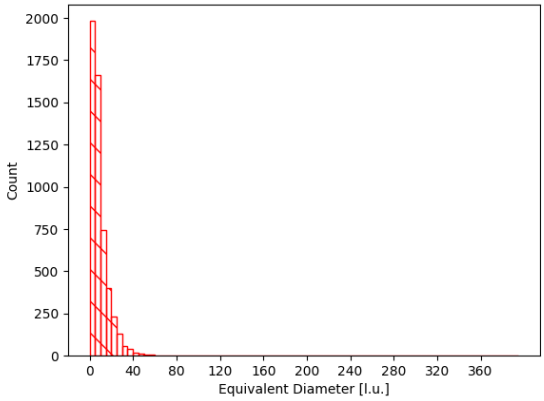

(c) CRT distribution

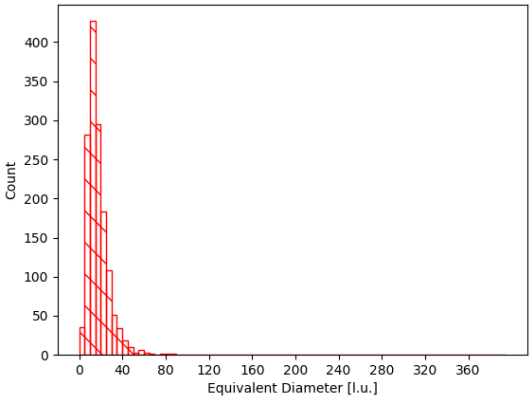

Source – Elaborated by the author

From the Figure 43, it is possible to see the random method had the highest quantity of elements but, they are mainly small size elements. On the other hand, the EDT method presented a slight increase in elements size regarding the random method, but in general, both methods had lower values for fluid flow particle size. Differently, the CRT method presented a lower quantity of elements but with a higher size. It may show why the NWP relative permeability is higher for the CRT method and, in general, similar to the random and EDT methods.

Figure 44 – Histogram of equivalent diameter for wetting phase.

(a) Random distribution

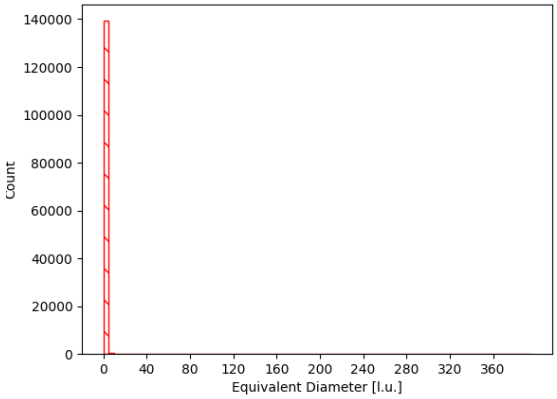

(b) EDT distribution

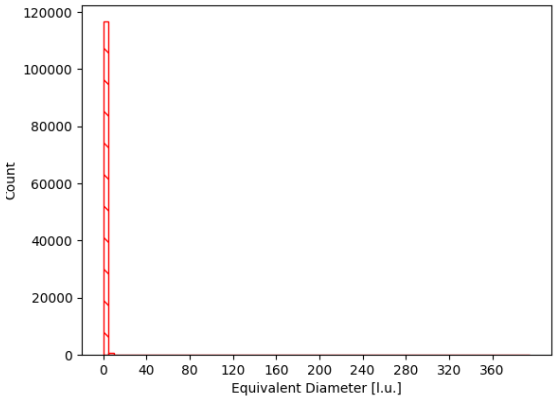

(c) CRT distribution

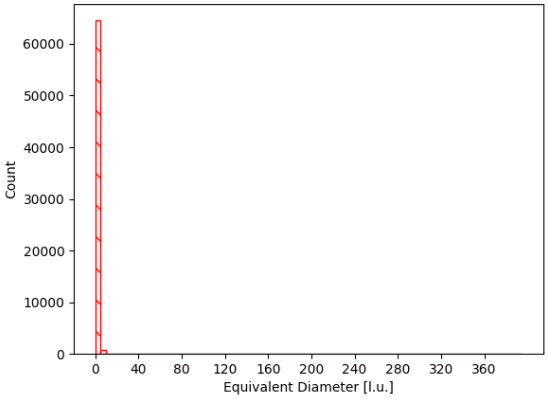

Source – Elaborated by the author

From Figure 44, it is possible to see the random and EDT methods had the highest values for the number of elements. In comparison to the CRT method, the random and EDT methods obtained almost the double value in terms of the number of elements. The size distribution is generally small for all methods, which is in accordance with the porosity of the porous medium.

Regarding the WP relative permeability curves, the random and EDT methods presented the higher values while the CRT method presented the lower values. Over

again, the reason may be strongly related to the connectivity of the phases.

4.3.3 Drainage Flooding (DRE)

In order to compare our results, the relative permeability curves obtained for Raeini, Blunt, and Bikeljic (2014) were used as benchmarks. In their work, Raeini, Blunt, and Bikeljic (2014) used a Berea sandstone with $400 \times 246 \times 256$ size, effective porosity of 18.5%, and predicted permeability of $1.24\ D$, which are similar to the Berea sandstone used in this work.

In their drainage simulations, the WP filled the Berea sandstone and the NWP was injected with a contact angle of 0° between the grain walls and the fluid–fluid interface. The capillary number was equal to 1.5×10^{-5}, in order to maintain a capillary-fingering displacement. The densities and viscosities of both fluids were equal and the contact angle (between the grain walls and the fluid-fluid interface) was assumed as zero during the drainage.

Also, before the simulation starts, a small portion of the image (8%) toward the inlet was filled with the injected phase to ensure there are always cells at the inlet containing the injected phase. The contact angle between the fluid-fluid interface was also set to zero, at the inlet.

Regarding the simulation, the flow equations were solved using a volume-of-fluid-based finite volume method with a filtered surface force formulation developed for efficient modelling of two-phase flow at low capillary numbers. The methodology is well explained at (RAEINI; BLUNT; BIJELJIC, 2012).

As simulation parameters, (RAEINI; BLUNT; BIKELJIC, 2014) considered a zero-gradient boundary condition for all variables, including pressure and velocity, at the outlet and, a fixed average value boundary condition for the dynamic pressure and a relaxed-fixed velocity for the injection of one phase, at the inlet.

The relative permeability curves are obtained from transient two-phase flow simulations. Each point of the Raeini, Blunt, and Bikeljic (2014) curve represents the average value over a time interval. This averaging helps to reduce the high-frequency fluctuations introduced by the pore-scale events.

The results obtained by the simulation of initial distribution methods and the drainage flooding results obtained by Raeini, Blunt, and Bikeljic (2014) can be observed in Figure 45.

By comparing the relative permeabilities curves for random, EDT, and CRT methods with the curves for the drainage flooding, the CRT method presented the best resemblance. However, according to Ramstad, Idowu, and Nardi (2011), the correlation between simulated drainage curves in the transient flow compared to experimental curves obtained under steady-state conditions may request caution.

From Figure 45, it is possible to see the cross-over point between CRT method

Figure 45 – Relative permeability curves comparison between the initial distribution methods and the results for drainage obtained by Raeini, Blunt, and Bikeljic (2014).

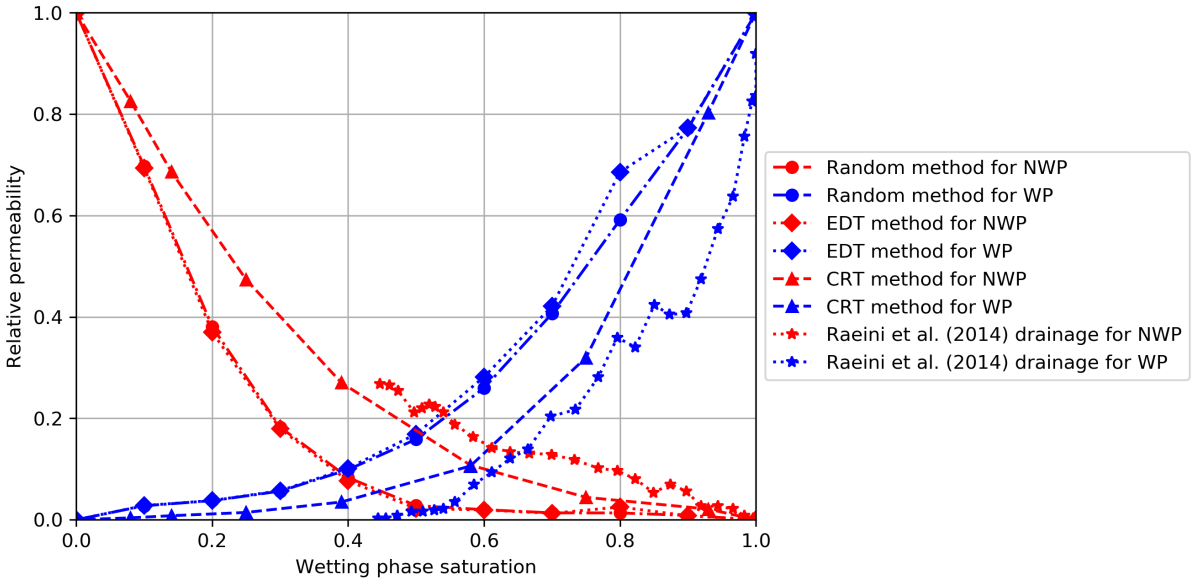

Source – Elaborated by the author

($S_w = 0.65$) and drainage ($S_w = 0.58$) is closer than the cross-over point between the random and EDT methods (0.40) and drainage. Also, it is possible to see the Berea sandstone did not present the WP overconnectivity, which was seen for the artificial 2D image, regarding the CRT method. For the Berea sandstone, the WP relative permeabilities for the CRT method were the lower observed values - which was also in agreement with the drainage flooding results. This observation may be associated with the phase connectivity since for the artificial image high size elements were observed, while for the Berea sandstone, these elements were not found.

Another observation from Figure 45 is regarding the NWP relative permeability curves. For the artificial image, the random and EDT methods presented the highest NWP relative permeability values. Otherwise, for the Berea sandstone, both methods presented the lowest values.

As exposed previously, it was believed the higher NWP relative permeability values for the random and EDT methods happened due to the lubrication effect. Otherwise, since the opposite was observed for the Berea sandstone it may be not an ordinary result.

According to Dou and Zhou (2013) the lubricating effect is significant in the heterogeneous porous media but not in the homogeneous porous media. It happened because the homogeneity of porous media restrains the lubrication effect. Therefore, the lubricating effect is strongly dependent on the heterogeneities of porous media.

For Churcher et al. (1991), the Berea sandstone has a similar degree of pore-

throat size correlation. Nevertheless, the degree of heterogeneity was not studied either for the artificial image or the Berea sandstone used in this work and, the Berea sandstone used by Churcher et al. (1991) research did not seem to be the same as the used here. Being so, it is not possible to confirm the relationship between lubrication effect and heterogeneity for this work.

Regarding the relative permeability absolute differences, Tables 9 and 10 summarise the results for NWP and WP. The column RAE presents the relative permeability values for Raeini, Blunt, and Bikeljic (2014) work.

Table 9 – Absolute NWP relative permeability differences regarding initial distribution methods and Raeini, Blunt, and Bikeljic (2014) drainage.

S_w	**RAE**	**RAN**	**EDT**	**CRT**	**|RAE-RAN|**$[\%]$	**|RAE-EDT|**$[\%]$	**|RAE-CRT|**$[\%]$
0.45	0.2681	0.0550	0.0500	0.2190	21.31	21.81	4.91
0.50	0.2198	0.0280	0.0221	0.1762	19.18	19.77	4.36
0.60	0.1492	0.0199	0.0192	0.1002	12.93	13.00	4.90
0.70	0.1287	0.0136	0.0127	0.0629	11.51	11.60	6.58
0.80	0.0965	0.0134	0.0251	0.0378	8.31	7.14	5.87

Source – Elaborated by the author

Table 10 – Absolute WP relative permeability differences regarding initial distribution methods and Raeini, Blunt, and Bikeljic (2014) drainage.

S_w	**RAE**	**RAN**	**EDT**	**CRT**	**|RAE-RAN|**$[\%]$	**|RAE-EDT|**$[\%]$	**|RAE-CRT|**$[\%]$
0.45	0.0027	0.1288	0.1353	0.0575	12.61	13.26	5.48
0.50	0.0161	0.1587	0.1692	0.0762	14.26	15.31	6.01
0.60	0.0858	0.2598	0.2815	0.1312	17.40	19.57	4.54
0.70	0.2037	0.4066	0.4213	0.2569	20.29	21.76	5.32
0.80	0.3592	0.5914	0.6857	0.4541	23.22	32.65	9.49

Source – Elaborated by the author

From Tables 9 and 10, it is possible to observe the random and EDT methods presented higher absolute differences regarding the drainage relative permeability values, varying from 7.14% to 21.81% for NWP and from 12.61% to 32.65% to WP. However, the CRT method presented lower differences, remaining bellow 6.58% to NWP and 9.49 to WP.

Raeini, Blunt, and Bikeljic (2014) also compared their drainage relative permeability curves with experimental results found in literature (OAK; BAKER; THOMAS, 1990; AKBARABADI; PIRI, 2013; KREVOR; PINI; BENSON, 2012; FULCHER; ERTEKIN; STAHL, 1985), as seen in Figure 46.

Figure 46 – Comparison between Raeini, Blunt, and Bikeljic (2014) simulations and experimental results

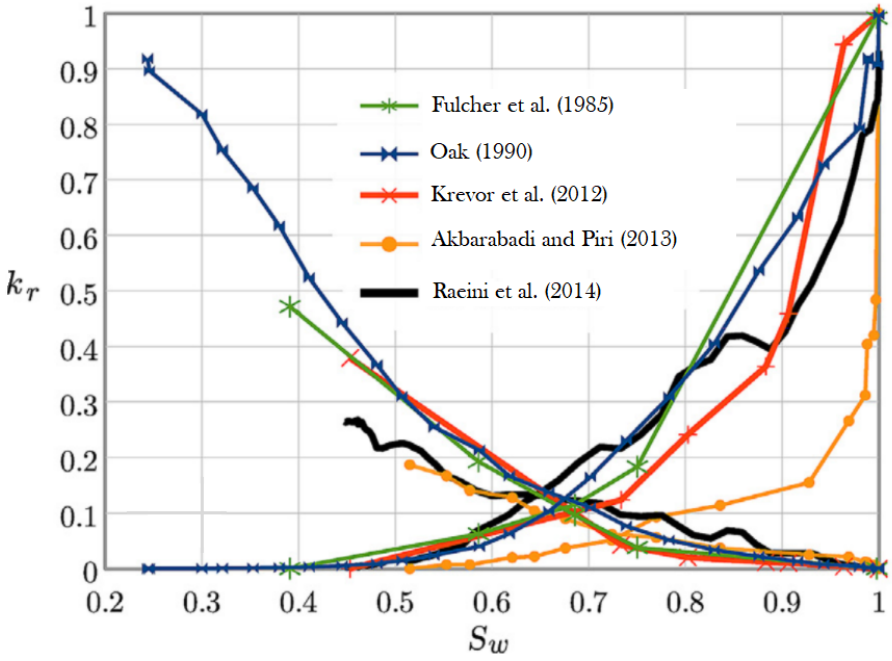

Source – Adapted from Raeini, Blunt, and Bikeljic (2014)

By analysing our results regarding the experimental curves, the random and EDT method did not resemble any of the experimental data, mainly due to the lower cross-over saturation level, that shifted the curves to the left. Otherwise, the CRT method agreed with Fulcher, Ertekin, and Stahl (1985) relative permeability curves.

5 CONCLUSION

This study has been performed to explore the effect of the initial distribution of phases in the relative permeability curves. The motivation behind it was based on the increasing use of computational simulations to predict the multiphase fluid flow and its associated properties.

The study observed the connectivity of phases was strongly related to the initial distribution of phases, which leaded relative permeability to present different values regarding the method used for initial distribution.

These differences were investigated by the carrying out simulations for an artificial two-dimensional porous medium and a three-dimensional sandstone. The porous medium was considered strongly wetting for the wetting phase, with a contact angle equal to 0°. For the artificial 2D image, a higher contact angle was also considered to analyse the role of the lubrication effect.

A drainage flooding was preceded to the artificial 2D image with the contact angle equal to 0° to verify which of the distribution methods would be likely to resemble the physical displacement observed in reservoir condition. For the Berea sandstone rock, the results were compared with Raeini, Blunt, and Bikeljic (2014) simulations and the experimental data available in their work.

From this study some key findings can be summarised, like the following:

i. The initial distribution of phases may lead to different phases connectivity patterns related to the final distribution of phases that affect directly the relative permeability values;

ii. For the artificial image, the CRT method showed a good agreement for NWP relative permeability curve and random and EDT methods for the WP relative permeability curve, regarding the drainage flooding simulation;

iii. For the WP relative permeabilities, the CRT method allowed the wetting phase to flow even for a saturation level for which WP should be static. This is observed for the entire WP relative permeability curve indicating CRT method overpredicts the WP relative permeability values for the artificial 2D image;

iv. For the higher contact angle simulations, the results obtained for the random and EDT methods corroborate with the supposition that by the increase of contact angle the relative permeability of NWP should decrease, and the relative permeability of WP should increase. Nevertheless, the CRT method results were opposite direction. By analysing the quantity and the size of phase elements, it was found out the results were intrinsically related to the phases connectivity;

v. For both strongly and partially wetting conditions in the artificial 2D image, the random and EDT methods presented a higher quantity and higher size phase elements for NWP. It reflected on higher values for relative permeability curves;

vi. For Berea sandstone, the random and EDT methods presented a higher NWP quantity of phase elements, otherwise, the size was smaller than for the CRT method. It incurred in lower NWP relative permeabilities for random and EDT methods;

vii. For the WP, the three methods presented small phase elements. Nevertheless, the random and EDT methods had the higher quantities for this measurement. It may explain the higher values observed for the WP relative permeability curves for random and EDT methods;

viii. By comparing the relative permeability curves for Berea sandstone the CRT method showed agreement with Raeini, Blunt, and Bikeljic (2014) and Fulcher, Ertekin, and Stahl (1985) results.

The findings from this work shed lights on the role of initial distribution of phases in the connectivity and, the correlation of phases connectivity and relative permeability.

5.1 SUGGESTION FOR FUTURE RESEARCHES

As suggestions for future studies: the suitability of CRT methods could be studied for a range of contact angles; the drainage flooding for the Berea sandstone image used in this work could be simulated with the same capillary number and using the steady-state flow, as in the initial distribution methods simulations, to better understand the results observed and to analyse the phases connectivity; the understanding of how to control the drainage simulation for other saturation values may be useful to reproduce the entire relative permeability curve and; the understanding of the homogeneity or heterogeneity of the samples could be inferred to verify the expressiveness of the lubrication effect.

REFERENCES

AKBARABADI, M.; PIRI, M. Relative permeability hysteresis and capillary trapping characteristics of supercritical CO2/brine systems: an experimental study at reservoir conditions. **Advances in Water Resources**, 2013.

ALBERTAZZI, Armando; SOUZA, André R. de. **Fundamentos de metrologia científica e industrial**. Ed. by Manole. [S.l.]: Manole, 2008.

ALIZADEH, A H; PIRI, M. Three-phase flow in porous media: a review of experimental studies on relative permeability. **Reviews of Geophysics**, p. 468–521, 2014.

ALPAK, F O; BERG, S; ZACHAROUDIOU, I. Prediction of fluid topology and relative permeability in imbibition in sandstone rock by direct numerical simulation. **Advances in Water Resources**, p. 49–59, 2018.

ALPAK, F. O.; ZACHAROUDIOU, I., et al. Direct simulation of pore-scale two-phase visco-capillary flow on large digital rock images using a phase-field lattice Boltzmann method on general-purpose graphics processing units. **Computational Geosciences**, 2019.

AMAEFULE, J.; HANDY, L. The effect of interfacial tensions on relative Oil/Water permeabilities of consolidated porous media. **SPE Journal**, 1982.

APOURVARI, S N; ARNS, C H. Image-based relative permeability upscaling from the pore scale. **Advances in Water Resources**, p. 161–175, 2016.

ASSIS ZAMPIROLLI, Francisco de. **Transformada de Distância por Morfologia Matemática**. 2003. PhD thesis – Universidade Estadual de Campinas.

BERG, S et al. Connected pathway relative permeability from pore-scale imaging of imbibition. **Advances in Water Resources**, p. 24–35, 2016.

BIRD, R. B.; STEWART, W. E.; LIGHTFOOT, E. N. **Transport Phenomena**. [S.l.]: John Wiley and Sons, 2006.

BLUNT, M. J. **Multiphase flow in permeable media: a pore scale perspective**. Ed. by Cambridge University Press. [S.l.]: Cambridge University Press, 2017.

BULTREYS, T. et al. Investigating the relative permeability behavior of microporosity-rich carbonates and tight sandstones with multiscale pore network models. **J. Geophys. Res.Solid Earth**, 2016.

CHANG, L. C. et al. Effect of connectivity and wettability on the relative permeability of NAPLs. **Environmental Geology**, 2008.

CHEN, L; KANG, Q, et al. Pore-scale modeling of multiphase reactive transport with phase transitions and dissolution-precipitation processes in closed systems. **Physical Review**, 2013.

CHEN, S; DOOLEN, G D. Lattice Boltzmann method for fluid flows. **Annual Review of Fluid Mechanics**, p. 329–364, 1998.

CHURCHER, P. L. et al. Rock Properties of Berea Sandstone, Baker Dolomite, and Indiana Limestone. **Society of Petroleum Engineering**, 1991.

COSENTINO, L. **Integrated Reservoir Studies**. [S.l.]: Editions TECHNIP, 2001.

DAI, Z et al. An integrated framework for optimizing CO2 sequestration and enhanced oil recovery. **Enviromental Science Tecnology**, p. 49–54, 2013.

DANIELSSON, P. E. Euclidean Distance Mapping. **Computer Graphics and Image Processing**, 1980.

DONG, Hu. **Micro-CT Imaging and Pore Network Extraction**. 2007. PhD thesis – Imperial College London.

DONNEZ, P. **Essentials of reservoir engineering**. [S.l.]: Editions TECHNIP, 2007.

DOU, Zhi; ZHOU, Zhi-Fang. Numerical study of non-uniqueness of the factors influencing relative permeability in heterogeneous porous media by lattice Boltzmann method. **International Journal of Heat and Fluid Flow**, p. 23–32, 2013.

EZEKWE, Nnaemeka. **Petroleum reservoir engineering practice**. Ed. by Prentice Hall. [S.l.]: Prentice Hall, 2011.

FULCHER, R. A.; ERTEKIN, T.; STAHL, C. D. Effect of capillary number and its constituents on two-phase relative permeability curves. **Journal of Petroleum Technology**, 1985.

GHASSEMI, A.; PAK, A. Numerical study of factors influencing relative permeabilities of two immiscible fluids through porous media using lattice Boltzmann method. **Journal of Petroleum Science and Engineering**, p. 135–145, 2011.

GINZBURG, I. Equilibrium-type and link-type lattice Boltzmann models for generic advection and anisotropic-dispersion equation. **Advances in water resources**, p. 1171–1195, 2005.

GUNSTENSEN, A K et al. Lattice Boltzmann model for immiscible fluids. **Physical Review**, 1991.

GUNSTENSEN, A. K. et al. Lattice Boltzmann model of immiscible fluids. **Physics Review**, 1991.

GUO, Y.; LIU, X.; XUO, X. A Unified Detail-Preserving Liquid Simulation byTwo-Phase Lattice Boltzmann Modeling. **IEEE Computer Society**, 2017.

GUO, Z; SHU, C. **Lattice Boltzmann Method and Its Applications in Engineering**. [S.l.]: World Scientific, 2013. DOI: https://doi.org/10.1142/8806.

HALLIDAY, I; HOLLIS, A P; CARE, M C. Lattice boltzmann algorithm for continuum multi- component flow. **Physical Review**, 2007. DOI: doi:10.1103/PhysRevE.76.026708.

HUANG, H; SUKOP, M; LU, Y X. **Multiphase Lattice Boltzmann Methods: Theory and application**. [S.l.]: John Wiley and Sons, 2015. v. 1.

JIANG, F; TSUJI, T. Estimation of three-phase relative permeability by simulating fluid dynamics directly on rock-microstructure images. **Water Resources Research**, p. 11–32, 2016.

KANG, Q et al. Pore scale modeling of reactive transport involved in geologic CO2 sequestration. **Transport Porous Media**, p. 197–213, 2010.

KREVOR, S. C. M.; PINI, R.; BENSON, S. M. Relative permeability and trapping of CO2 and water in sandstone rocks at reservoir conditions. **Advances in Water Resources**, 2012.

KRÜGER, T et al. **Lattice Boltzmann Method: Principles and Practice**. [S.l.]: Springer, 2017.

LANDRY, C J; KARPYN, Z T; AYALA, O. Relative permeability of homogenous-wet and mixed-wet porous media as determined by pore-scale lattice Boltzmann modeling. **Water Resources Research**, p. 3672–3689, 2014.

LANG, N. et al. Estimating the 3D Pore Size Distribution of Biopolymer Networks from Directionally Biased Data. **Biophysical Journal**, 2013.

LI, Z et al. A lattice Boltzmann investigation of steady-state fluid distribution, capillary pressure and relative permeability of a porous medium: Effects of fluid and geometrical properties. **Advances in Water Resources**, p. 153–166, 2018.

LIU, Z et al. Pore-scale characterization of two-phase flow using integral geometry. **Transport Porous Media**, p. 99–117, 2017.

LONGAIR, Mark. **Find Connected Regions Plugin**. 2006. Source: `https://www.longair.net/edinburgh/imagej/find-connected-regions/`.

LYONS, Willian. **Working guide to reservoir engineering**. Ed. by Elsevier. [S.l.: s.n.], 2010.

MAURER, C.; RAGHAVAN, V. A Linear Time Algorithm for Computing Exact Euclidean Distance Transforms of Binary Images in Arbitrary Dimensions. **IEEE Transactions on Pattern Analysis and Machine Intelligence**, 2003.

MOHAMED, A. A. **Lattice Boltzmann Method: fundamentals and engineering applications with computer codes**. [S.l.]: Springer, 2011.

MOSTAGHIMI, P.; BLUNT, M. J.; BIJELJIC, B. Computations of absolute permeability on micro-CT images. **Math Geosci**, 2012.

OAK, M J; BAKER, L E; THOMAS, D C. Three-phase relative permeability of Berea sandstone. **Journal of Petroleum Tecnology**, 1990.

OLIVEIRA, G. et al. The influence of microporosity on porosity-permeability correlation in carbonate rocks. **International Congress of the Brazilian Geophysical Society**, 2019.

ØREN, P E; BAKKE, S; ARNTZEN, O J. Extending predictive capabilities to network models. **Society of Petroleum Engineers**, p. 324–336, 1998.

PAN, C.; LUO, L. S.; MILLER, C. T. An evaluation of lattice Boltzmann schemes for porous medium flow simulation. **Computers and Fluids**, 2006.

PHILIPPI, P. C. et al. From the continuous to the lattice-Boltzmann equation: the discretization problem and thermal models. **Physical Review**, 2006.

QIAN, Y. H.; D'HUMIÈRES, D.; LALLEMAND, P. Lattice BGK Models for Navier-Stokes Equation. **Europhysics Letters**, 1992.

RAEINI, A. Q.; BLUNT, M. J.; BIKELJIC, B. Direct simulations of two-phase flow on micro-CT images of porous media and upscaling of pore-scale forces. **Advances in Water Resources**, 2014.

RAEINI, A.Q.; BLUNT, M.J.; BIJELJIC, B. Modelling two-phase flow in porous media at the pore scale using the volume-of-fluid method. **Computers and Fluids**, 2012.

RAMSTAD, T; IDOWU, N; NARDI, C. Relative permeability calculations from two-phase flow simulations directly on digital images of porous rocks. **Transport Porous Media**, p. 487–504, 2011.

ROSA, Adalberto José; SOUZA CARVALHO, Renato de;
XAVIER, José Augusto Daniel. **Engenharia de reservatórios de petróleo**. Ed. by Interciência. [S.l.]: Interciência, 2006.

ROSENFELD, A.; PFALTZ, J. L. Sequential Operations in Digital Picture Processing. **Journal of the ACM**, 1966.

ROTHMANN, D; KELLER, J. Immiscible cellular-automaton fluids. **Journal of Statistical Physics**, p. 1119–1127, 1988.

SANTOS, L. O. E.; FACIN, P. C.; PHILIPPI, P. C. Lattice-Boltzmann model based on field mediator for immiscible fluids. **Physical Review**, 2003.

SATTER, A.; IQBAL, G. M.; BUCHWALTER, J. **Practical Enhanced Reservoir Engineering: Assisted with Simulation Software**. [S.l.]: PennWell Corporation, 2007.

SCHINDELIN, J et al. Fiji: an open-source platform for biological-image analysis. **Nature Methods**, 2012. DOI: doi:10.1038/nmeth.2019.

SCHLÜTER, S et al. Pore scale displacement mechanisms as a source of hysteresis for two-phase flow in porous media. **Advances in Water Resources**, p. 2194–2205, 2016.

SHAN, X; CHEN, H. Lattice Boltzmann model for simulating flows with multiple phases and components. **Physical Review**, 1993.

SHI, Y; TANG, G H. Relative permeability of two-phase flow in three-dimensional porous media using lattice Boltzmann method. **Internation Journal of Heat and Fluid Flow**, p. 101–113, 2018.

SPENCER, T J; HALLIDAY, I; CARE, C M. Lattice Boltzmann equation method for multiple immiscible continuum fluids. **Physical Review**, 2010.

SUKOP, M. C.; THORNE, D. T. **Lattice Boltzmann Modelling:An Introduction for Geoscientists and Engineers**. [S.l.]: Springer, 2006.

SWIFT, M R et al. Lattice Boltzmann simulations of liquid-gas and binary fluid systems. **Physical Review**, 1996.

TORELLI, J. C. et al. A High Performance 3D Exact Euclidean Distance Transform Algorithm for Distributed Computing. **World Scientific**, 2010.

WOLF-GLADROW, Dieter A. **Lattice-Gas Cellular Automata and Lattice Boltzmann Models: An Introduction**. [S.l.]: Springer, 2005.

YIOTIS, A. G. et al. A lattice Boltzmann study of viscous coupling effects in immiscible two-phase flow in porous media. **Colloids and Surfaces**, 2007.

ZHANG, D; PAPADIKIS, K; GU, S. A lattice Boltzmann study on the impact of the geometrical properties of porous media on the steady state relative permeabilities on two-phase immiscible flows. **Advances in Water Resources**, p. 61–79, 2016.

ZHAO, H et al. Relative permeability of two immiscible fluids flowing through porous media determined by lattice Boltzmann method. **International Communications in Heat and Mass Transfer**, p. 53–61, 2017.

APPENDIX A – RELATIVE PERMEABILITY ABSOLUTE DIFFERENCES FOR WP

The characteristic WP relative permeability curve for CRT method indicates an overprediction for all the saturation levels. It is observed since the drainage flooding returns a value closer to zero for a wetting saturation equal to 35%. It results in the analysis that, at that saturation level, the wetting phase should be almost static in the porous medium.

In order to present the size of the gap observed for the WP for CRT method, Table 11 brings the analysis of absolute difference of the initial distribution methods.

Table 11 – Absolute relative permeability differences of WP regarding initial distribution methods.

S_w	**RAN**	**EDT**	**CRT**	**|RAN-EDT|[%]**	**|RAN-CRT|[%]**	**|EDT-CRT|[%]**
1.00	1.0000	1.0000	1.0000	0.00	0.00	0.00
0.90	0.6918	0.7049	0.8651	1.31	17.33	16.02
0.80	0.4925	0.5222	0.7285	2.97	23.60	20.63
0.70	0.3642	0.3770	0.6331	1.28	26.89	25.61
0.60	0.2493	0.2436	0.5687	0.57	31.94	32.51
0.50	0.1112	0.1159	0.4982	0.47	38.70	38.23
0.40	0.0435	0.0538	0.4025	1.03	35.90	34.87
0.30	0.0056	0.0124	0.2735	0.68	26.79	26.11
0.20	0.0029	0.0038	0.1982	0.09	19.53	19.44
0.10	0.0028	0.0016	0.0746	0.12	7.18	7.30
0.00	0.0000	0.0000	0.0000	0.00	0.00	0.00

Source – Elaborated by the author

As seen, the differences for intermediate saturation between CRT and random or EDT methods, 40% and 50%, ranged from 34.87% to 38.70%. Therefore, for high end saturation levels the differences achieved values from 7.18% to 23.60%. In the other hand, the WP relative permeability curve for random and EDT method did not present differences higher than 2.97% for all the interval.

APPENDIX B – RELATIVE PERMEABILITY ABSOLUTE DIFFERENCES FOR WP REGARDING CONTACT ANGLE INCREASE

According to Ghassemi and Pak (2011), in a strongly wetting system, non-wetting fluid tends to occupy a larger pore space, while the wetting phase tends to occupy a smaller pore space. Otherwise, when the system is not strongly wetting due to the increase of the contact angle, the fluid displacement is reorganise in a totally different way.

As the initial distribution methods vary for this work, Tables 12 and 13 presents the results for absolute differences for relative permeability.

Table 12 – Absolute relative permeability differences of NWP regarding initial distribution methods.

S_w	RAN	EDT	CRT	|RAN-EDT|[%]	|RAN-CRT|[%]	|EDT-CRT|[%]
1.0	0.0000	0.0000	0.0000	0.00	0.00	0.00
0.9	0.0011	0.0009	0.0014	0.02	0.03	0.05
0.8	0.0734	0.0580	0.0081	1.54	6.53	4.99
0.7	0.1387	0.1047	0.0536	3.40	8.51	5.11
0.6	0.1825	0.1841	0.1236	0.16	5.89	6.05
0.5	0.3165	0.2965	0.2249	2.00	9.16	7.16
0.4	0.3719	0.3941	0.2785	2.22	9.34	11.56
0.3	0.5424	0.5216	0.4297	2.08	11.27	9.19
0.2	0.6673	0.6758	0.5715	0.85	9.58	10.43
0.1	0.6093	0.7759	0.7678	16.66	15.85	0.81
0.0	1.0000	1.0000	1.0000	0.00	0.00	0.00

Source – Elaborated by the author

Table 13 – Absolute relative permeability differences of WP regarding initial distribution methods.

S_w	**RAN**	**EDT**	**CRT**	**|RAN-EDT|[%]**	**|RAN-CRT|[%]**	**|EDT-CRT|[%]**
1.0	1.0000	1.0000	1.0000	0.00	0.00	0.00
0.9	0.7092	0.7404	0.8187	3.12	10.95	7.83
0.8	0.5818	0.6292	0.7054	4.74	12.36	7.62
0.7	0.4181	0.4786	0.6161	6.05	19.80	13.75
0.6	0.2979	0.3387	0.4541	4.08	15.62	11.54
0.5	0.2088	0.2228	0.3221	1.40	11.33	9.93
0.4	0.1362	0.1399	0.2297	0.37	9.35	8.98
0.3	0.0557	0.0757	0.1412	2.00	8.55	6.55
0.2	0.0121	0.0351	0.1067	2.30	9.46	7.16
0.1	0.0008	0.0003	0.0442	0.05	4.34	4.39
0.0	0.0000	0.0000	0.0000	0.00	0.00	0.00

Source – Elaborated by the author

APPENDIX C – RELATIVE PERMEABILITY ABSOLUTE DIFFERENCES FOR BEREA SANDSTONE

The absolute differences for the NWP and WP relative permeabilities for the Berea sandstone can be seen in Tables 14 and 15.

Table 14 – Absolute differences for NWP relative permeability for Berea sandstone

S_w	RAN	EDT	CRT	|RAN-EDT|[%]	|RAN-CRT|[%]	|EDT-CRT|[%]
1.0	0.0000	0.0000	0.0000	0.00	0.00	0.00
0.9	0.0086	0.0078	0.0249	0.08	1.63	1.71
0.8	0.0134	0.0251	0.0378	1.17	2.44	1.27
0.7	0.0136	0.0127	0.0629	0.09	4.93	5.02
0.6	0.0199	0.0192	0.1002	0.07	8.03	8.10
0.5	0.0280	0.0221	0.1762	0.59	14.82	15.41
0.4	0.0830	0.0767	0.2619	0.63	17.89	18.52
0.3	0.1826	0.1796	0.4011	0.30	21.85	22.15
0.2	0.3810	0.3702	0.5702	1.08	18.92	20.00
0.1	0.6969	0.6935	0.7792	0.34	8.23	8.57
0.0	1.0000	1.0000	1.0000	0.00	0.00	0.00

Source – Elaborated by the author

Table 15 – Absolute differences for WP relative permeability for Berea sandstone

S_w	RAN	EDT	CRT	|RAN-EDT|[%]	|RAN-CRT|[%]	|EDT-CRT|[%]
1.0	1.0000	1.0000	1.0000	0.00	0.00	0.00
0.9	0.7718	0.7732	0.7226	0.14	4.92	5.06
0.8	0.5914	0.6857	0.4541	9.43	13.73	23.16
0.7	0.4066	0.4213	0.2569	1.47	14.97	16.44
0.6	0.2598	0.2815	0.1312	2.17	12.86	15.03
0.5	0.1587	0.1692	0.0762	1.05	8.25	9.30
0.4	0.0988	0.1014	0.0387	0.26	6.01	6.27
0.3	0.0564	0.0573	0.0218	0.09	3.46	3.55
0.2	0.0376	0.0379	0.0115	0.03	2.61	2.64
0.1	0.0276	0.0279	0.0051	0.03	2.25	2.28
0.0	0.0000	0.0000	0.0000	0.00	0.00	0.00

Source – Elaborated by the author

For the NWP relative permeability, Table 14, the absolute differences were lower than 2% between random and EDT methods. Nevertheless, between the random and CRT methods and EDT and CRT methods, this values increased, mostly for intermediate saturation levels, varying from 17.89% to 22.15%.

For the WP relative permeability, Table 15 the absolute differences between random and EDT methods were lower than 2%, except for $S_w = 0.8$ that presented a difference equal to 9.43%. For EDT and CRT methods, the higher differences were observed for higher wetting phase saturation, varying from 12.86% to 23.16%.